Site-directed mutagenesis of the metallo-β-lactamase VIM-7 from the opportunistic human pathogenic bacteria *Pseudomonas aeruginosa*

KJE-3900

Susann Skagseth

Master Thesis in Chemistry

Faculty of Science and Technology

University of Tromsø

May, 2012

Acknowledgements

Abbreviations

$\Delta\varepsilon$:	Extinction coefficient
A:	Ampere
Amp:	Ampicillin
AU:	Absorbance Unit
BME:	β–mercaptoethanol
bp:	base pair
BSA:	Bovine Serum Albumin
Cam:	Chloramphenicol
CV:	Column Volume
Da:	Dalton
ddH$_2$O:	Double-distilled water
dNTP:	Deoxyribonucleotide
E. coli:	*Escherichia coli*
EDTA:	Ethylene Diamine-Tetra-acetic Acid
Etest:	Epsilometer test
Hepes:	4-(2-hydroxyethyl)-1-piperazineethanesulfonic acid
IPTG:	Isopropyl-β-D-1-thiogalactopyranoside
k_{cat}:	Turnover number in Michaelis-Menten kinetics
K$_m$:	Dissociation constant for enzyme-substrate (ES) complex in Michael-Menten equation
LB:	Lysogeny Broth
LDS:	Lithium dodecyl sulphate
MBL:	Metallo-β-lactamase
MIC:	Minimum inhibitory concentration
min:	Minutes
mRNA:	messenger RNA
OD:	Optical density
o/n:	overnight
P. aeruginosa:	*Pseudomonas aeruginosa*
Pa:	Pascal
PBP:	Penicillin-binding protein
PCR:	Polymerase chain reaction
PEG:	Polyethylene glycol

PEG MME:	Polyethylene glycol monomethyl ether
rpm:	Rounds per minute
SB:	Sample buffer
SBL:	Serine-β-lactamase
SDS-PAGE:	Sodium dodecyl sulphate-polyacrylamide gel electrophoresis
SOB:	Super Optimal Broth
TAE:	Tris-acetate-EDTA
TEV:	Tobacco Etch Virus
TGX:	Tris-Glycine-Extended
VIM:	Verona integron-encoded metallo-β-lactamase
wt:	wild type

Abstract

The metallo-β-lactamases (MBLs) are enzymes with the ability to hydrolyse the β-lactam antibiotics. The worldwide emergence of the antibiotic resistant MBLs poses an increasing clinical threat. The VIM enzymes are a growing family of carbapenemases with a wide geographic distribution in Europe, South America and the USA. The VIM-7, the first VIM enzyme to be discovered in the USA, is the most divergent member of the VIM-enzymes with the closest similarity to VIM-1 with a 77% amino acid identity. The VIM-7 has a conserved D120 in the active site, which, in catalysis, plays an important role. The Y224 residue present in the VIM-2, which currently is the most widespread MBL, is though to have an impact on the activity. Three site-directed mutations of the VIM-7, with a previously solved structure, were made; D120A, D120N and H224Y respectively. All three mutants and the VIM-7 wt were sequenced, and the mutants VIM-7 D120A and VIM-7 H224Y with the VIM-7 wt, containing an N-terminal hexahis-tag and cleavage site, were produced, affinity purified and tested in a nitrocefin activity assay. The nitrocefin activity assay showed that the VIM-7 D120A mutant was inactive. In addition, the VIM-7 H224Y mutant was purified using gel filtration. A crystal was obtained of the VIM-7 H224Y mutant, and the crystal structure was solved. Enzyme kinetic studies were performed on the VIM-7 wt and the VM-7 H224Y, which resulted in the VIM-7 H224Y to have a significantly higher catalytic efficiency towards specific antibiotic substrates than the VIM-7 wt. The VIM-7 D120A mutant would not hydrolyse the antibiotic substrate ertapenem, and was not tested with other antibiotics. The inactive VIM-7 D120A and the active VIM-7 H224Y showed that by mutating one single amino acid, the D120 and the H224 residues, it has a significant effect on the activity of the VIM-7.

Keywords

Contents

Aim of study

The aim of this project was to produce three different site-directed mutations, each close to the active site to investigate how the mutants would affect the specificity of VIM-7 against a series of antibiotics. The mutants were expected to have different effects on the activity compared to the wild type. The mutants were expressed and purified before a biochemical characterization was performed. An optimistically aim was to perform crystallization trials and structure determination of one of the VIM-7 mutants.

Introduction

Antibiotic resistance has been known for 65 years, but the number of antibiotic resistant organisms and their breadth of resistance is increasing [1]. The metallo-β-lactamases (MBLs), present in many clinically important human bacterial pathogens, represent a growing challenge to the effectiveness of β-lactams, which are still the most widely prescribed class of antibiotics [2]. The MBLs encoded on transferable genes are easily spread, which makes surveillance studies and MBL inhibitor studies important [3]. In this study, mutations on the MBL VIM-7 will be performed to understand the selected residues' importance, in the active site, for enzyme activity.

β-lactams vs. metallo-β-lactamases – in the fight against resistance

For the last 60 years, β-lactams have been the most widely used antibiotics. β-lactams includes the following classes; penicillins, cephalosporins, monobactams and carbapenems, and they inhibit a transpeptidase involved in the cell wall biosynthesis [4]. A common feature of the molecular structure of the β-lactam antibiotics is a four-atom ring known as a β-lactam (Figure 1). The β-lactams are the largest group of antibiotics prescribed in Norway with a total human usage of 45% of all antibiotics used [5].

Some bacteria develop a resistance to β-lactam antibiotics by producing enzymes called β-lactamases, which hydrolyses the amide bond of the β-lactam ring. This makes the β-lactamases very important clinically. The β-lactamases are classified into four classes A-D [6, 7]. These are again divided into two superfamilies; the serine β-lactamases (SBLs), which entail class A, C and D, and metallo-β-lactamases (MBLs), which is class B of the Amber classification of β-lactamases [8]. According to the Bush-Jacoby classification of β-lactamases, the MBL belong to group 3 [9]. SBLs are characterized, as the name implies, by a serine moiety in the active site [10], while the MBLs are characterized by one or two metal ions, usually zinc, that functions as cofactors for enzyme activity [11]. The MBLs are further divided into subgroups B1, B2 and B3 according to their structural features and sequence identity, where most MBLs belong to group B1 [12]. All β-lactam antibiotics are hydrolysed by MBLs, with the monobactam aztreonam as an exception. Clinically, the MBLs are important because they are not inactivated by useful inhibitors, while many of the SBLs are inactivated [13, 14]. The MBLs are often expressed in combination with other β-lactamases in the same organism, and they have a broad substrate profile.
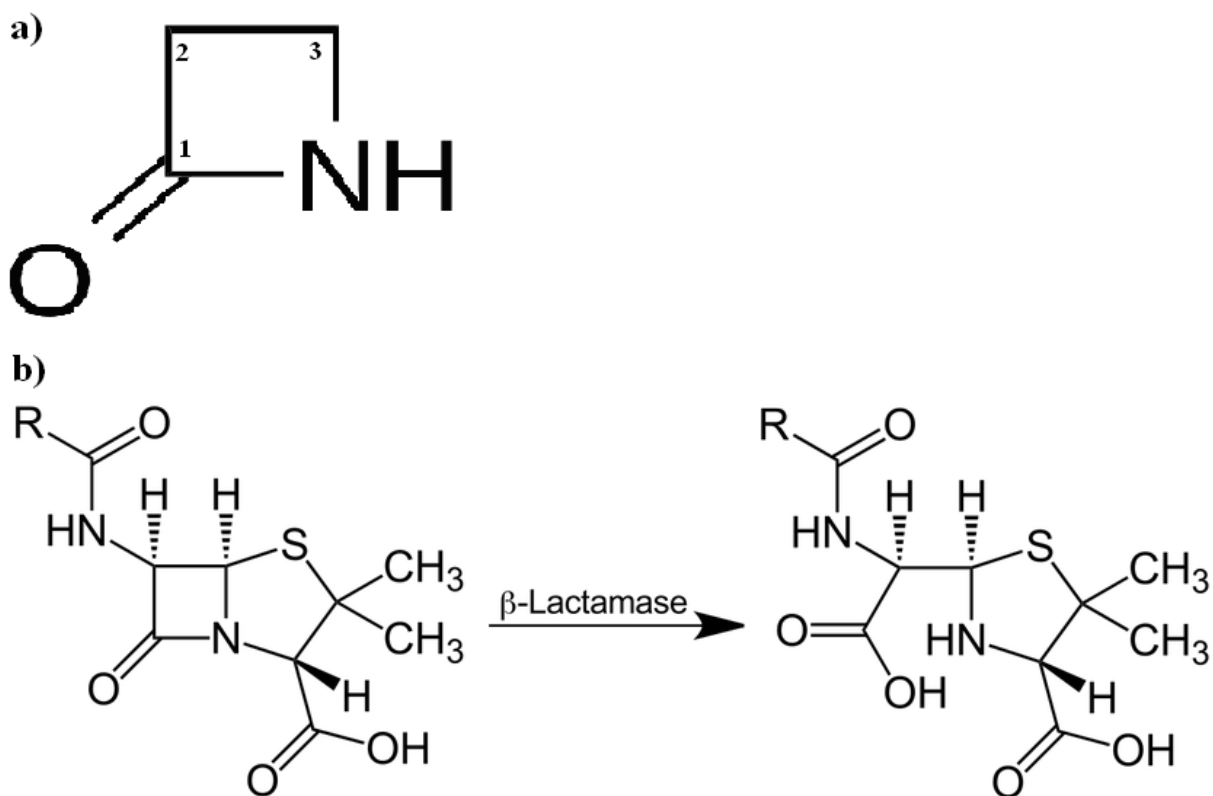
Figure 1: The cleavage of the β-lactam ring by the β-lactamases. a) The β-lactam ring. **b)** The action of β-lactamases on the β-lactam antibiotics. The C1-N bond of the β-lactam ring is broken by the β-lactamase, and the β-lactam antibiotics' properties are deactivated. Figures obtained from Wikipedia.

In the 1960s, the first discovery of MBL was made, in a strain of *Bacillus cereus* [15, 16]. The MBLs are known to be expressed by at least twenty different strains, this including *Pseudonomas aeruginosa* [17, 18]*, Klebsiella pneumoniae* [19]*, Serratia marcescens* [20]*, Aeromonas hydrophila* [21]*, Aeromonas veronii* [22]*, Stenotrophomonas maltophilia* [23]*, and *Bacteroids fragilis* [24, 25], where some of the strains are human pathogens.

As mentioned earlier, the MBLs need one (subclass B2) or two (subclass B1 and B3) active-site zinc ions for β-lactam hydrolysis. The location of the zinc atoms, in the B1 subclass, is at the opening in the wide groove between two β-sheets (Figure 2). The zinc ions are bridged with a water/hydroxide ion, and differences in the dizinc center and the substrate binding sites contribute in determining the MBLs catalytic efficiency towards the bound substrate. Although the MBLs have a low level of overall amino acid similarity, they share the αββα sandwich structure consisting of two β-sheets at the core and five external α-helices (Figure 2) [26]. The MBL proteins include the enzymes thiolesterases, which are members of the glyoxalase II family. The thiolesterases catalyse the hydrolysis of S-D-lactoyl-glutathione for it to form glutathione and D-lactic acid [27, 28].

9
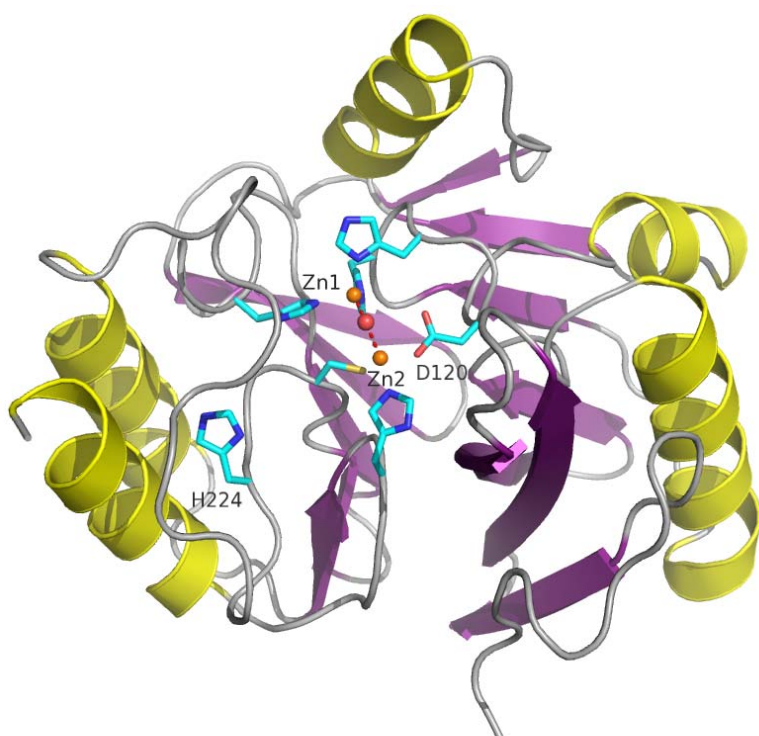
Figure 2: The structure of VIM-7 which belongs to the MBL molecular class B1. The Zn ions are in indicated by orange spheres, and the bridging water molecule in red. The figure is made in PyMOL using the VIM-7 structure obtained from RCSB PDB ID: 2Y87 [29].

Pseudomonas aeruginosa

The MBL VIM-7 was found in *P. aeruginosa*, which is a common bacterium that can cause disease in humans and animals [30]. *P. aeruginosa* is found in most man-made environments in the world in addition to soil, water and skin flora. Not only does it thrive in normal atmosphere, but also in hypoxic atmosphere, meaning atmosphere where the dissolved oxygen in water is below the level necessary to sustain most animal life. Because the bacteria can survive on most surfaces, it is also found in and on medical equipment, such as catheters, which causes cross-infections in hospitals. On the other hand, the bacteria are able to decompose hydrocarbons and have been contributory in breaking down tarballs and oil from oil spills [31]. One of the most opportunistic bacterial pathogens in patients with chronic pulmonary diseases such as cystic fibrosis and diffuse panbronchiolitis, is *P. aeruginosa* [32].

Verona integron-encoded metallo-β-lactamase 7 (VIM-7)

The Verona integron-encoded metallo-β-lactamase (VIM) was first reported in Italy in 1996 [33], hence, numbered 1, and the VIM is a growing family of carbapenemases, which now have a wide geographic distribution in Europe [34-37], South America [38], and have also been found in the United States [39]. VIM-1 was discovered in 1996 in *P. aeruginosa (P. aeruginosa)* at the University of Verona in Italy, and is the origin to the name VIM. In most countries in Europe the VIM-2 has been isolated from several strains, and is today the dominant type of VIM [40]. The VIM MBLs belong to the B1 subgroup, which has two flexible loops thought to interact with bound substrate and inhibition molecules [26]. The VIM enzymes are mostly occurring in *P. aeruginosa, Pseudonomas putida (P. putida)* [35], and occasionally in Enterobacteriaceae [41]. Due to the world-wide distribution, the VIM-enzymes are the most clinically important MLBs. VIM-7 was the first MBL reported from the United States. In a clinical isolate of *P. aeruginosa* from Texas, the VIM-7 was identified on a 24 kb plasmid [42]. The VIM-7, compared to other VIM-type MBLs, differ the most in terms of the amino acid sequence. VIM-7 is closest related to VIM-1 and VIM-4 with a 77% sequence identity and a 74% sequence identity to VIM-2 [3]. The VIM-7 amino acid and nucleotide sequence is shown in figure 3 below. The secondary structure elements and sequence alignment of VIM-7 and VIM-2 are shown in figure 4 below, including β-sheets and α-helices.

Enzyme kinetic studies of VIM-7 have shown that it efficiently hydrolyzes the β-lactams penicillins and carbapenem, except for ertapenem. For the β-lactams cephalosporins, the reported activity was found to be variable [43].

```
  1   M   F   Q   I   R   S   F   L   V   G   I   S   A   F   V   M   A   V   L   G
  1   ATGTTTCAAATTCGCAGCTTTCTGGTTGGTATCAGTGCATTCGTCATGGCCGTACTTGGA

 21   S   A   A   Y   S   A   Q   P   G   G   E   Y   P   T   V   D   D   I   P   V
 61   TCAGCAGCATATTCCGCACAGCCTGGCGGTGAATATCCGACAGTAGATGACATACCGGTA

 41   G   E   V   R   L   Y   K   I   G   D   G   V   W   S   H   I   A   T   Q   K
121   GGGGAAGTTCGGCTGTACAAGATTGGCGATGGCGTTTGGTCGCATATCGCAACTCAGAAA

 61   L   G   D   T   V   Y   S   S   N   G   L   I   V   R   D   A   D   E   L   L
181   CTCGGTGACACGGTGTACTCGTCTAATGGACTTATCGTCCGCGATGCTGATGAGTTGCTT

 81   L   I   D   T   A   W   G   A   K   N   T   V   A   L   L   A   E   I   E   K
241   CTTATTGATACAGCGTGGGGGGCGAAGAACACGGTAGCCCTTCTCGCGGAGATTGAAAAG

101   Q   I   G   L   P   V   T   R   S   I   S   T   H   F   H   D   D   R   V   G
301   CAAATTGGACTTCCAGTAACGCGCTCAATTTCTACGCACTTCCATGACGATCGAGTCGGT

121   G   V   D   V   L   R   A   A   G   V   A   T   Y   T   S   P   L   T   R   Q
361   GGAGTTGATGTCCTCCGGGCGGCTGGAGTGGCAACGTACACCTCACCCTTGACACGCCAG

141   L   A   E   A   A   G   N   E   V   P   A   H   S   L   K   A   L   S   S   S
421   CTGGCCGAAGCGGCGGGAAACGAGGTGCCTGCGCACTCTCTAAAAGCGCTCTCCTCTAGT

161   G   D   V   V   R   F   G   P   V   E   V   F   Y   P   G   A   A   H   S   G
481   GGAGATGTGGTGCGCTTCGGTCCCGTAGAGGTTTTCTATCCTGGTGCTGCGCATTCGGGC

181   D   N   L   V   V   Y   V   P   A   V   R   V   L   F   G   G   C   A   V   H
541   GACAATCTTGTGGTATACGTGCCGGCCGTGCGCGTACTGTTTGGTGGCTGTGCAGTTCAT

201   E   A   S   R   E   S   A   G   N   V   A   D   A   N   L   A   E   W   P   A
601   GAGGCGTCACGCGAATCCGCGGGTAATGTTGCCGATGCCAATTTGGCAGAATGGCCTGCT

221   T   I   K   R   I   Q   Q   R   Y   P   E   A   E   V   V   I   P   G   H   G
661   ACCATTAAACGAATTCAACAGCGGTATCCGGAAGCAGAGGTCGTCATCCCCGGCCACGGT

241   L   P   G   G   L   E   L   L   Q   H   T   T   N   V   V   K   T   H   K   V
721   CTACCGGGCGGTCTGGAATTGCTCCAACACACAACTAACGTTGTCAAAACGCACAAAGTA

261   R   P   V   A   E   -
781   CGCCCGGTGGCCGAGTAA
```

Figure 3: The protein coding sequence of the VIM-7 gene. The amino acid sequence is shown above and nucleotide sequence below. Numbering of sequences is given to the left. In this thesis a construct for A26-E265 was cloned. A26 is indicated in bold. The selected sites for mutations, here indicated as D117 and H200, while according to the BBL standard numbering scheme [12] is D120 and H224 are indicated in bold. Figure obtained from researcher Hanna-Kirsti Schrøder Leiros.
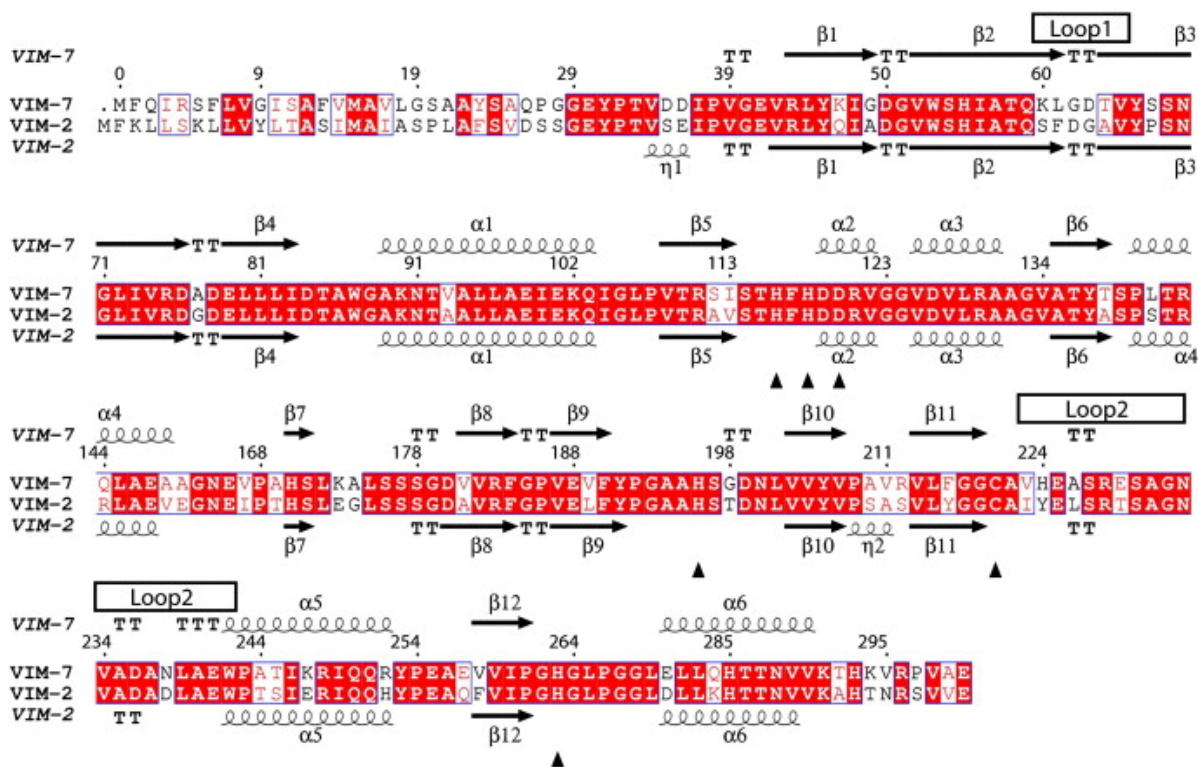
Figure 4: Sequence alignment and secondary structure elements of VIM-7 and VIM-2. The residues of VIM-7 and VIM-2 are numbered according to the standard numbering scheme for class B beta-lactamases [44]. The residues binding the zinc are indicated with triangles (▲). PDB ID: 2YZ3 [29].

Selected site-directed mutations of VIM-7

In this thesis, a D120A mutant, D120N mutant and a H224Y mutant of VIM-7 were made. Previous studies of D120 residue mutations in other MBLs have shown to have an impact on the activity of the enzyme. The 224 position was proposed to play a role in the activity, as the VIM-2 had a tyrosine amino acid at the 224 residue, and VIM-7 had a histidine amino acid.

Studies have shown that the D120 residue in the active site is important for MBLs to binding of Zn and therefore for proper binding of substrate to the enzyme [4, 45]. The aspartic acid (D) residues can have three major functions in enzymes: 1) contribute in coordination of the Zn ions to ensure the optimal position for catalytic activity, and therefore 2) hydrogen bonding with active site residues and substrates, and 3) shuttling protons from and to groups in the active site [4]. The coordination of Zn ions is done by D120, with unbound oxygen located directly above the bridging group in the active site (Figure 5). The interactions of the D120 residue with water molecules in the active site are important to transfer protons and a possible nucleophilic attack by the metal-bridging water/hydroxide on the β-lactam carbonyl

13

carbon of the amide bond. Hence, the D120 residue plays an important role in the enzymatic activity of the MBL [4]. It has also been hypothesized that D120, in addition to being a metal-binding ligand, electrostatically interacts with the bridging hydroxide, properly positioning it for nucleophilic attack on the substrate. The incoming water molecule acts as a proton donor to the nitrogen leaving group of the substrate [45]. One proposed reaction mechanism is shown in figure 6. The carboxylate side chain of D120 binds directly with the metal-bridging water/hydroxide, via hydrogen bonding, and with the Zn ion.

Samuelsen et al [43], showed that the catalytic efficiency for cephalosporins was generally higher for VIM-1 and VIM-2, compared to the catalytic efficiency of VIM-7. The cephalosporin moxalactam was the only exception of the nine cephalosporin substrates tested. The catalytic efficiency of the carbapenems was similar between VIM-7 and VIM-2, while the efficiency of the penicillins was higher for VIM-7, compared to the VIM-1 and VIM-2. By studying the active site of VIM-1, VIM-2 and VIM-7 (Figure 5), there are some differences. Most VIMs have histidine at the 224 position, while VIM-2 has a tyrosine. It was suggested that the Tyrosine-224 of the VIM-2 interacts with the charged R2 substituents of some β-lactams (present in some cephalosporin substrates), and that the tyrosine hydroxyl group makes a second-shell metal-ligand interaction by hydrogen bonding via a water molecule. A substitution of Tyr-224 with histidine was suggested to disrupt this interaction [43].
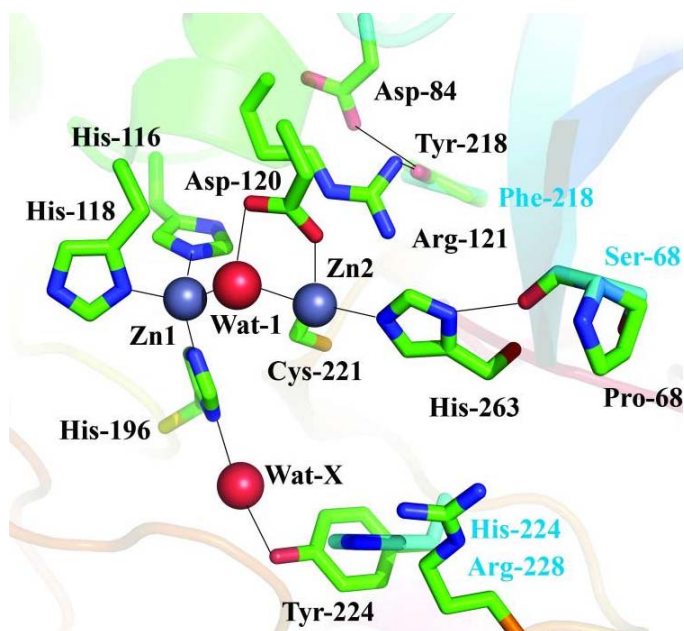
Figure 5: The active sites of VIM-2. Active site residues for VIM-2 are shown in green. Light cyan coloured residues represent the aligned residues in VIM-1 and VIM-7. The atom colours are; carbon is shown in green, oxygen in red, nitrogen in blue and sulphur in yellow. The two zinc ions (Zn1 and Zn2) are marked as grey, and the two water molecules (Wat-1 and Wat-X) as red spheres. The numbering of the residues is according to the BBL standard numbering scheme [12]. Thin gray lines show the metal-ligands and hydrogen bonds. The VIM-1 and VIM-7 models' side chains are of Ser68, Phe218 and His224 are shown in cyan. Figure adapted from Samuelsen et al [43].
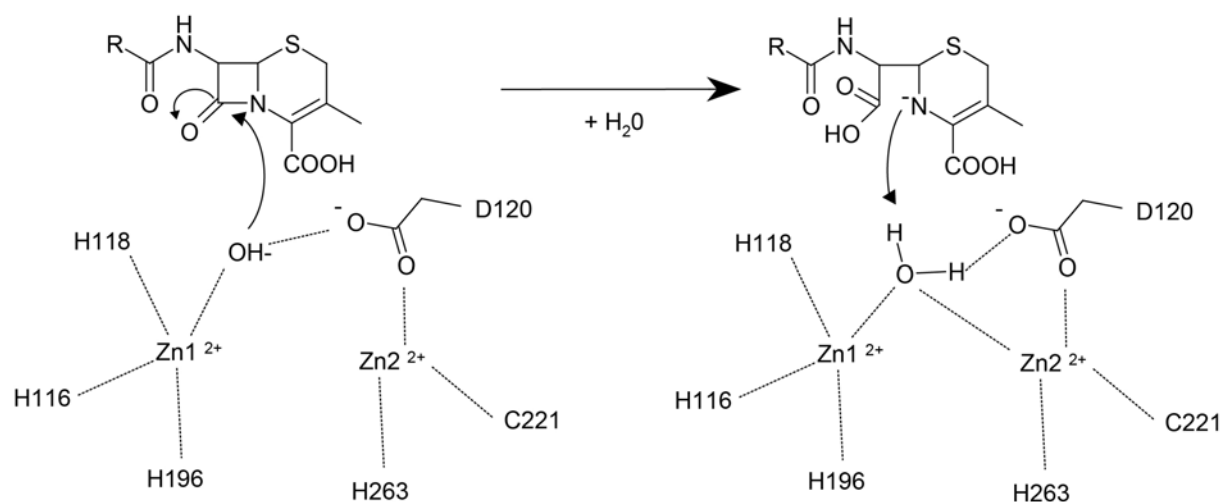
Figure 6: The proposed reaction mechanism showing the role of the D120 residue in the active site of the VIM-7. The D120 orients the metal-bound water/hydroxide (OH⁻) for it to make the initial nucleophilic attack on the bound cephalosporin substrate. Another water molecule protonates the amide nitrogen and replaces the first water/OH⁻ at the bridging position. Hypothesis published by Crisp et al [45].

Classification of antibiotics

More than 12 000 antibiotics with a variety of modes of action and with different specificities have been extracted from different microorganisms, since the late 1920s when penicillin was first discovered [46, 47]. The first use of the term "antibiotic" in the present sense was by the American microbiologist Waksman and his colleagues in 1941 [48]. Waksman [49] defined antibiotic as following; "an antibiotic is a chemical substance, produced by micro-organisms, which has the capacity to inhibit the growth of and even to destroy bacteria and other micro-organisms." A common classification system is based on the biological activity of the antibiotics [50]; group 1, bacteriostatic antibiotics, where the growth of the bacteria is inhibited (the bacteria is kept in the stationary growth), and group 2, bactericidal antibiotics, where the bacteria is killed. The biological activity can be estimated for group 1 by measuring the minimal inhibitory concentration (MIC). MIC is the lowest concentration of antibiotics needed to inhibit the growth of a microorganism. For group 2, the minimal bactericidal concentration (MBC) is measured, which is the lowest concentration of antibiotics that kills the bacteria.

Several other classification systems have been developed based on; chemical origin (natural, semisynthetic, or synthetic), or their mechanism of action is shown in figure 7, a spectrum of activity, or chemical structure. The specificity of the activity is classifies as; broad-spectrum, where the antibiotics affect a wide variety of bacteria, and narrow-spectrum, where antibiotics affect specific types of bacteria, like Gram-negative or Gram-positive bacteria. It has been proposed and partly proved that the development of antibiotic resistance is associated with overuse of broad-spectrum antibiotics [51].
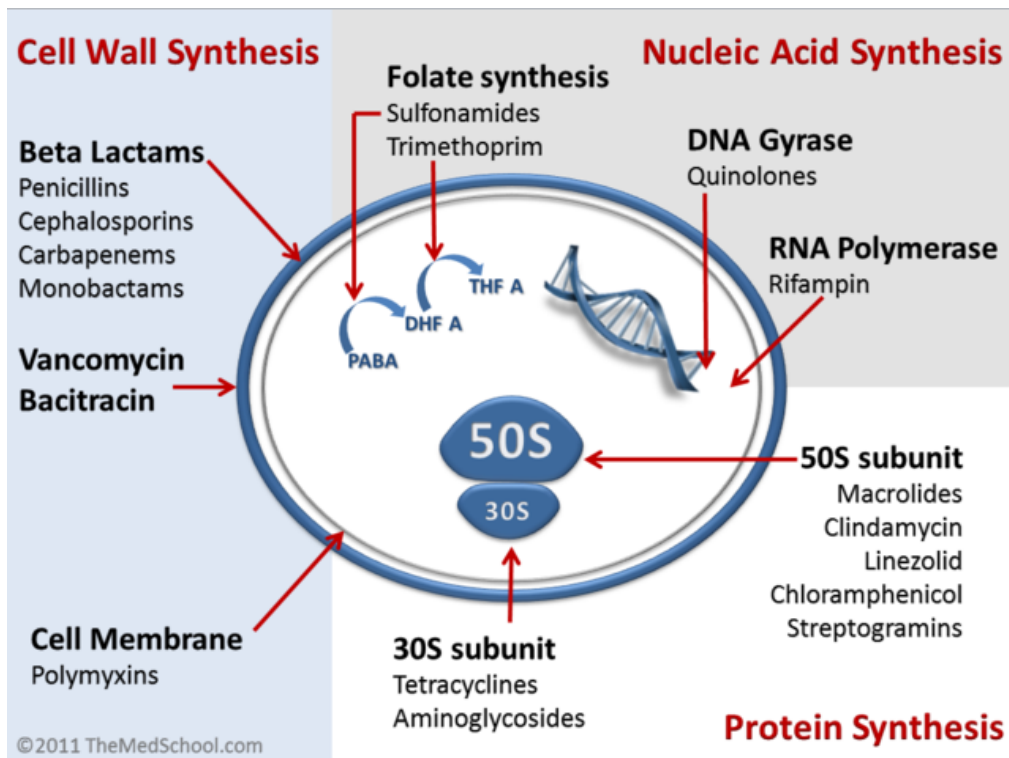
Figure 7: Antibiotics mechanism of action on the bacteria cell. The different classes of antibiotics are shown here in β-lactams affects the cell wall synthesis. Figure obtained from Wikipedia.

Every year, over 100 000 tons of antibiotics are produced, worldwide, with annual sales of about $35 billion, this including antibiotics used as animal growth promoters and in animal feed. In the antibiotic market, the sales are driven by four leading drug classes: the cephalosporins (27%), macrolides (20%), quinolones (17%), and penicillins (17%). These four drug classes, together, account for more than 80% of the global antibacterial sales [46].

Macrolides

Macrolide is a term used to describe drugs containing a macrocyclic lactone ring of 12 or more elements (figure 8). The macrolides with 14-, 15-, and 16-membered rings are a widely used family of antibiotics [52]. By binding to the large ribosomal subunit in the peptidyl transferase center, the macrolides cause cell growth to stop due to inhibition of protein synthesis [53, 54]. Clinical applications of macrolides are; in the treatment of upper respiratory tract infections [55] and as immunomodulatory medication, as they have the ability to lower inflammation [52, 56].
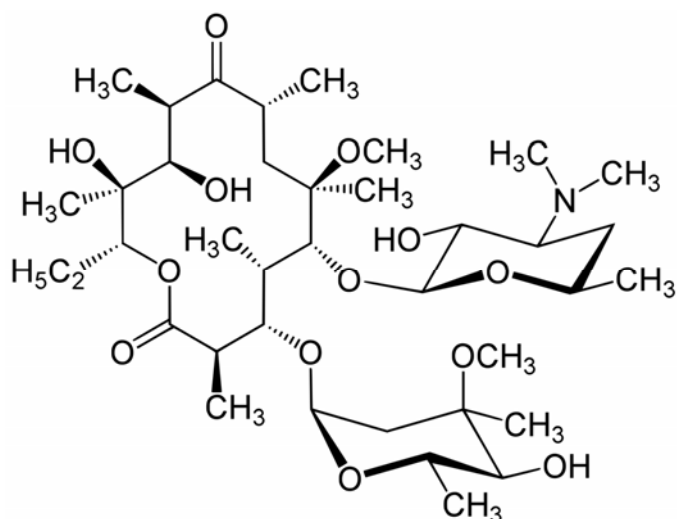
Figure 8: The chemical structure of Clarithromycin. The macrolide ring is the cyclic ester (lactone) to the left. Figure obtained from Wikipedia.

Quinolones

The quinolones are a group of broad-spectrum antibiotics [57, 58], which are produced synthetically. The chemical structure of the quinolone backbone is shown in figure 9. In the clinical use of quinolones, the majority has a fluoride substitute on the central ring system, and belongs to the subgroup called flouroquinolones [59]. The mechanism of action of quinolones is to prevent bacterial DNA from unwinding and duplicate, this is done by inhibiting the bacterial DNA gyrase (gram-negative bacteria) or the topoisomerase IV enzyme (gram-positive bacteria) [60, 61]. The result of the inhibition is bacterial cell death.
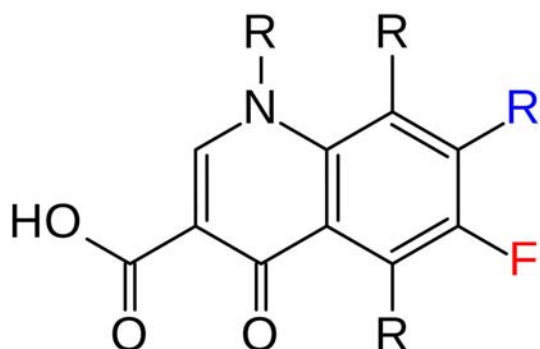
Figure 9: The chemical structure of the quinolone backbone. The blue R (to the right) is usually piperazine when the connection has fluorine. Figure obtained from Wikipedia.

β-lactam antibiotics

The β-lactams antibiotics are a broad group of antibiotics, where all antibiotic agents have a β-lactam ring in their structure (Figure 1a), which includes the antibiotics; carbapenems, cephalosporins, penicillin, and monobactams [62]. The β-lactam antibiotics function by inhibiting the synthesis of the peptidoglycan layer of the cell walls of Gram-positive and -negative bacteria. Especially in Gram-positive bacteria this peptidoglycan layer is important for cell wall structure. Transpeptidases known as penicillin-binding proteins (PBPs) facilitate the final transpeptidation step in the synthesis of peptidoglycan. A β-lactam ring is found in the structure of all β-lactam antibiotics. The β-lactam antibiotics' ability to reach the PBP intact and their ability to bind to the PBP, decides how efficient they are as antibiotics. The various functional groups have been chemically added to the cyclic amide ring in the β-lactam series, which have formed a family of active compound with different specificities [63, 64].

The inhibition of the cell wall biosynthesis triggers the release of bacterial autolysin, leading to cell lysis and death [65]. Measured by sales up until 2003, the β-lactams compounds was to be found in more than half of all commercially available antibiotics [66]. In the following, a selection of relevant β-lactams will be presented.

Penicillin

The chemical structure of a penicillin backbone [67] is shown in figure 10 below. The core skeleton of a penicillin antibiotic is named penem. The side chain R varies [68].

Penicillin is the oldest known β-lactam antibiotic, and it was discovered by a coincidence. Sir Alexander Fleming was trying to multiply the penicillium fungi in the lab in 1928 [69]. Ernst Boris Chain and Sir Howard Walter Florey, at Oxford, contributing in bringing penicillin's potential for medical use to maturation and, together with Fleming, received the Nobel Prize in Physiology or Medicine in 1945 [70].

Examples of penicillins; benzylpenicillin (also known as penicillin G), ampicillin [71], cyclacillin [72].
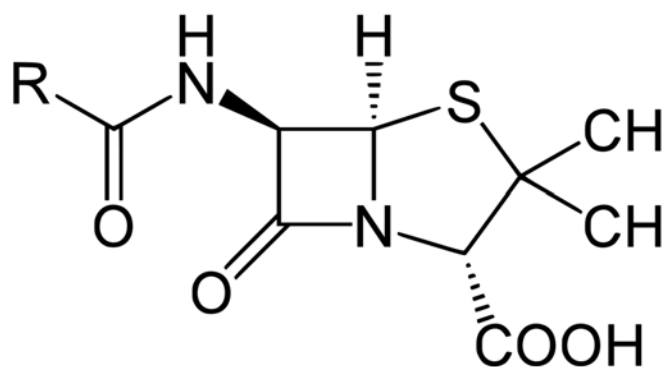
Figure 10: The chemical structure of the penicillin backbone. The R group of the penicillin is variable. The β-lactam ring is located to the left, and a thiazolidine ring to the right. Figure obtained from Wikipedia.

Monobactam

In contrast to other β-lactams, the monobactams have a β-lactam ring which is not fused to another ring (figure 11). The only marketed monobactam is aztreonam. The synthetically produced aztreonam is specific towards aerobic gram-negative bacteria [73, 74]. Aztreonam has not been used a lot clinically, because the third-generation cephalosporins available have a broader spectrum of activity [75].
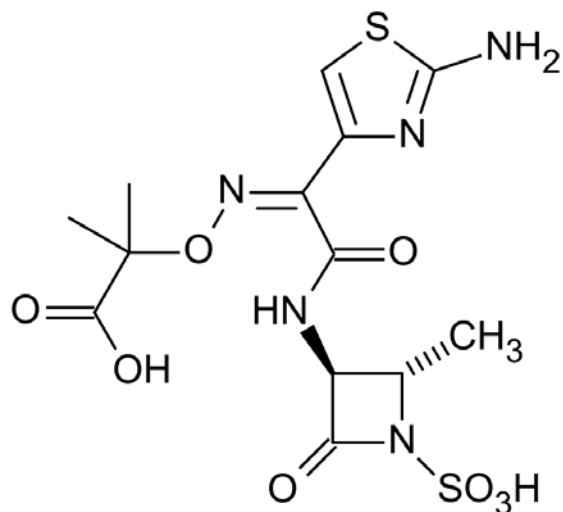
Figure 11: The chemical structure of the monobactam, Aztreonam. The β-lactam ring is to the right below. Figure obtained from Wikipedia.

Carbapenems

The carbapenem class of β-lactams have a broad spectrum of antibiotic activity, with a structure that contributes to a strong resistance towards most β-lactamases (Figure 12) [76]. Originally, the carbapenems were developed from thienamycin, as a natural product of *Streptomyces cattleya*. The thienamycin, however, was chemically instable, and was followed by the N-formimidoyl derivate, imipenem [77]. Other examples of carbapenems are meropenem [78] and ertapenem [79].
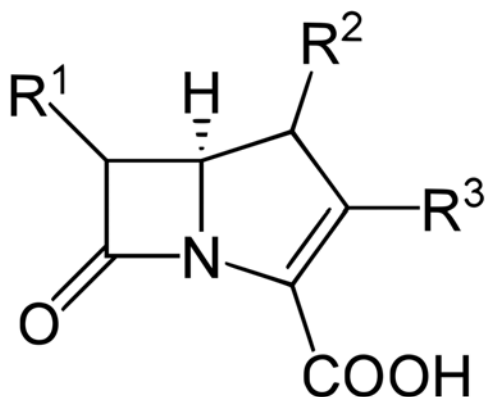
Figure 12: The chemical structure of the carbapenem backbone. The β-lactam ring is located to the left, and the R groups are variable. Figure obtained from Wikipedia.

Cephalosporins

The cephalosporins, together with cephamycins, are a subgroup of β-lactam antibiotics cephems [80]. Originally, the cephalosporins were derived from the fungus *Acremonium*, which was previously known as cephalosporium [81]. Cephalosporins and cephamycins are very similar, the difference is a methoxyl group in the 1 position of the cephamycin and an acetoxy group at 2 position of the cephalosporin, while cephamycins have other substituents after the acetoxy group [82] (position 1 and 2 indicated in figure 13). The similarity between the cephalosporins and the cephamycins is the reason for the cephamycines sometimes being termed as cephalosporins. Originally, the cephamycins was produced by *Streptomyces* [83], but synthetic antibiotics have also been produced. Cefoxitin is an example of a cephamycin [84]. The cephalosporins are normally classified into "generations" according to their antimicrobial properties [75]. The first-generation cephalosporins were the first cephalosporins entitled, while later, cephalosporins with more extended-spectrum were named second-generation cephalosporins. Each new generation of cephalosporins has a spectrum more concentrated towards Gram-negative bacteria. Examples of cephalosporins; cefacetrile [85] (first-generation), cefuroxime [86] and cefoxitin (second-generation),

ceftazidime [87] (third-generation), cepefime [88] (fourth-generation), and ceftobiprole [89] (fifth-generation).
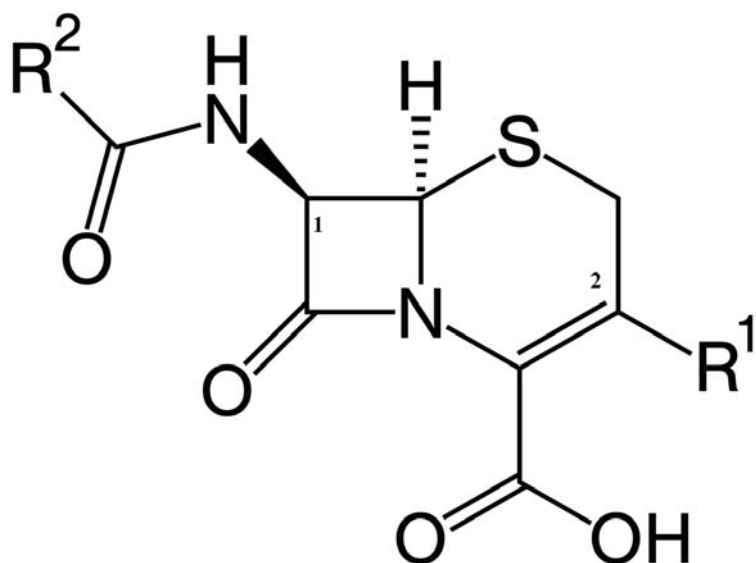
Figure 13: The chemical structure of the backbone of cephalosporin. The β-lactam ring is located to the left. The numbers 1 and two at the carbons indicate where the difference between cephalosporins and cephamycins is. R1 and R 2 are variable groups. Figure obtained from Wikipedia.

Nitrocefin

Nitrocefin is not an antibiotic, but a chemical compound widely used to detect the activity of β-lactamases [90-93] and used in kinetic analysis [94-96]. Nitrocefin is characterized as a chromogenic cephalosporin. Cephalosporins has an absorbance at around 260 nm [97], while the nitrocefin has an absorbance of 482 nm [98]. A reason for nitrocefin having an absorbance is due to highly conjugation with the R2 group[98]. The amide bond in the β-lactam ring of nitrocefin is hydrolysed by β-lactamases, resulting in a color change from yellow to red (figure 14).
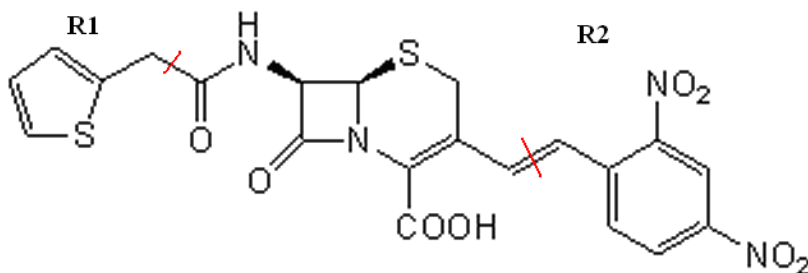
Figure 14: The chemical structure of nitrocefin. The β-lactam ring is the second ring from the left, connected to a dihydrothizine ring. The R1 and R2 groups are indicated by red lines. Figure obtained from EMD Millipore.

Antibiotic resistance

Since the early 1940s, drug resistance has been known, and although many international reports, including the report of the World Health Organization [99], the problem grows and evolves from decade to decade.

The global public health is threatened by the current increase in antibiotic resistance, which involves all major microbial pathogens and antimicrobial drugs [1]. There are several reasons for the global concern when it comes to antibiotic resistance; i) it kills, ii) increases the cost of health care, iii) prevents control of infectious diseases, and iv) endangers the health care gains to society.

Antibiotic resistance appears when a microorganism survives being exposed to an antibiotic. Antibiotic resistance is a type of drug resistance. Resistant organisms, which include viruses, bacteria and some parasites, are able to combat attack by antimicrobial medicines (like antibiotics, antivirals, and antimaterials) making the standard treatments become ineffective. The resistant infections might also spread to other people. Some bacteria have been characterized as multiple antibiotic resistant. Severe clinical problems and the cost of lives are posed by drug resistant strains, especially in developing countries. The spread is often aided by poor sanitation conditions, and new effective but more expensive, antibiotics are not reached because of small healthcare budgets [100]. For example, a re-emergence of tuberculosis, which often is multidrug resistant, has occurred since the 1980s, and has been enhanced by human immunodeficiency virus infections (HIV) [101]. The β-lactamases with their broad-spectrum activities do also destroy the latest generations of cephalosporins and penicillin [102]. Carbapenem-drugs are often the 'last resort' of serious infections of Gram-negative bacteria, and the carbapenems are inactivated by strains bearing the MBLs [76, 103]. The MBLs are thus considered a great threat to humans.

Bacteria become antibiotic resistant as the genes encoding the resistance are spread from one bacterium to another through plasmids, bacteriophages, naked DNA or transposons. Some complex transposons have integrons that are used for integrating different antibiotic resistance genes [104]. An integron is a mobile DNA element with the ability to capture and carry genes, and the antibiotic resistance genes are located on gene cassettes, which can exist as free circular DNA. A recombination event integrates the gene cassette into the integron. Chromosomal genes can be transferred by naked DNA. The naked DNA is released from one microorganism and can be taken up by another bacterium. This was the mechanism for penicillin resistance [105, 106]. Bacteria, being mobile, can easily be transferred from one person to another and it can spread between countries [107].

When patients have an emergence of resistant bacteria as a result of using antibiotics, it normally occurs through a process named 'selective pressure'. Studies have shown that small numbers of bacteria, that are basically resistant towards antibiotics, are normally harbored in healthy persons [108]. Resistant bacteria are usually held back by large numbers of antibiotic-susceptible organisms. The organisms susceptible to the antibiotic at the site of infection are eliminated by the use of the antibiotic. The antibiotic is further spread in adequate concentrations to all sites in the body. When the numbers of natural flora is decreased by the administration of an antibiotic, which allows resistant bacteria to proliferate, a selective pressure has happened [109].

Several different causes for antibiotic resistance have been proposed; i) unnecessary use of antibiotics by humans, ii) availability over-the-counter in many countries, iii) patient failure to follow prescribed course of treatment, iv) misuse by health professionals, v) use in animal feeds in low doses, vi) antibiotic application in family pets, agriculture, and aquaria, and vii) eating raw or undercooked foods [110].

There are some actions for limiting the development of antibiotic resistance; only use antibiotics for bacterial infections, if possible, identify the causative organism, finish the full treatment (not stop antibiotics as soon as symptoms diminish), and use the right antibiotics (not rely on broad-spectrum antibiotics).

Enzyme kinetics

The enzyme kinetics is used to study the catalytic efficiency of different antibiotics on MBLs. Living systems depend on chemical reactions which, on their own, would occur at extremely slow rates. Enzymes are catalysts which reduce the needed activation energy so these reactions proceed at rates that are useful to the cell.

In this thesis, the Michaelis-Menten equation is used to study the enzyme kinetics of VIM-7, and its mutants' hydrolysis of β-lactam substrates. The Michaelis-Menten model is given below (equation 1), by relating reaction rate (V_0) to the concentration of a substrate [S], which describes the rate of enzymatic reactions [111, 112].

$$(1) \quad V_0 = \frac{V_{max}[S]}{K_m + [S]}$$

The V_{max} and K_m are kinetic constants, where V_{max} represents the maximum rate achieved by the system, while K_m represents the substrate concentration at which the reaction rate is half of V_{max} (Figure 15). K_m indicates how efficiently an enzyme selects its substrate and converts it to product.

The German biochemist Leonor Michaelis and the Canadian physician Maud Menten proposed a mathematical model of the reaction involving an enzyme, E, binding to a substrate, S, to form a complex of enzyme and substrate, ES, which is then converted into a product, P, and the enzyme, (equation 2).

$$(2) \quad E + S \underset{k_r}{\overset{k_f}{\leftrightarrow}} ES \overset{k_{cat}}{\to} E + P$$
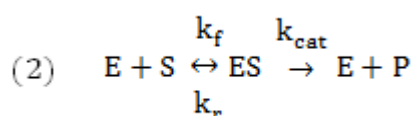
The k_f, k_r and k_{cat} are the rate constants that describe the rate of the ES complex formation, and formation of product and the reverse formation of substrate from the complex. The double arrows between S and ES show that the enzyme-substrate binding is a reversible process. In order to convert this equation into analysis of V_{max} and K_m, we have to assume that the concentration of ES is steady during the kinetic reaction and the formation of ES from E + P is negligible, since the concentrations of product is rather low at the start of the reaction. The k_{cat} is known as the turnover number, and tells the maximum number of substrate molecules converted to product per enzyme molecule per second. K_m tells the binding affinity of the substrate to the enzyme. When dividing k_{cat}/K_m, you get an estimate of the enzymes efficiency catalysis [113].

In enzyme kinetics the reaction rate, V_0, can not further increase at very high substrate concentration, which means it will reach a maximum value of V_{max} [114]. The Michaelis-Menten equation (equation 1) can be illustrated by a curve (Figure 15) with the following assumptions made:

- There is no allostericity or cooperation, and the mechanism does not involve intermediate or product inhibition.

- The total enzyme concentration does not change over time.

- The concentration of the substrate-bound enzyme [ES], and the unbound enzyme $[E]_0$, are changing more slowly than the concentration of the product and substrate. The change of substrate-enzyme complex is set to zero over time.
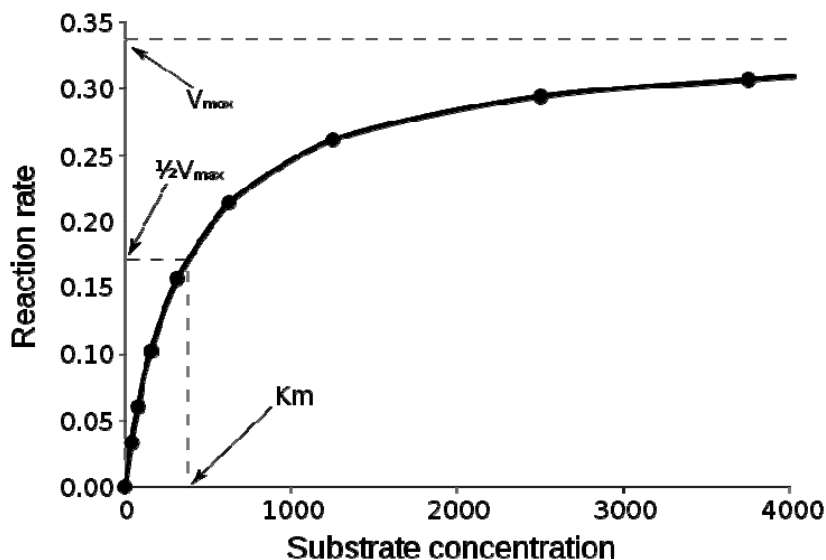
Figure 15: The Michaelis-Menten kinetics curve. The saturation curve shows the relationship between substrate concentration and the reaction rate of an enzyme and shows how the kinetic constants K_m and V_{max} can be derived. V_{max} represents the maximum rate of the reaction, and K_m is defined by the substrate concentration where the V_{max} is half.

Materials and methods

Table 1: Content of buffers and solutions used for cloning of VIM-7, protein expression and purification of the VIM-7 wt and the mutants.

	Contents
LB	1% (w/v) bacto tryptone, 0.5% (w/v) bacto yeast extract, 1% (w/v) NaCl, in ddH$_2$O
LB-agar	1% (w/v) bacto tryptone, 0.5% (w/v) bacto yeast extract, 1% (w/v) NaCl, 1.5% (w/v) agar-agar, in ddH$_2$O
TB	1.2% (w/v) peptone, 2.4% (w/v) yeast extract, 72 mM K$_2$HPO$_4$, 17 mM KH$_2$PO$_4$, 0.4% glycerol
SOB	2% (w/v) bacto-peptone, 0.5% (w/v) Yeast extract, 10 mM NaCl, 2.5 mM KCl, in ddH$_2$O
Cam	35 mg/ml Chloramphenicol in 100% Ethanol
Amp	100 mg/ml Ampicillin in ddH$_2$O
IPTG	0.4 mM Isopropyl-β-D-1-thiogalactopyranoside in ddH$_2$O
TAE-buffer	40 mM Tris, 20 mM acetic acid, 1 mM EDTA
Buffer A	50 mM Tris-HCl pH 7.5, 150 mM NaCl, 100 µM ZnCl$_2$
Buffer B	50 mM Tris-HCl pH 7.5, 150 mM NaCl, 100 µM ZnCl$_2$, 10 mM Imidazole
Buffer C	50 mM Tris-HCl pH 7.5, 150 mM NaCl, 100 µM ZnCl$_2$, 1 M Imidazole
Buffer D	50 mM Tris-HCl pH 7.5, 150 mM NaCl, 1 mM EDTA, 1 mM BME
Buffer E	50 mM Hepes pH 7.2, 100 µM ZnCl$_2$.
Buffer F	50 mM Hepes pH 7.2, 100 µM ZnCl$_2$, 1 mg/ml Bovine Serum Albumin
Buffer G	10 mM Tris-HCl pH 8.0, 1 mM EDTA

Cloning of VIM-7

The VIM-7 protein, originating from the *bla*$_{VIM-7}$ gene (M1-E265 figure 4) from the *P. aeruginosa* strain 07-406 [42], subcloned in a pET26b(+) vector by Samuelsen et al [43], was cloned. At the N-terminal of the sequence of *bla*$_{VIM-7}$, there is a 25 residue long region which gives high scores in the programme SignalP [115, 116].This indicates that the gene has a signal sequence which might cause the produced protein to be transported out of the nucleus to the periplasm. To avoid secretion of the protein to the periplasm, the primers were designed to allow the protein coding sequence to start at Ala26, hence, removing the signal sequence. By this strategy the construct would encode amino acids A26-E265 of VIM-7.

Three primers were designed based on the nucleotide sequence of the bla_{VIM-7} gene (EMBL Bank Entry: AM778842.1) [42]. The first primer, the VIM-7 Ala26 forward primer, encodes a hexahistidine tag (His-tag) at the N-terminal (shown in italic below), that allows for affinity purification of the tagged recombinant protein from endogenous proteins in the bacterial host *E. coli.* In addition, a TEV protease specific cleavage site (shown in underline below) was cloned following the his-tag, which allows for tag-removal. Finally, this primer contained a gene-specific sequence complementary to the bla_{VIM-7} (shown in bold, italic and underlined below).

The VIM-7 reverse primer encodes a gene specific sequence (shown in bold, italic and underlined), in addition to an *att*B2 site (shown in bold and underlined) followed by a stop codon (shown in bold below).

Following gene-specific amplification with VIM-7 Ala26 fwd and VIM-7 rev, a PCR with adapter primer was performed to include the Gateway *att*B1 (shown in italic and underlined below) and *att*B2 recombination sequences to perform the Gateway cloning. In addition, this primer contained a Shine-Dalgerno sequence, seven nucleotides upstream from the start codon, (shown normal in red below), that allows the ribosome to bind the mRNA and initiate protein synthesis. The start codon ATG (shown in bold below) is placed after the Shine-Dalgerno sequence, followed by a His-tag (shown in italic).

Overview of primers:

- VIM-7 Ala26 fwd
  5' - *CATCACCATCACCATCAC***GAAAACCTGTATTTCCAGGGAGCA GCACAGCCTGGCGGTGAATATCCG** - 3'

- VIM-7 rev (reverse and complementary of DNA)
  5' - **GGGGACCACTTTGTACAAGAAAGCTGGGTCTTA CTCGGCCACCGGGCGTACTTTG** - 3'

- Forward Primer 2: attB1-His fwd (adapter primer)
  5 – *GGGGACAAGTTTGTACAAAAAAGCAGGCT*TCGAAGGAGATAGAACC **ATG***CATCACCATCACCATCAC* - 3'

Polymerase chain reaction (PCR) is a scientific technique for generating large quantities of a specific DNA sequence *in vitro* [46]. The Phusion PCR consisted of 1x HF buffer (Thermo Science), 200 µM dNTP mix (Thermo Science), 0.5 µM forward primer (VIM-7 Ala26 fwd, described above), 0.5 µM reverse primer (VIM-7 rev, described above), approximately 100 ng VIM-7 pET26b(+) template, 0.02 U/µl Phusion polymerase (Thermo Science), and nuclease-free water to a final volume of 50 µl. The solutions were mixed by

tapping the PCR tubes before it was collected by a quick centrifugation. Amplification was performed with the following cycle conditions in a PTC-200 Peltier Thermal Cycler (VWR): first, the initial denaturation at 95°C for 5 min, second, 30 cycles of [denaturation at 95°C for 30 sec, annealing at 55°C for 30 sec, and elongation at 72°C for 45 sec] third, extension at 72°C for 5 min. The tubes were kept on 4-10ºC after the PCR.

The PCR product contained a sequence coding for a hexahis-tag, a TEV cleavage site, the bla_{VIM-7} gene specific sequence (corresponding to A26-E265) and an attB2 site. To inspect the whether the amplification was successful or not, an agarose gel electrophoresis method was performed. A 0.8% agarose gel was made by weighing out agarose powder and mixed with 400 ml of 1x TAE buffer (tris-acetate-EDTA) (Table 1). The agarose solution was heated for about 4 min until the solution was dissolved. The melted agarose solution was cooled to 60°C before use. Agarose solution containing 0.05% (w/v) RedSafe nucleic acid staining solution (ChemBio) was poured into a gel casting tray. The comb was placed in the casting tray to generate a row of wells which samples are loaded into once the gel has solidified and comb been removed. The samples were added 5 µl 10x TAE loading buffer, before loading in to the agarose gel wells. 6 µl of 100 bp DNA Ladder and 6 µl of 1 kb DNA Ladder (Invitrogen) were used as DNA standards. 1x TAE buffer was added to the chamber to cover the gel, and the agarose gel was run at 90 V for approximately 45 min to separate DNA fragments based on size and charge. The PCR product was extracted from the gel and purified according to the Ultra-Sep Gel Extraction Protocol (Omega Bio-Tek).

The adapter amplification of the product was performed in a second round of PCR to include both the Gateway attB1 (from the first PCR) and the attB2 recombination sequences for the Gateway cloning. The PCR reaction was performed as previously described, using the forward primer 2 (described above) and the same reverse primer as before. The PCR product was analysed by agarose gel electrophoresis reaction, as described previously. The DNA was extracted and purified described above.

The PCR product contained an attB1 site, a Shine-Dalgarno part, a start codon, a hexahis-tag, a TEV-cleavage site, the bla_{VIM-7} gene specific sequence (corresponding to A26-E265), a stop codon, and an attB2 site (Figure 16).

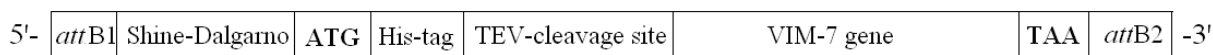| 5'- | attB1 | Shine-Dalgarno | ATG | His-tag | TEV-cleavage site | VIM-7 gene | TAA | attB2 | -3' |

Figure 16: The VIM-7 PCR product used in the Gateway cloning. The PCR product contained an *att*B1, a Shine-Dalgarno sequence to help the ribosome bind the mRNA to initiate protein synthesis, a start codon (ATG) for translation, a hexahis-tag (His-tag), a TEV-cleavage site, a bla_{VIM-7} gene specific sequence (corresponding to A26-E265, here termed VIM-7 gene) , a stop codon (TAA) to end translation, and an *att*B2 sites. The *att*B1 and *att*B2 sites contribute in incorporating the gene in the entry clone in the Gateway cloning system.

The cloning was performed according to the Gateway cloning protocol (Life Technologies) and was initiated by a BP Clonase II reaction [117] [118]. The BP reaction contained 150 ng of the purified PCR product, 150 ng donor vector (pDONR221), and TE buffer to a final volume of 10 µl (buffer G in Table 1). The recombination reaction was incubated at room temperature o/n.

The BP reaction product was trated with 1 µl Proteinase K, before 2 µl of the reaction was transformed to *E. coli* chemically competent DH5α cells. The cells were incubated with DNA on ice for 25-30 min, before heat-shock at 42ºC for 45 sec in a water bath. The cells were incubated in 1 ml SOC media (Table 1) at 37ºC for 1 hour, before the cells were pellet by centrifugation at 13 000 rpm at room temperature, and spread on a Lysogeny Broth (LB)-agar (Table 1) plates containing 10 mg/ml kanamycin (Kan) antibiotic. The plates were incubated at 37 ºC o/n.

Mini cultures were prepared of a few (2-5) colonies from the transformation, and grown in 3 ml Terrific Broth (TB) media (Table 1) with 10 mg/ml Kan. The mini cultures were grown at 37ºC o/n at 250 rpm shaking. Plasmids from the mini cultures were purified according to the ZR Plasmid Miniprep-Classic Protocol (Zymo Research) [119].

A PCR screen was performed to analyse whether the recombination to donor vector was successful. The PCR contained 1x Thermo polymerase buffer (Thermo), 2 mM $MgSO_4$, 200 µM dNTP mix, 0.3 µM M13 forward and reverse primers, 100 ng genomic DNA, 0.02 U/µl VENT DNA polymerase (Bio Labs), and nuclease-free water to a final volume of 25 µl. The PCR cycles were as described above. The PCR product was analysed with agarose gel electrophoresis, as previously described.

The mini cultures that indicated a correctly recombined VIM-7 pDONR221 product, shown by PCR screens and electrophoresis with a product of approximately 1000 bp, was Sanger sequenced. The sequencing PCR reaction contained the chemicals; 1x sequencing buffer, 3.2 pmol of either the M13 forward or the M13 reverse primer, 1x BigDye v3.1, 200 ng template, and nuclease-free water to a final volume of 20 µl. The PCR setup was with the

following cycle conditions in a PTC-200 Peltier Thermal Cycler (VWR); first, the initial denaturation at 96°C for 5 min, second, 25 cycles of [denaturation at 96°C for 10 sec, annealing at 50°C for 5 sec, and elongation at 60°C for 4 min]. The tubes were kept on 4-10ºC after the PCR. The sequencing products were sent to the University Hospital of Northern Norway [120]. The returned sequences were analysed and confirmed using the program BioEdit Sequence Alignment Editor Version 7.0.9.0 [121].

After the sequences were verified the cloning was continued with a LR Clonase II reaction performed according to the Life Technologies Protocol [118]. The LR reaction contained 100 ng entry clone (the VIM-7 pDONR221), 150 ng/µl pDEST14 destination vector, and TE buffer (buffer G in Table 1) to a final volume of 10µl. The LR reaction was treated with proteinase and transformed into *E. coli* cell DH5α, as described above. Mini cultures were set up with colonies from the agar-plate in TB-media containing 100 mg/ml Amp and 35 mg/ml Cam at 37°C o/n. The mini cultures were purified according to the ZR Plasmid Miniprep-Classic Protocol (Zymo Research) [119], described above. Finally, a PCR screen was performed as described above, but using T7 promoter and T7 terminator primers. The PCR product contained a start codon, hexaHis-tag, TEV cleavage site, the VIM-7 gene (A26-E265), and a termination codon (Figure 17).

The products were analysed by agarose gel electrophoresis, as previously described, to verify correct recombination into the pDEST14 vector. The cloning of VIM-7 wt into pDEST14 expression vector was completed, where "VIM-7 wt" corresponds to the A26-E265 (Figure 4).
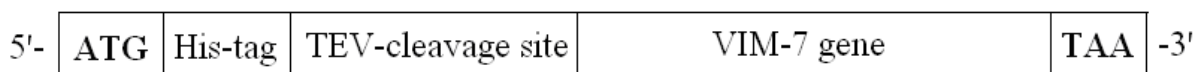
Figure 17: The VIM-7 gene recombined into the expression vector pDEST14 by the Gateway cloning system. The his-tag and TEV-cleavage site is intact to facilitate purification of the target protein, and a start codon and termination codon is present for translation of the VIM-7 gene (A26-E265).

Point mutations in the VIM-7 wt pDEST14 construct

Forward and reverse oligonucleotide primers, one pair for each of the three point mutations leading to substitution of D120A, D120N and H224Y in VIM-7 wt, were designed. The site-directed mutagenesis was performed by using the Quikchange Lightning Site-Directed Mutagenesis Kit protocol (Stratagene). The mutations were incorporated into the VIM-7 wt-pDEST14 construct by a PCR. The sequencing PCR protocol is described above. The paternal plasmid DNA was removed according to the Quikchange Site-Directed Mutagenesis Kit (Stratagene) by adding 1 µl DpnI restriction enzyme to the mutagenesis reaction and incubated at 37ºC for 1 hour. Incubation at 72ºC for 10 min inactivated the DpnI. The pDEST14 vector specific PCR colony screens were performed to find clones encoding an approximately 1000 bp product, as previously described. The PCR reaction was performed by using T7 promoter and T7 terminator primers. Results were analysed with agarose gel electrophoresis, as previously described, before positive clones were analysed with Sanger Sequencing, as described above.

The mutagenesis primers constructed are as follows, where the red lower case letter shows the mutation and red colour shows codons:

VIM-7 D120A fwd
5'-TTCCATGACGcTCGAGTCGGTGGAGTTGATGTCCTCCGGGCGGCT-3'

VIM-7 D120A rev
5'- ACCGACTCGAgCGTCATGGAAGTGCGTAGAAATTGAGCGCGTTAC-3'

VIM-7 D120N fwd
5'-TTCCATGACaATCGAGTCGGTGGAGTTGATGTCCTCCGGGCGGCT-3'

VIM-7 D120N rev
5'-ACCGACTCGATtGTCATGGAAGTGCGTAGAAATTGAGCGCGTTAC-3'

VIM-7 H224Y fwd
5'-TGTGCAGTTtATGAGGCGTCACGCGAATCCGCGGGTAATGTTGCC-3'

VIM-7 H224Y rev
5'-TGACGCCTCATaAACTGCACAGCCACCAAACAGTACGCGCACGG-3'

Preparation of Z-competent cells of Rosetta2(DE3)pLysS and BL21(DE3)star/pRARE/pLysS

Z-competent *E. coli* cells are, by a method developed by Zymo Research, made chemically competent that completely eliminates the need for heat shock and related procedures. Z-competent *E. coli* are chemically competent cells used for simple and efficient DNA transformation.

Glycerol stocks of Rosetta2(DE3)pLysS (Novagen) and BL21(DE3)star/pRARE/pLysS (Novagen) were each spread on different LB-agar plate (Table 1) containing 34 µg/ml Cam and incubated at 37°C overnight (o/n). Single colonies of Rosetta2(DE3)pLysS and BL21(DE3)star/pRARE/pLysS cells from the LB-agar plates were each inoculated into 1 ml SOB media (Table 1) and incubated at 37°C o/n. 50 ml SOB containing 34 µg/ml Cam were inoculated with 1:100 pre-culture Rosetta2(DE3)pLysS or BL21(DE3)star/pRARE/pLysS. The mini culture was incubated to reach a cell density (OD) of log phase (0.4-0.6). The cultures were cooled on ice for 10 min, before pelleting the cells by centrifugation at 4°C at 3500 rpm for 10 min. The pellet was washed in 5 ml cold 1x Wash Buffer, and collected as described above. The pellet was gently resuspended in 5 ml 1x Competent Buffer. Wash and Competent buffer were from the Z-Competent *E. coli* Transformation Kit & Buffer Set (Zymo Research) [122]. Finally, the cells were distributed in 100 µl aliquots in pre-frozen eppendorf tubes, and stored at -70°C.

Protein expression of recombinant VIM-7 wt and mutants

In order to test what strain was most optimal to use in production of the proteins, a small scale expression experiment was set up for testing the recombinant VIM-7 wt-pDEST14 and the three mutants in both *E. coli* Rosetta2(DE3)pLysS and *E. coli* BL21 (DE3) star/pRARE/pLysS. The small scale expression of the cells were performed in 20 ml LB-media (Table 1) containing 100 mg/ml Amp and 34 mg/ml Cam, and were grown at 37ºC to reach log phase OD 600 0.5-0.7. The expression was induced at different temperatures; 37ºC for 4 hours and 20ºC o/n, with 0.4 mM Isopropyl-β-D-1- thiogalactopyranoside (IPTG).

For large scale protein expression, the three different mutants of VIM-7 were expressed in *E. coli* Rosetta2(DE3)pLysS cells with the use of two litres times 1 LB-media (Table 1) with 100 µg/ml Amp and 34 µg/ml Cam. The cultures were grown at 37°C, and the growth was monitored by measuring the cell density at OD 600 nm in a spectrophotometer to reach a value of 0.5-0.7. The cultures were then induced with 0.4 mM IPTG and grown at

either at 20°C o/n or at 37°C for 4 hours. The cells were harvested by centrifugation at 5000 rpm for 18 min at 4°C in a Beckman Avanti centrifuge. The culture media was discarded, and the pellets frozen at -20°C for later use.

Cell disruption

Each pellet from the large scale protein expression was resuspended in 30 ml buffer A (Table 1) together with one tablet of SigmaFAST EDTA-free protease inhibitor cocktail (Sigma). The cells were disrupted by sonication for 9.9 sec pulses with amplitude of 25%, a max temperature of 8°C for 35 min by the Vibra-Cell sonicator (Sonics). The supernatant of the sonication product containing soluble proteins was obtained by centrifuging at 14.000 rpm for 30 min at 4°C.

SDS-PAGE

Sodium dodecyl sulphate-polyacrylamide gel electrophoresis (SDS-PAGE) was used to analyse the protein expression and quality after each purification steps. After purification, SDS-PAGE analysis was performed in order to choose fractions for further analysis. Fractions were loaded on 4-20% Mini-PROTEAN TGX Precast Gels (Bio-Rad) and performed according to the protocol [123]. 25 µl of the purification fractions for SDS-PAGE analysis were pooled and 10 µl of 3xSample buffer (SB) were added. 1x SB consists of 4xNuPage LDS Sample buffer (Invitrogen), 100 µl MilliQ water and 150 µl 14.3 M BME. To denature proteins, all gel samples were boiled at 95°C for 3-5 min before they were loaded onto the gel. Routinely, 5 µl of Mark12 Unstained Standard (Invitrogen) was used as a molecular weight marker. 10 µl of the protein samples were loaded to the gel. The gel was in a 1xTris-Glycine buffer at 200 V, 90 mA and 12.5 W for about 40 min. The gel was rinsed three times with MilliQ water, and heated in a microwave oven in between. The water was discarded before adding 20-30 ml SimpleBlue SafeStain (Invitrogen) to the gel. The gel was again heated as described before and placed on an orbital shaker for 15-60 min. The stain was then discarded, and the gel destained in MilliQ water on the orbital shaker o/n.

Protein purification

Affinity purification

In order to separate the VIM-7 proteins, which are tagged with a hexahistidine tag, from the other *E. coli* proteins, affinity purification is performed. Histidine tags have an affinity for nickel or cobalt ions. Imidazole is used for elution, because of its ability to act as a metal ion ligand. The VIM-7 proteins are separated from other untagged protein, the hexahistidine tag is cleaved off in dialysis, and the VIM-7 proteins are separated from the tagged proteins in the second affinity purification step.

For the purification a 1 ml HisTrap High Performance (HP) column, the ÄKTA explorer Fast Protein Liquid Chromatography (FPLC) system and the computer program Unicorn 5.0 (GE Healthcare United Kingdom) were used. The buffers used in the affinity purification were the buffer B and the buffer C (Table 1). The flow rate was set to 1 ml/min and the maximum pressure set to 0.5 MPa. The lysate were loaded onto a 50 ml super loop connected to the ÄKTA explorer FPLC system. To prepare the 1 ml HisTrap HP column, it was first washed with 20% ethanol, then with ddH$_2$O, and finally with buffer B (Table 1). The purification was done with loading the lysate with buffer B (Table 1) over 17-42 column volumes (CV), before a 10 mM-1 M imidazole gradient over 15 CV, and the size of the eluate fractions collected were 1 ml.

TEV cleavage by dialysis

Dialysis was used to perform the TEV protease cleavage of the hexahistidine tag attached. TEV is named after where it was found, the Tobacco Etch Virus, and the TEV protease is a highly site-specific enzyme. TEV recognise the amino acid sequence ENLYFQ(G/S), and performs a cleavage between the Q and G/S residue [124]. Dialysis is a purifying step, in a way that it separates the molecules in the solution according to their ability to diffuse through a semi permeable membrane with different cut offs. Small molecules like salt, water and such, move through the membrane in the direction of decreasing concentration.

The selected fractions from the HisTrap purification, which from the SDS-PAGE indicated the target protein, were pooled for dialysis with TEV protease. The fractions, together with TEV protease, with a TEV concentration of 1:100 of the protein concentration [125], were injected in the Slide-A-Lyzer Dialysis Casette (Extra strength); cut off 10 kDa

(Thermo Sciences). The dialysis buffer D (Table 1) was used during the dialysis, and the dialysis was performed o/n at 4°C.

Gel filtration of VIM-7 H224Y mutant

Gel filtration is a size-exclusion chromatography method, where the molecules in the solution are separated by size. The motivation for this purification method was to get as pure protein as possible for the enzyme kinetic studies.

Gel filtration was carried out on an ÄKTA Explorer FPLC system using a Hiload 16/60 200 prep grade Superdex column (Amersham Bioscience), with maximum pressure of 0.5 MPa and flow rate of 1.5 ml/min. The buffer A (Table 1) was used for gel filtration.

Protein concentration measurement

The Nanodrop 2000c Spectrophotometer (Thermo Sciences) was used to measure the protein concentrations, in order to calculate the amount of protein in the samples. 1 µl of buffer B (Table 1) was used as blank, and 1 µl of protein sample was used during the measurement, when measuring protein concentration after affinity purification. The gel filtration buffer A (Table 1) was used as blank for measurements after gel filtration. By using the online program Protparam at ExPasy [126], the molecular weight and the extinction coefficient was determined, based on the sequence.

Table 2: Extinction coefficient and molecular weight of the proteins VIM-7 wt, VIM-7 D120A and VIM-7 H224Y as determined by Protparam (ExPASy) [126].

Protein	Extinction coefficient, $\Delta\varepsilon$	Molecular weight (Da)
VIM-7 wt	26 930	25 591.8
VIM-7 D120A	26 930	25 547.8
VIM-7 H224Y	28 420	25 617.9

Epsilometer test

To determine whether VIM-7 wt, VIM-7 D120A and VIM-7 H224Y are receptive to the action of specific antibiotic, the Epsilometer test (E-test) was performed. The E-test is based on a LB-agar medium inoculated with the test organism and the diffusion of a microbial gradient from a coated plastic strips into the agar. Directly from the scale on the strips the minimum inhibitory concentrations (MIC), which are the zone where the growth inhibition intersects the strip, are read [127]. This laboratory test is common in medicine, where the medical doctor is seeking guidance in the concentration of the antibiotics and which antibiotic is suitable for the patient. The enzymes were transformed into *E. coli* Rosetta2(DE3)pLysS cells, and they were spread on LB-agar plates containing 100 µg/ml Amp and 35 µg/ml Cam, and incubated at 37ºC o/n. Single colonies were inoculated in a water solution containing NaCl, for the solution to obtain a cell density of 0.5. Cotton sticks were dipped in the solution containing protein, and a cross was streaked on a LB-agar plate, before the solution was spread on the whole plate by rotating it and moving the cotton stick towards the middle and back. Rectangular strips, E-tests (bioMérieux, Marcy l'Etoile), containing increasing concentration of selected antibiotics; ertapenem, meropenem, imipenem, cefuroxime, ceftazidime, cefoxitin, piperacillin, aztreonam, and amoxicillin, were placed on the agar plate with the protein solution and incubated at 37ºC over night. The MIC of the proteins was read by researcher Ørjan Samuelsen at University Hospital of Northern Norway the next day.

Activity testing by using nitrocefin

In order to test the VIM-7 wt and the mutants D120A and H224Y for their activity, the substrate nitrocefin (Merck) was used in a colorimetric enzyme assay. Nitrocefin changes colours from yellow to red, when there is an active enzyme present. The nitrocefin hydrolysis the product and can be detected spectrophotometrically at 482 nm. The measurements were performed on a UV spectrophotometer SpectraMax M2^e (Molecular Devices) and analysed with the SoftMax Pro 5.2 software (Molecular Devices). In this assay, the proteins were used with a concentration of 0.1 µM made by diluting it in an enzyme kinetic buffer F (Table 1). The presence of Bovine Serum Albumin (BSA) in the enzyme stock solution protects the β-lactamases from denaturation at low protein concentration, and allows for reproducible and reliable measurements of the initial rate of enzyme-catalyzed hydrolysis of the substrate [128]. The nitrocefin concentration was 100 µM in all assays. Directly before starting the experiment,

10 µl protein solution was mixed with 40 µl of 100 µM nitrocefin and 50 µl of enzyme kinetic buffer E (Table 1). The temperature used during the measurements was 25°C.

Enzyme kinetics

In order to measure the specific efficiency of the enzymes VIM-7 wt, VIM-7 D120A and VIM-7 H224Y, enzyme kinetics studies were performed. The specific efficiency represents the ability of the enzyme to convert substrate into product.

The antibiotics ertapenem, meropenem, cefuroxime, ceftazidime, cefepime and cefoxitin were dissolved in buffer E (Table 1). The substrates concentration of the stock solutions were determined by measuring the absorbance by using the spectrophotometer and the software described above, and the extinction coefficient of each substrate (Table 3). The solutions for kinetic analyses were made in the range of 2-1000 µM for each antibiotic.

The proteins VIM-7 wt, VIM-7 D120A and VIM-7 H224Y were diluted in buffer F (Table 1). The absorbance of the substrate nitrocefin was measured at 482 nm in a 96-well flat bottom non-binding surface plate, while the absorbance of the other substrates was measured using 96-well falcon UV microplates. This is because the antibiotics, apart from nitrocefin, interact with the plastic in the non-binding surface.

Table 3: Extinction coefficients, plate-specific extinction coefficients, and wavelengths for the substrates used for performing the enzyme kinetics studies.

Substrates	Extinction coefficient ($\Delta\varepsilon$)	Plate-specific coefficient ($\Delta\varepsilon$, OD/µM)	Wavelength (nm)
Nitrocefin	17400	0.00645	482
Ertapenem	-6920	0.00710	300
Cefuroxime	-7600	0.00252	260
Ceftazidime	-9000	0.00431	260
Cefepime	-10000	0.00392	260
Cefotixin	-7700	0.00231	260
Meropenem	-6500	0.00306	300

The program GraphPad Prism was used to analyse the results of the kinetics experiments.

Crystallization of VIM-7 H224Y mutant

Crystallization trials were set up with the hanging drop method [129] for the VIM-7 H224Y mutant, using a protein concentration of 17 mg/ml and a reservoir solution with 20-25% polyethylene glycol monomethyl ether 2000, 0.1 M calcium acetate, 0.1 M sodium cacodylate pH 5.0 with 8 mM BME [29]. Each drop formulation was made by mixing 1 µl of 17 mg/ml protein and 1 µl of reservoir solution, with a reservoir volume of 500 µl. The plates were stored at room temperature.

Additionally, trials were also set up with the Phoenix DT crystallization robot (Rigaku) with the sitting drop method [130]. The screen used, named KCSG, was made by researcher Kenneth Johnson (Norstruct, Uit). In the sitting drop method the drops contained 200 nl of VIM-7 H224Y protein and 200 nl of reservoir solution, and the wells contained 60 µl reservoir solution. The trials were stored at room temperature.

A crystal of the VIM-7 H224Y mutant obtained from the robot was cryoprotected by researcher Hanna-Kirsti Schrøder Leiros, and sent to Max-LAB in Lund, Sweden for x-ray data collection. The crystal structure refinement was performed by researcher Hanna-Kirsti Schrøder Leiros. The antibiotic substrate Ceftazidime was docked into the crystal structure of the VIM-7 H224Y mutant, *in silico,* by using the molecular visualization program PyMOL. The docking was performed using the structure of the VIM-7 (PDB ID: 2Y87 [29]), which has been docked with ceftazidime, superimposed on the solved crystal structure of the VIM-7 H224Y mutant.

Results

Cloning and mutagenesis of VIM-7 wt

The bla_{VIM-7} gene originated from *P. aeruginosa* [42], subcloned into pET26b(+) vector by Samuelsen et al [43], was successfully cloned into the expression vector pDEST14 performed using the Gateway cloning system. First, the bla_{VIM-7} gene, corresponded to amino acid sequence A26-E265, was cloned to contain an N-terminal hexahis-tag and a TEV cleavage site, an *att*B and an *att*B2 recombination site for the Gateway system, and start and termination codon (Figure 16). Then the bla_{VIM-7} gene was cloned into the donor vector pDONR221 in a BP Clonase II reaction. The bla_{VIM-7} sequence was verified by Sanger sequencing, before the gene was cloned into the expression vector pDEST14 in a LR Clonase II reaction. The new gene contained the N-terminal hexahis-tag, a TEV cleavage site and start and termination codons (Figure 17). The cloned gene of bla_{VIM-7} sequence was called "VIM-7 wt".

Three different site-directed mutations, VIM-7 D120A, VIM-7 D120N and H224Y, were successfully performed by using the Quikchange Lightning Site-Directed Mutagenesis Kit (Stratagene). To screen for positive mutation clones, T7 forward and reverse vector-specific primers were used in a Phusion PCR reaction to amplify fragments of correct size, an approximately 1000 bp product (Figure 18). The PCR screens were used to select clones for Sanger sequencing. The PCR products were separated by size and charge on a 0.8% (w/v) agarose gel prestained with 0.05% RedSafe DNA stain. As a references for estimating the size of DNA fragments, both 100 bp DNA Ladder and 1 kb DNA Ladder were used as DNA markers. Positive control with pDEST14 and negative control (without plasmid) were also run, to make sure that the PCR screening was performed without complications. The positive clones were analysed by Sanger sequencing for the presence of the desired mutation.
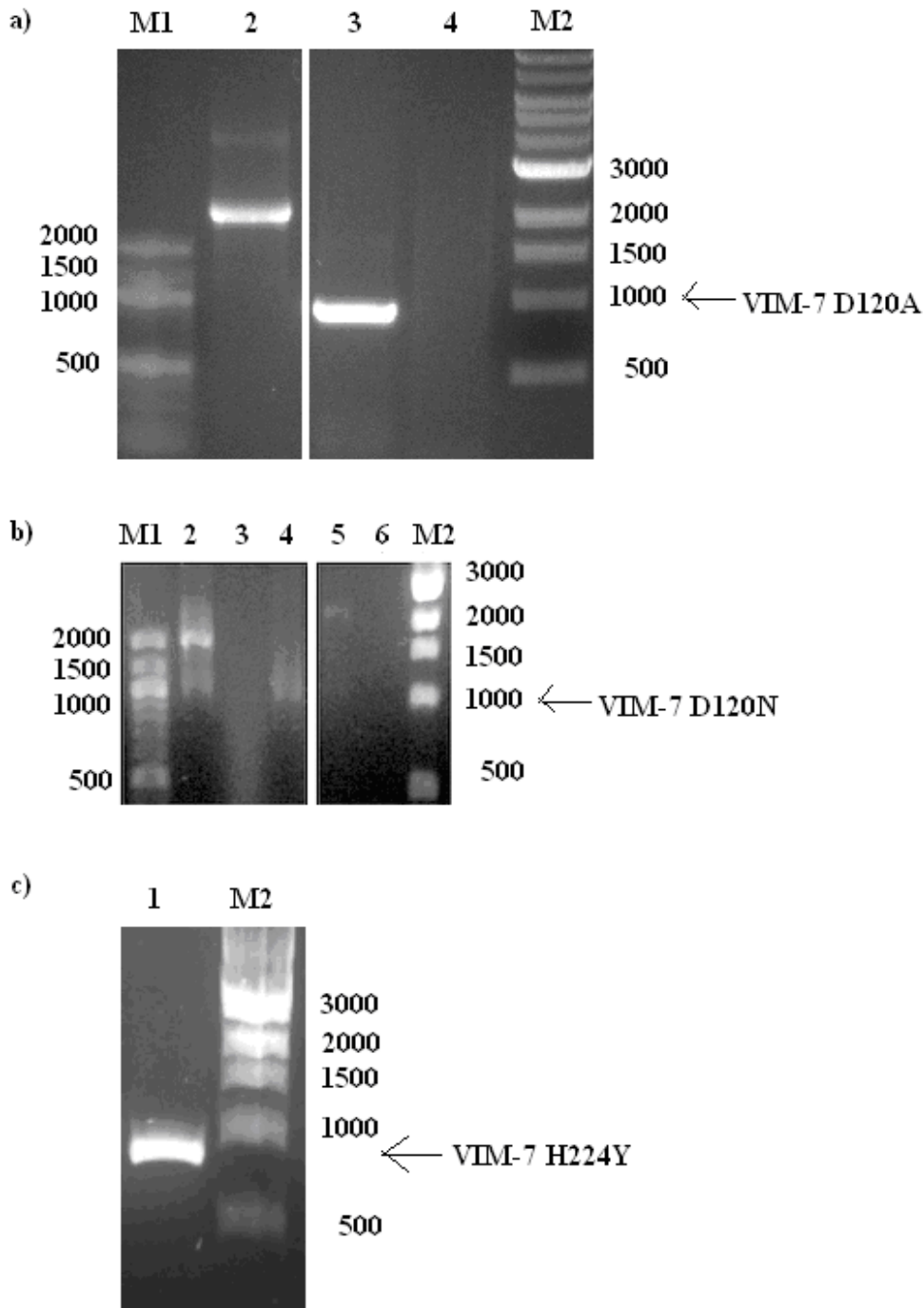
Figure 18: PCR screening of positive a) VIM-7 D120A mutants, b)VIM-7 D120N mutants, and c)VIM-7 H224Y mutants, all in pDEST14 expression vector. PCR using vector-specific T7 primers were performed to screen for positive VIM-7 mutant clones in pDEST14 vector. PCR products were size separated by agarose gel electrophoresis. Agarose gel analysis showing; 100 bp DNA marker (M1), 1 kb DNA Ladder (M2). Relevant marker bands are indicated by size (bp) on the left and the right side of the gel image, and positive amplification of VIM-7 mutants are indicated with an arrow. **a)** Positive control amplification of a 2030 bp product from pDEST14 (lane 2), VIM-7 D120A mutant amplification (lane 3), and negative control without DNA template (lane 4). **b)** VIM-7 D120N mutant amplification of individual clones (lane 2,3 and 4), positive control amplification of a 2030 bp product from pDEST14 (lane 5), negative control without DNA template (lane 6). **c)** VIM-7 D120N mutant amplification (lane 1).

The VIM-7 wt was sequenced after cloning in the donor vector pDONR221 in the Gateway cloning system. The VIM-7 wt was then recombined from donor vector pDONR221 to the expression vector pDEST14, but the cloning product was not sequenced to the expression vector. The mutants were sequenced both in forward and reverse direction, and the mutants were in the expression vector pDEST14.

According to the agarose electrophoresis gel analysis of the VIM-7 D120N mutant, an approximately 1000 bp product is weakly visible for two of three amplification reactions (Figure 18b, lane 2 and 4). All three were sent for sequencing, and only one plasmid contained the correct sequence. Lane 2 (Figure 18b) had insertions as analysed by Sanger sequencing, and was not used further.

Clones containing the desired mutations, D120A, D120N and H224Y were identified by PCR screenings and by Sanger sequencing. T7 primer specific amplifications from the VIM-7 D120N pDEST14 plasmid are not as clear. The VIM-7 D120A pDEST14 plasmid and the VIM-7 H224Y pDEST14 plasmid were amplified as expected.
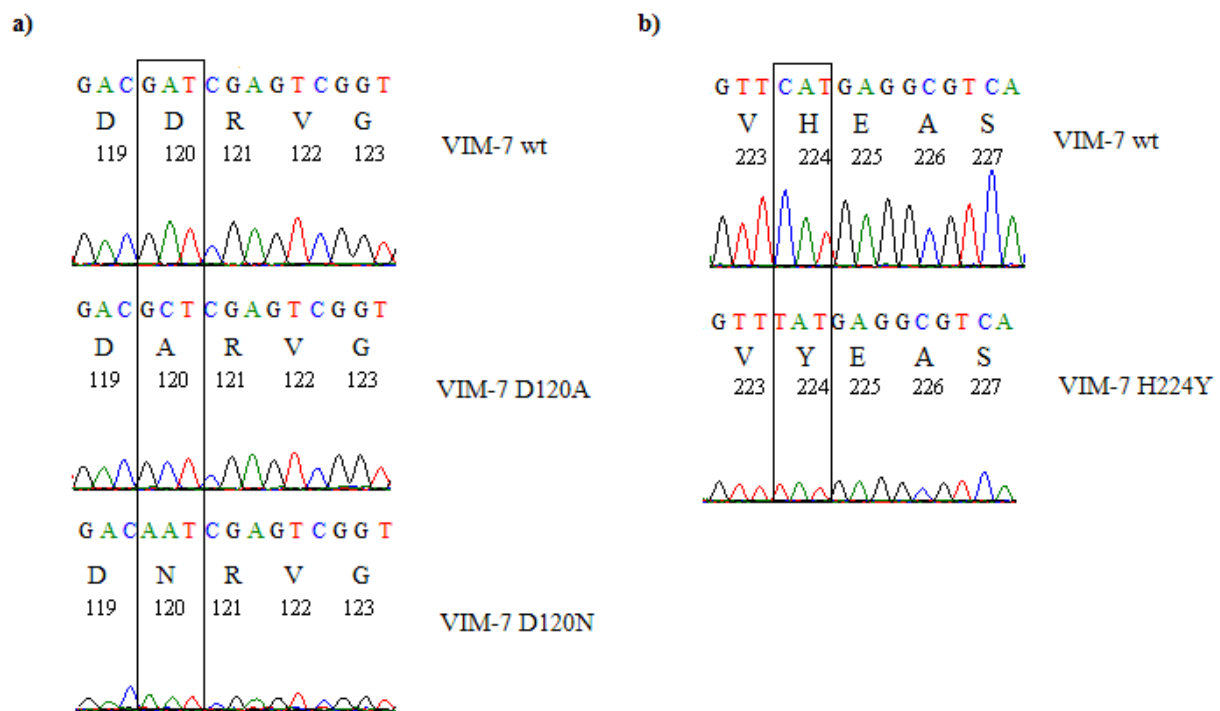
Figure 19: Chromatogram selections of the sequences of VIM-7 wt compared to the mutants. a) VIM-7 wt sequence (showing only amino acids D119-G123) as it is cloned into the pDONR221 vector compared to the VIM-7 D120A mutant (middle panel) and the VIM-7 D120N mutant (lower panel), both of the latter sequences in the pDEST14 vector. **b)** VIM-7 wt sequence (showing only amino acids V223-S227) in the pDONR221 vector compared to the VIM-7 H224Y mutant in the vector pDEST14.

The peaks in the chromatogram show that the VIM-7 D120N mutants are not as distinct as the peaks in the VIM-7 wt and the VIM-7 D120A mutant (Figure 19a). For Sanger sequencing the read lengths are routinely 800-1200 base pairs long [131]. The read length of the sequence encoding VIM-7 D120N is approximately 500 base pairs. With a short read length like this, the mutant is near the end of the sequence, and the sequencing intensity is not as strong as it would have been in with a longer reading length. An overload of DNA template might lead to a large number of small fragments [132].

To conclude, the mutagenesis for all three point mutations was performed successfully, and the mutations were all confirmed by Sanger sequencing.

Small and large scale protein expression

To find out whether the recombinant VIM-7 wt and the mutant proteins, containing a hexahis-tag and a TEV cleavage site, were inducible with 0.4 mM IPTG from the pDEST14 vector, two different *E. coli* strains were used, and induced at two different temperatures, 37ºC and 20ºC. The strains used were Rosetta2(DE3)pLysS and BL21(DE3)star/pRARE/pLysS strains, and the temperatures of induction was 37°C for approximately 4 hours, or 20°C o/n, respectively (data not shown). The VIM-7 wt, VIM-7 D120A mutant and VIM-7 H224Y mutant were induced by both *E. coli* strains, and Rosetta2(DE3)pLysS was chosen for large scale protein expression.
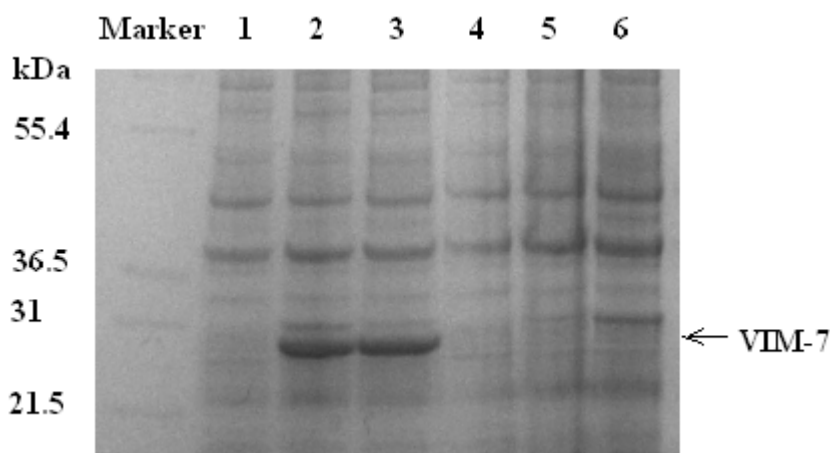
Figure 20: SDS-PAGE analysis of recombinant protein expression of VIM-7 wt and mutant VIM-7 D120N at different temperature in Rosetta2(DE3)pLysS. SDS-PAGE analysis with the protein marker Mark12 (Marker), showing molecular weight band values to the left (as kilodaltons, kDa). Lane 1-3 shows VIM-7 wt; lane 1) before induction with 0.4 mM IPTG, lane 2) was after induction at 37°C for 4 hours, and lane 3) after induction at 20°C o/n. Lane 4-6 shows VIM-7mutant D120N; lane 4) before induction with 0.4 mM IPTG, lane 5) after induction at 37°C for 4 hours, and lane 6) after induction at 20°C o/n. The strain Rosetta2(DE3)pLysS was used for all enzymes. Positive application of VIM-7 is indicated with an arrow.

The recombinant VIM-7 D120N mutant was, however not inducible (lane 5 and 6, Figure 20). The experiment was repeated three times, however, with unsuccessful results. Several buffers were used in order to check solubility, and the VIM-7 wt and the VIM-7 D120A and H224Y mutants were soluble in all of the buffers (data not shown).

The VIM-7 wt, VIM-7 D120A and VIM-7 H224Y mutants were expressed in both strains and at both temperatures to an equal level (data not shown).

In order to check whether the VIM-7 D120N mutant was observable in large scale, it was attempted to produce in large scale. The VIM-7 wt, VIM-7 D120A and VIM-7 H224Y mutants were all produced successfully in 1 litre large scale expression in Rosetta2(DE3)pLysS, while the VIM-7 D120N mutant was expressed, even in large scale production.

Purification of VIM-7 wt, VIM-7 D120A and VIM-7 H224Y

To perform kinetics studies and set up crystallization trials, the proteins VIM-7 wt and the mutants were purified. The pellets containing the Rosetta2(DE3)pLysS with the target protein were dissolved in lysis buffer A (Table 1), before they were disrupted by sonication for the proteins to exit the cells. Purification was done by the affinity purification method [113] using a HisTrap HP 1 ml column with a flow rate of 1 ml/min, and a pressure of 0.5 MPa. The column was washed, and the lysate was loaded to the column. The buffer B (Table 1) was used on the column over 17-42 CV for the absorbance 280 to decrease before an imidazole gradient ranging from 10 mM-1M was used to elute the protein, by using buffer C (Table 1). The flowthrough was collected as 5 ml fractions, while the elution fractions were collected as 1 ml fractions. HisTrap purification method was performed before and after dialysis with TEV cleavage.

Based on analysis of the VIM-7 D120A mutant and the VIM-7 H224Y mutant amino acid sequences, the mass was expected to be about 26 kDa (Table 2), and the induced proteins were all corresponding to the expected mass.

Purification of VIM-7 wt

a)

b)
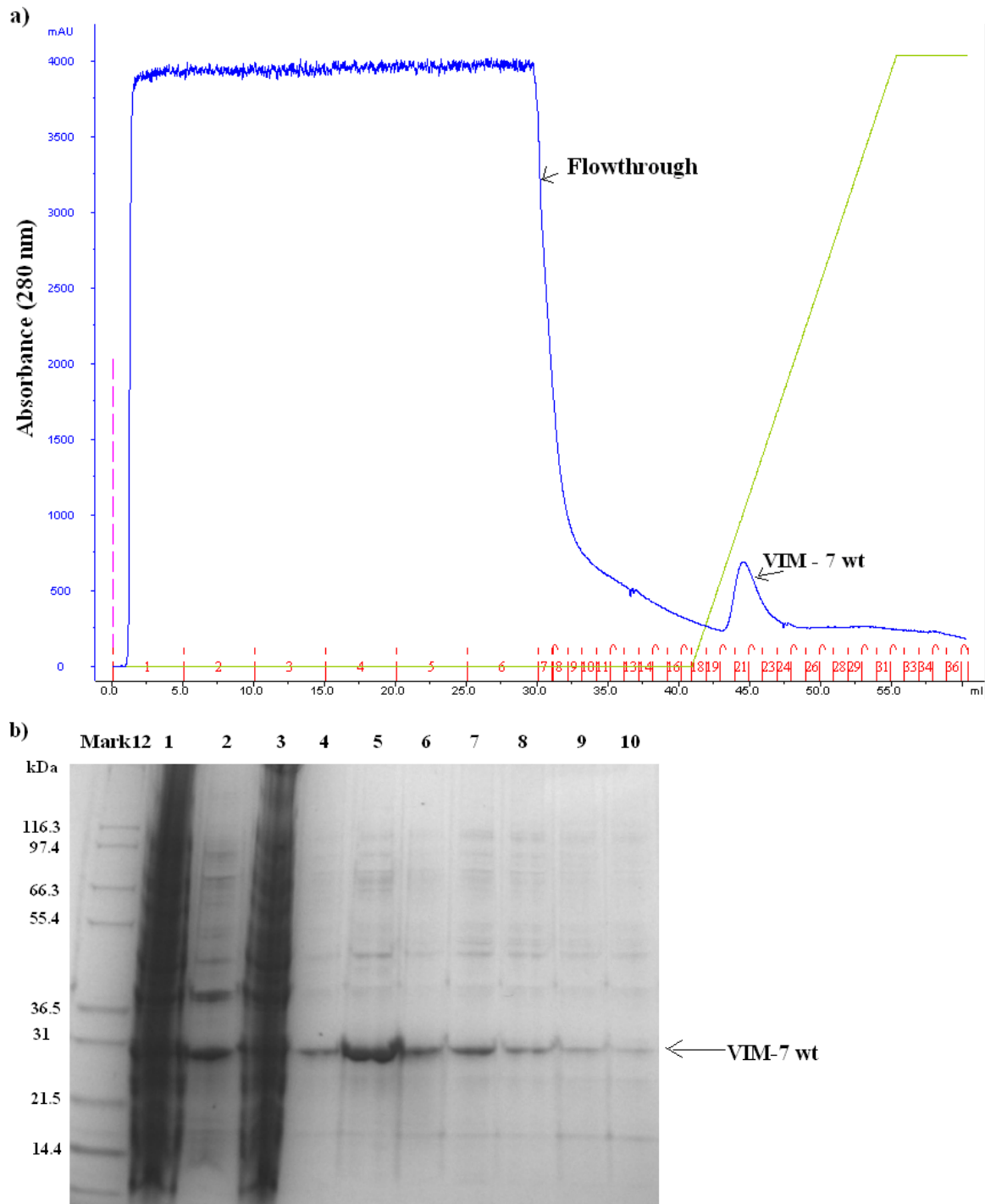
Figure 21: Affinity purification and SDS-PAGE analysis of VIM-7 wt. a) HisTrap purification with a 10-1000 mM imidazole gradient using a HisTrap HP 1 ml column over 15 CV with a flow of 1 ml/min and a collection of 1 ml fractions. The blue line indicates the absorbance at 280 nm and the green line indicate the 10-1000 mM imidazole gradient. The different peaks are marked with arrows, and the fractions are marked in red along the x-axis, while the absorbance is marked along the y-axis. The pink line shows injection of sample. **b)** The SDS-PAGE shows selected fraction from the HisTrap purification in a). The marker used is Mark12 Unstained Standard (Life Technologies), soluble fraction after sonication (lane 1), resuspended pellet after sonication (lane 2), flowthrough (lane 3), and fraction 20-26 (lane 4-10). VIM-7 wt is indicated with an arrow.

The elution peak of VIM-7 wt in the affinity purification chromatogram has a value of ca. 700 mAU (Figure 21a). The flowthrough fractions 1-6 were all pooled. Selected fractions from all steps of the purification were analysed by SDS-PAGE (Figure 21b).

The fractions 20-23 (lane 4-7, Figure 21b) were dialysed in a dialysis buffer D (Table 1) o/n with a magnetic stirrer at 4°C, with TEV (1:100 of protein concentration) added to the protein sample. To know the amount of protein in the fractions, the protein concentration was measured by Nanodrop. The VIM-7 wt protein concentration was 1.2 mg/ml before dialysis and TEV cleavage.

Affinity purification of VIM-7 wt was repeated after TEV digestion with the same conditions as earlier. The imidazole gradient was from 10-1000 mM over 15 CV, and in this purification, TEV, his-tagged TEV and other his-tagged proteins are eluted in the gradient. The cleaved VIM-7 wt protein is eluted in the flowthrough because of its inability to bind to the HisTrap column, whereas the uncleaved VIM-7 wt does bind.
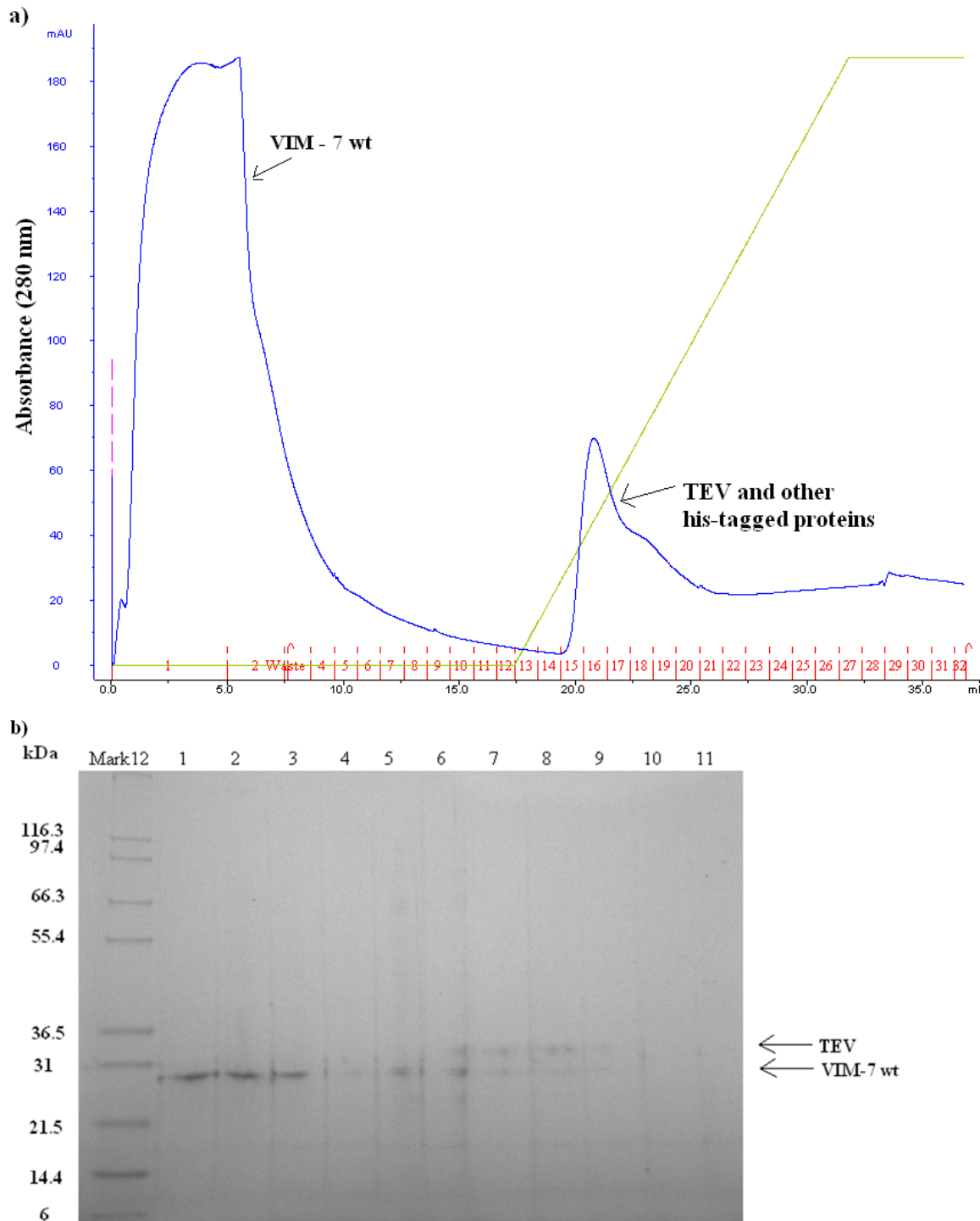
Figure 22: Affinity purification of VIM-7 wt and SDS-PAGE analysis after dialysis with TEV cleavage.
a) HisTrap purification after dialysis and TEV cleavage with a 10-1000 mM imidazole gradient using a HisTrap HP 1ml column. The first two fractions were 5 ml. The blue line shows the absorbance at 280 nm and the green line displays the imidazole gradient. The different peaks are marked, and the fractions are marked in red along the x-axis, while the absorbance is marked along the y-axis. The pink line shows injection of sample. **b)** SDS-PAGE showing selected fraction from the HisTrap purification in a). The marker used is Mark12 Unstained Standard (Life Technologies), flowthrough fraction 1 (lane 1), flowthrough fraction 2 (lane 2), flowthrough fraction 3 (lane 3), fraction 15-20 (lane 4-9), fraction 29 (lane 10), fraction 30 (lane 11). TEV and VIM-7 wt are indicated with arrows.

The peak of the VIM-7 wt had a maximum absorbance of 185 mAU (Figure 22a), verified by the SDS-PAGE analysis (Figure 22b). The VIM-7 wt was eluted in the flowthrough. TEV which contain his-tags and proteins, including VIM-7 wt, with his-tags still attached, eluted in the imidazole gradient.

The flowthrough fractions 1-3 (lane 1-3 in Figure 22b) all contained the VIM-7 wt protein, and were pooled. The protein concentration of the pooled fractions was 0.28 mg/ml, as determined by NanoDrop. The pooled fractions of 1-3 (lane 1-3, Figure 22b) were estimated to be reasonably pure. The fractions (lane 6-9, Figure 22b) from the peak in the gradient (Figure 22a), all contained TEV which had a mass of about 33 kDa. TEV and uncleaved VIM-7 wt in the SDS-PAGE analysis is observed in fractions 16-20 (Figure 22b) above the VIM-7 wt protein.

The affinity purification of VIM-7 wt was successful, and the pooled fractions of VIM-7 wt protein had a protein concentration of 0.28 mg/ml were estimated to be pure enough to perform the enzyme kinetic studies.

Purification of VIM-7 D120A mutant

The procedure for the purification of VIM-7 mutant D120A was identical to the purification of VIM-7 wt, described above.
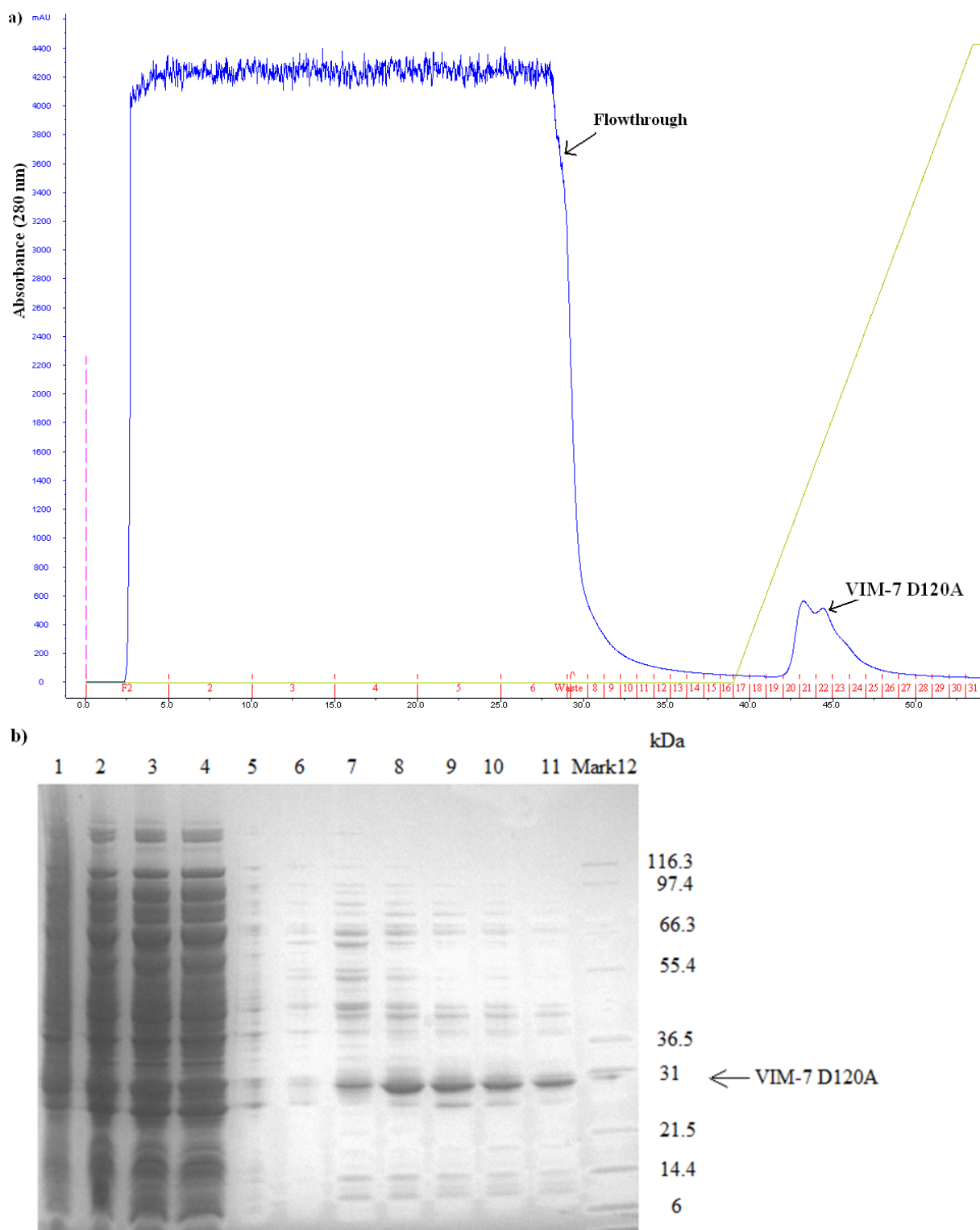
Figure 23: Affinity purification and SDS-PAGE analysis of VIM-7 mutant D120A. a) HisTrap purification using a HisTrap HP 1ml column. The blue line indicates the absorbance at 280 nm and the green line indicates the imidazole 10-1000 mM gradient. The different peaks are marked with arrows. The pink line shows injection of sample. **b)** SDS-PAGE showing selected fraction from the HisTrap purification. Sample from before sonication (lane 1), after sonication (lane 2), flow through fraction 1 (lane 3), flow through fraction 2 (lane 4), fraction 20-26 (lane 5-11). The marker used is Mark12 Unstained Standard (lane 12 as Mark12), and the masses are indicated to the right in the figure.

49

As for the purification of VIM-7 wt, the flowthrough fractions 1-7 were pooled and the SDS-PAGE analysis was performed. The peak of VIM-7 D120A mutant has an absorbance of maximum 500 mAU (Figure 23a), and was showed by SDS-PAGE analysis (Figure 23b). The target protein migrates according to its expected mass.

The fractions 22-26 (lane 7-11, Figure 23b) were pooled, TEV protease was added, and they were set for dialysis with TEV-cleavage o/n at 4ºC in a dialysis buffer D (Table 1). The protein concentration of the pooled fractions before dialysis was 1.3 mg/ml as measured by the Nanodrop.
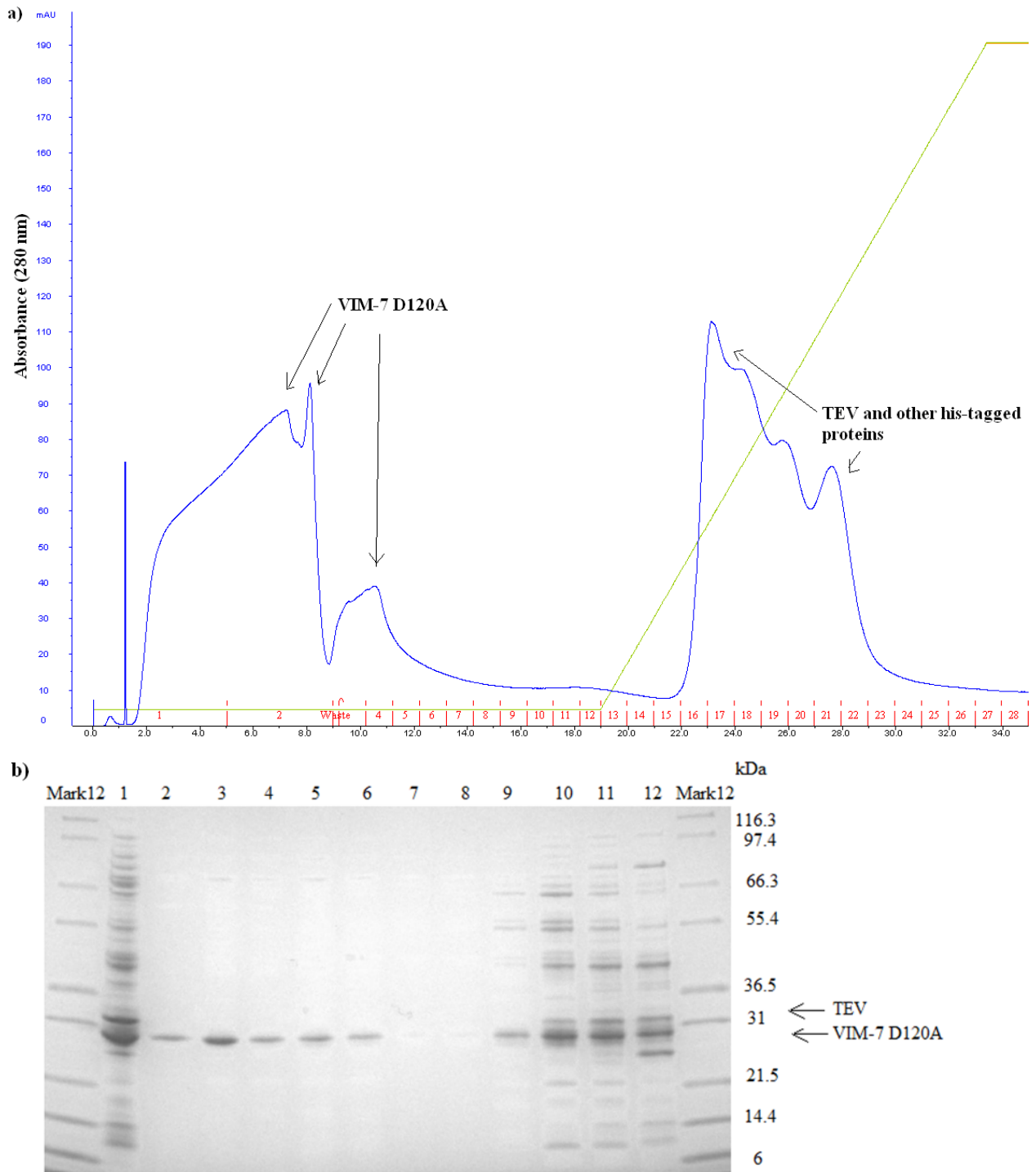
Figure 24: Affinity purification and SDS-PAGE analysis of VIM-7 D120A mutant after dialysis and TEV cleavage. a) HisTrap purification after TEV cleavage with a 10-1000 mM imidazole gradient (green line) using a HisTrap HP 1ml column. The first two fractions were 5 ml. The blue line indicates the absorbance at 280 nm (mAU). The different peaks are marked, and the fractions are marked in red along the x-axis, while the absorbance is marked along the y-axis. **b)** SDS-PAGE analysis showing selected fraction from the HisTrap purification after dialysis and TEV cleavage. The marker used is Mark12 Unstained Standard, sample after dialysis before purification (lane 1), flow through fraction 1 (lane 2), flow through fraction 2 (lane 3), fraction 4-6 (lane 4-6), fraction 16 (lane 7), and fraction 18-22 (lane 8-12).

51

The peaks with absorbance of 80, 95 and 30 mAU in fractions 1-6 (Figure 24a) shows from the SDS-PAGE analysis (Figure 24b) consistent in size to be the VIM-7 mutant D120A. There is not one consistent peak for the protein; this may be because of the pump changing the pressure on the column. After fraction 2, some protein appears to have been directed to waste, which causes the peak to drop to 15 mAU before the rest of the protein was injected into the column. The peaks at fraction 16-22 (Figure 24a) are his-tagged TEV, uncleaved VIM-7 D120A mutant and other proteins which have not cleaved off the His-tag, and the peaks have an absorbance of 85 and 110 mAU.

The flowthrough fractions 1 and 2 and fraction 4-6 (lane 2-6, Figure 24b) were pooled, and estimated to be reasonably pure for enzyme kinetic studies. Gel filtration purification was not performed, because it would reduce the total yield of the protein. A considerable amount of uncleaved VIM-7 D120A is in the fractions with TEV along with other proteins (lane 10-12, Figure 24b), due to insufficient amounts of TEV added to the dialysis to perform the TEV-cleavage.

The protein concentration of the pooled fractions lane 2-6 (Figure 24b) was 0.2 mg/ml. To use the protein for enzyme kinetics studies the fractions were pooled and concentrated with a Millipore centrifugal filter. The protein concentration of the fractions after up concentration was 7.8 mg/ml.

The TEV cleaved VIM-7 D120A mutant was successfully affinity purified, and the protein concentration estimated to 7.8 mg/ml, with estimated to be reasonable pure for further enzyme kinetic studies.

Purification of VIM-7 H224Y mutant
The procedure for the affinity purification and dialysis of VIM-7 mutant H224Y was identical to the previously described purification of VIM-7 wt.
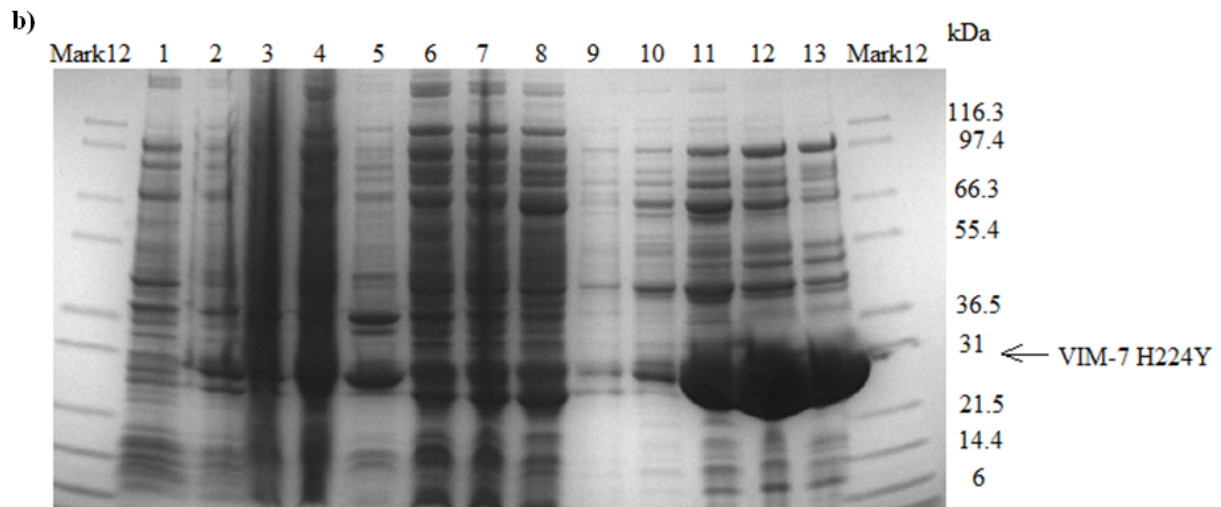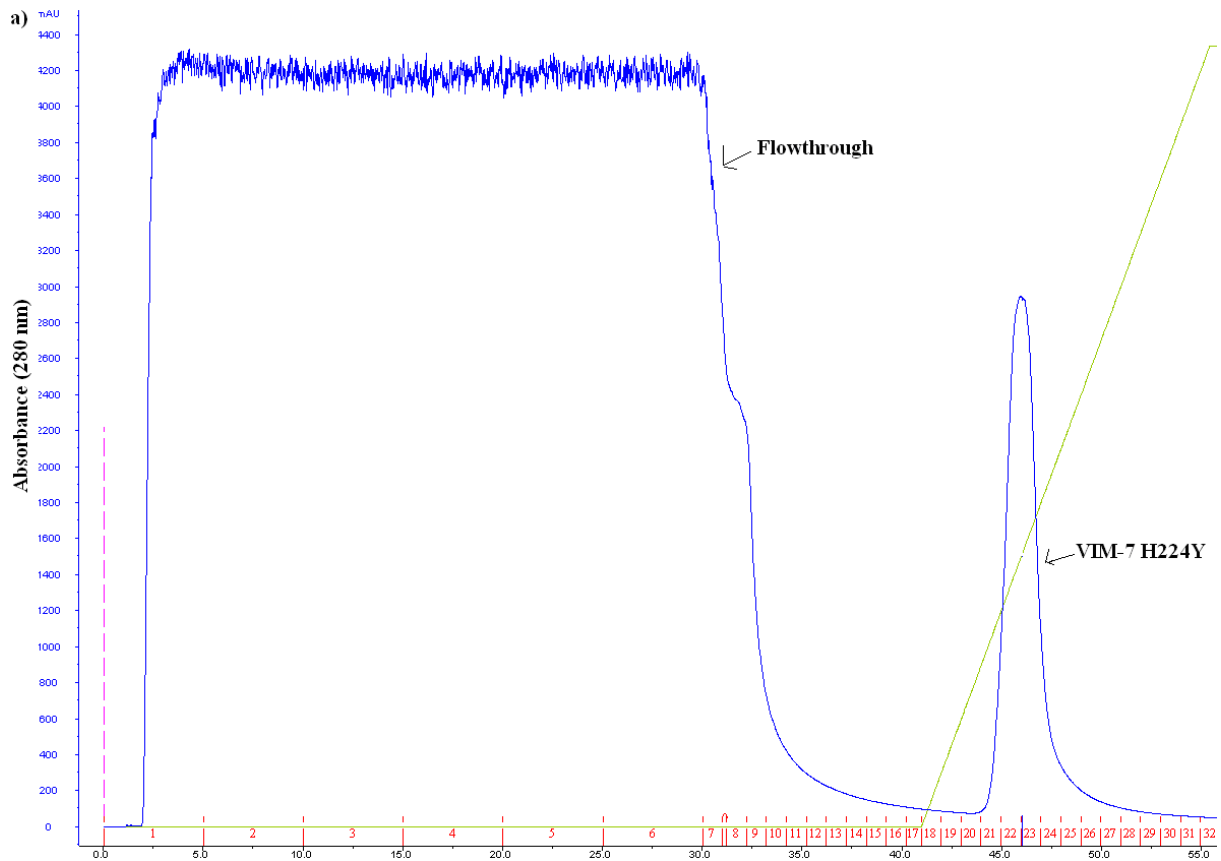
Figure 25: Affinity purification and SDS-PAGE analysis of VIM-7 H224Y mutant. a) HisTrap purification with a 10-1000 mM imidazole gradient (green line) using a HisTrap HP 1ml column over 15 CV with a flow of 1 ml/min and a collection of 1 ml fractions. The blue line shows the absorbance at 280 nm. The fractions are marked in red along the x-axis, while the absorbance is marked along the y-axis. The pink line shows injection of sample. **b)** SDS-PAGE analysis showing selected fraction from the first HisTrap purification of VIM-7 H224Y mutant. The molecular weight marker used is Mark12 Unstained Standard, before induction (lane 1), after induction (lane 2), before sonication (lane 3), after sonication supernatant (lane 4), after sonication pellet (lane 5), flow through (lane 6), fraction 8 (lane 7), fraction 9 (lane 8), fraction 21-25 (lane 9-13).

The peak of VIM-7 H224Y mutant has absorbance of 2944 mAU (Figure 25a). From the SDS-PAGE analysis (Figure 25b), it appears to be substantial amounts of VIM-7 H224Y mutant in the fractions 23-25 (lane 11-13, Figure 25b) from the peak (Figure 25a). The SDS-PAGE gel is clearly overloaded. By adding less amount of sample to the gel, the fractions for VIM-7 H224Y would be more defined.

A pink colour of fractions 23 and 24 (Figure 25a) of the VIM-7 H224Y mutant after the purification appeared. This is discussed later. The fractions 23-25 (lane 11-13, Figure 25b) were pooled, TEV was added, and they were dialysed with TEV-cleavage o/n. To get an estimate of the amount protein in the pooled fractions, the protein concentration was measured by Nanodrop to 7.7 mg/ml.
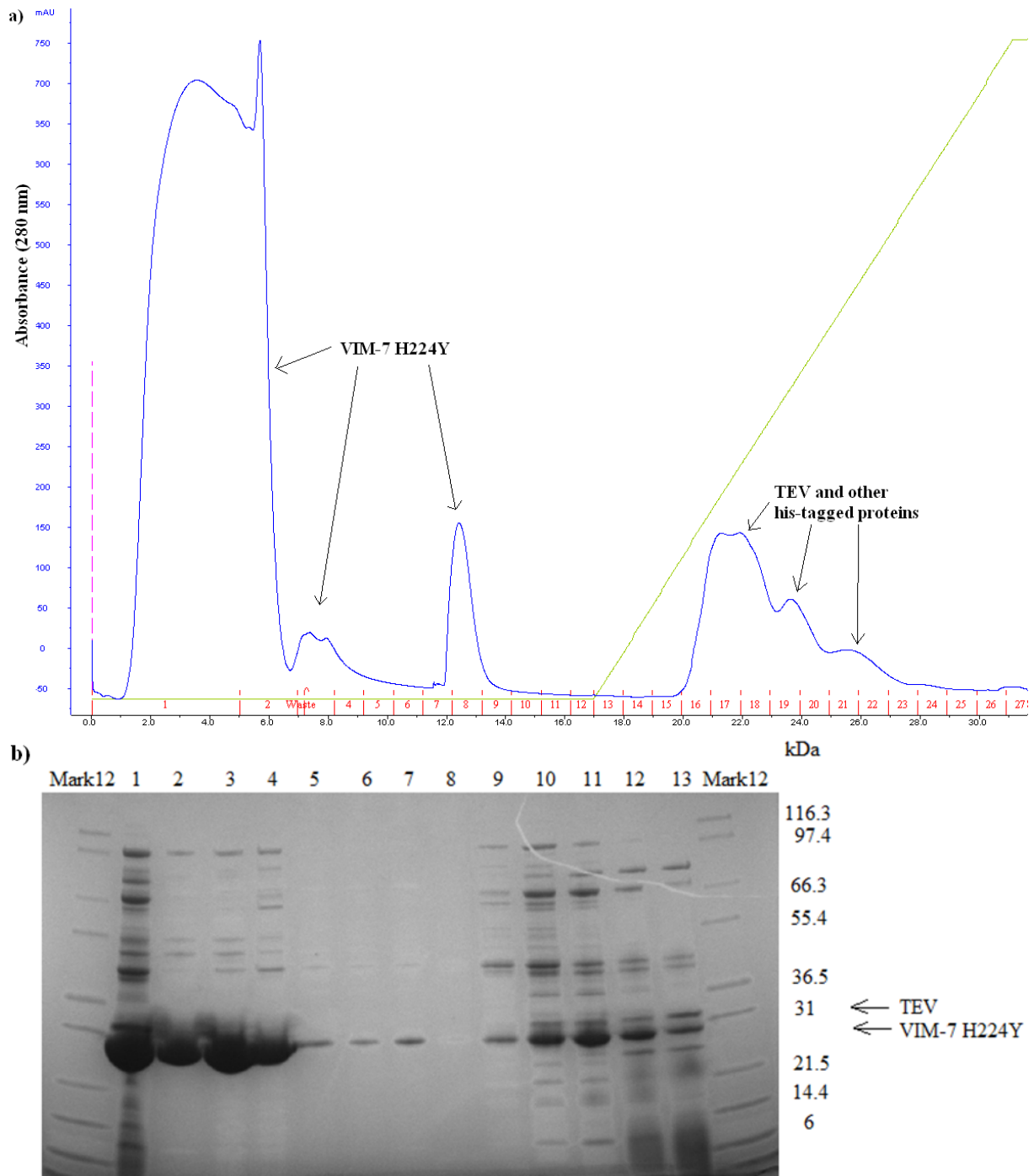
Figure 26: Affinity purification and SDS-PAGE analysis of VIM-7 H224Y mutant after dialysis and TEV cleavage. a) HisTrap purification with a 10-1000 mM imidazole gradient (green line) using a HisTrap HP 1ml column, was performed after TEV cleavage. The blue line indicates the absorbance at 280 nm. **b)** SDS-PAGE analysis shows selected fraction from the second HisTrap purification of VIM-7 mutant H224Y. The marker used is Mark12 Unstained Standard (Mark12), after dialysis (lane 1), flow through fraction 1 (lane 2), flow through fraction 2 (lane 3), fraction 3 (lane 4), fraction 7-9 (lane 5-7), fraction 16-21 (lane 8-13).

The peaks in fractions 1-4 and fraction 6 (Figure 26a) shows the VIM-7 H224Y mutant, as verified by SDS-PAGE analysis (Figure 26b) with a peak at 750 mAU. After fraction 2, some protein was directed to waste before injecting the rest of the protein onto the column, which causes the peak to drop before increasing again. The peaks at fractions 16-22 (Figure 26a) are TEV containing his-tags and other proteins with his-tags still attached, with peaks at 50 and 150 mAU.

The SDS-PAGE gel (Figure 26b) is overloaded, and by adding less amount of the VIM-7 H224Y mutant sample to the analysis, the target protein would be more defined and contaminants (approximately 40-97 kDa) would be less visible.

The fractions from both flowthroughs and fraction 3 (lane 2, 3 and 4, Figure 26b) were pooled, and estimated to be reasonably pure. To further purify and investigate the integrity of the protein, gel filtration purification was performed on flowthrough 2 (lane 3) and fraction 3 (lane 4) pooled. It appears to be some uncleaved VIM-7 H224Y mutant in the elution, fractions 17-21, (lane 9-13, Figure 26b) with TEV along with other proteins containing his-tags.

The fraction flowthrough 2 (lane 3) and fraction 3 (lane 4) was pooled and the protein concentration was 2.5 mg/ml. The protein concentration of the fraction flowthrough 1 (lane 2) was 1.3 mg/ml, and was concentrated by using a Millipore centrifugal filter. The protein concentration after up concentration was 20.1 mg/ml.

The affinity purification of recombinant VIM-7 H224Y mutant was successfully performed. Flowthrough 1 (lane 2) was roughly estimated to be 97% pure, and was used to set up crystallization trials. To perform enzyme kinetic studies, the flowthrough 2 and fraction 3 (lane 3-4, Figure 26b) were purified further by gel filtration purification.

Gel filtration of VIM-7 H224Y mutant
To perform a gel filtration, a HiLoad 16/60 column was used, with a flow rate of 1.5 ml/min, and a maximum pressure of 0.5 MPa. The fractions sizes were 3 ml. The buffer used for gel filtration was buffer A (Table 1).
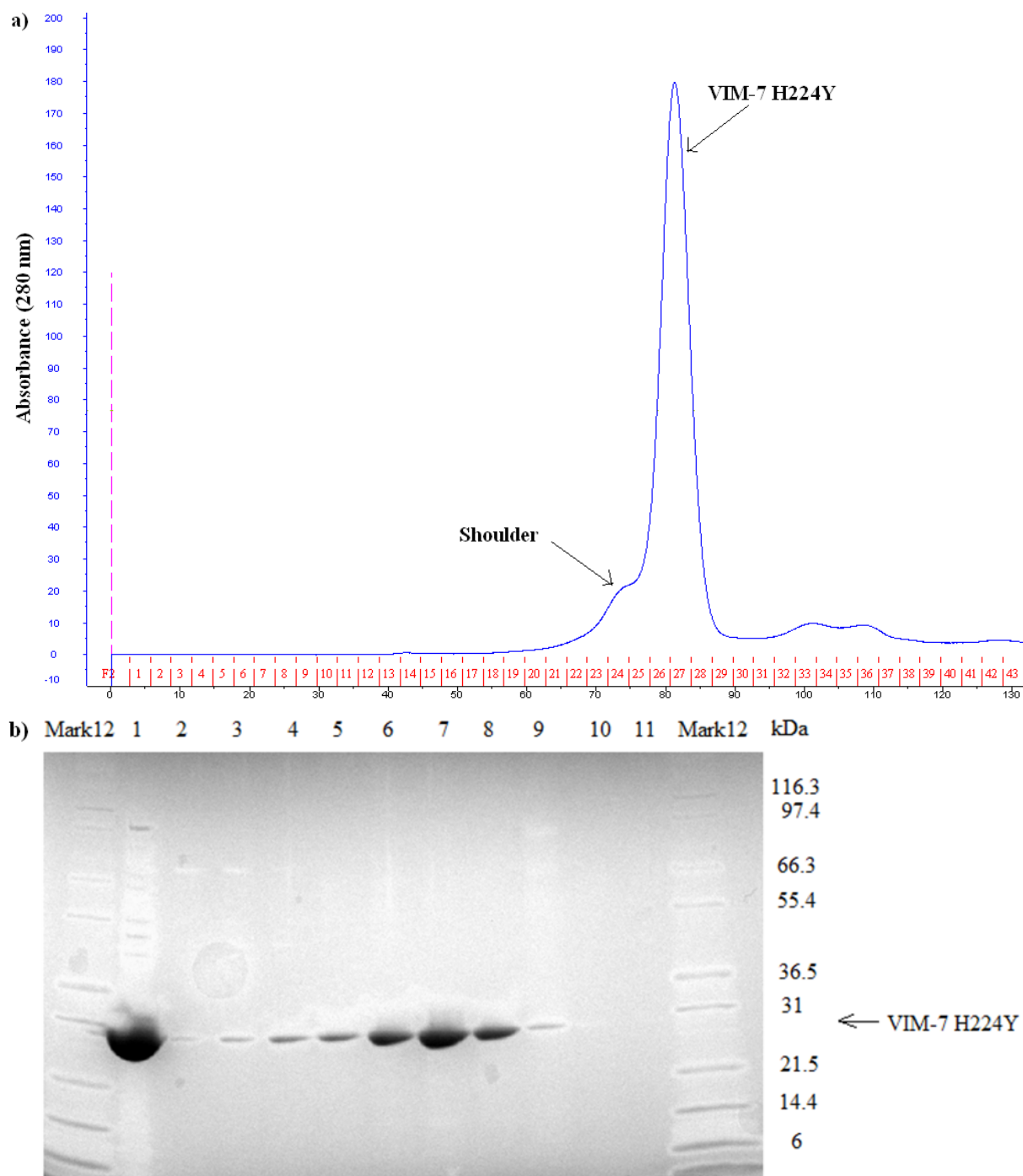
Figure 27: Gel filtration purification and SDS-PAGE analysis of VIM-7 H224Y mutant. a) Gel filtration purification Superdex HiLoad 16/60 column with a flow of 1.5 ml/min, a maximum pressure of 0.5 MPa and 3 ml fractions. The blue line indicates the absorbance at 280 nm. The peak is marked, and the fractions are marked in red along the x-axis, while the absorbance is marked along the y-axis. The pink line shows injection of sample. **b)** SDS-PAGE gel showing selected fraction from the gel filtration purification of VIM-7 mutant H224Y. The marker used is Mark12 Unstained Standard, before gel filtration (lane 1), fraction 22-29 (lane 2-9), fraction 33 (lane 10), fraction 38 (lane 11).

The peak in fractions 26-28 (Figure 27a) with a value of 190 mAU was analysed on a SDS-PAGE gel, which showed that is was the VIM-7 H224Y mutant. In order to confirm that the VIM-7 H224Y mutant is purer than before the gel filtration purification a SDS-PAGE analysis was performed on the selected fractions 22-29, 33 and 38. The analysis was performed with a sample of the VIM-7 H224Y mutant before gel filtration purification for comparison (lane 1, Figure 27b).

The shoulder (Figure 27a) might be a multimer or aggregates of the protein [133], which is shown in lane 2-5 (Figure 27b).

The protein was purer after gel filtration, and was considered reasonably pure. The fractions 26-28 (lane 6-8) were pooled and protein concentration measured to be 0.3 mg/ml. The pooled fractions were up concentrated to be 3.3 mg/ml. The protein from the gel filtrations was used further in the enzyme kinetics studies.

The purification of VIM-7 H224Y mutant was successfully, both for the affinity purification and gel filtration purification.

Epsilometer tests

The E-test was performed to study whether the VIM-7 wt, the VIM-7 D120A and the VIM-7 H224Y enzymes are receptive to specific antibiotics.

The results were read by researcher Ørjan Samuelsen, but the results showed no difference in MIC value between the VIM-7 wt, VIM-7 D120A and VIM-7 H224Y (Table 5). This is most likely due to the fact that VIM-7 was cloned into the pDEST14 expression vector, which is tightly regulated for leaky expression, and the genes to not be expressed without the presence of IPTG (Table 1).

Table 5: MIC values from the E-tests of the proteins VIM-7 wt, VIM-7 D120A and VIM-7 H224Y.

	Amoxicillin/Clavulanic acid	Piperacillin/Tazobactam	Ceftazidime	Cefoxitin	Aztreonam	Cefuroxime	Imipenem	Meropenem	Ertapenem
E. coli VIM-7 wt	12	2	0.19	2	0.032	1.5	0.38	0.064	0.023
E. coli VIM-7 D120A	8	2	0.125	2	0.032	0.75	0.38	0.047	0.023
E. coli VIM-7 H224Y	8	2	0.125	3	0.023	0.75	0.38	0.064	0.023

Activity testing by using nitrocefin

In order to examine the difference in activity between the VIM-7 wt and the VIM-7 D120A and H224Y mutants, an enzyme assay with the substrate nitrocefin was performed. By using the spectrophotometer SpectraMax and the software SoftMax and the extinction coefficient of the substrate, the substrate concentration of the stock solutions were determined. The nitrocefin was diluted in buffer E (Table 1). The proteins were diluted in buffer F with BSA (Table 1). The measurements were initiated by measuring 50 µl of buffer E together with 40 µl nitrocefin substrate. 10 µl of protein with a concentration of 0.1 µM was added to the solution, and the absorbance at specific wavelengths (Table 3) was measured at 25ºC for 20 min. The substrate nitrocefin was measured in a 96 well flat bottom non-binding surface microplate. The temperature used during the measurements was 25 °C.
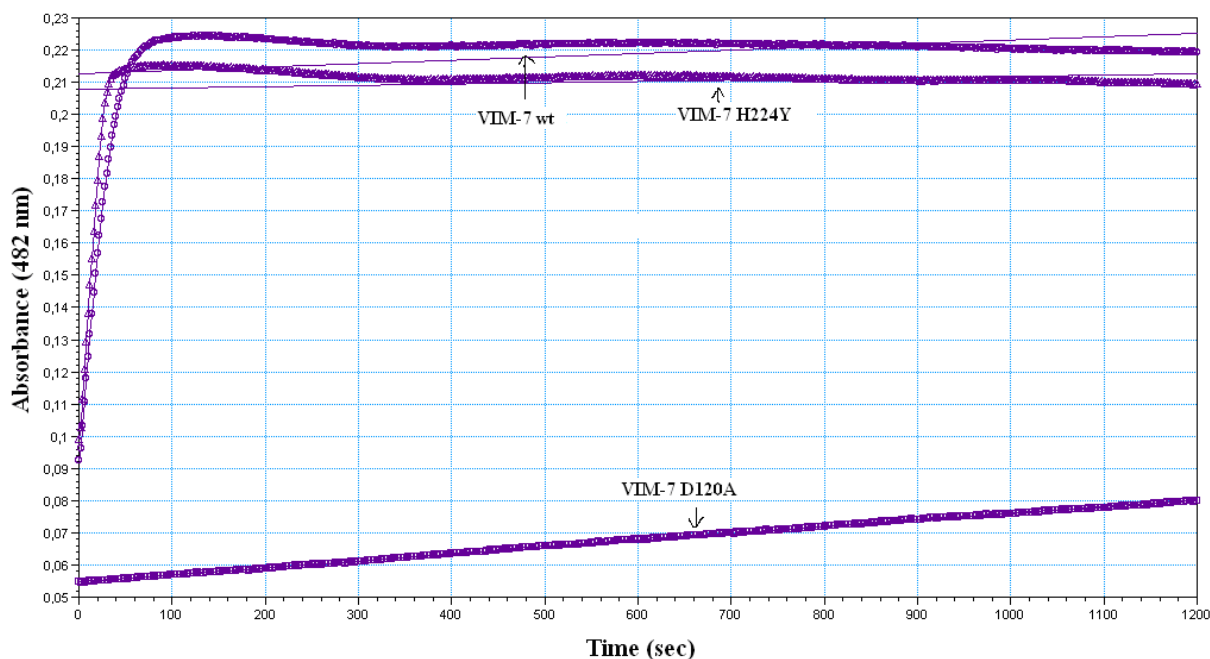
Figure 28: Activity measurements with nitrocefin. Nitrocefin was used as substrate for comparing the activity of VIM-7wt (o), VIM-7 H224Y mutant (Δ) and VIM-7 D120A mutant (□). All of the proteins had a concentration of 0.1 μM.

The VIM-7 H224Y mutant appeared to have an activity that was slightly lower than VIM-7 wt with the substrate nitrocefin (Figure 28). The VIM-7 D120A mutant, on the other hand, turned out to have very low activity (Figure 28).

This measurement was also performed with different antibiotics (results shown in the appendix). The results from these enzyme activity tests were used to find what concentration of the enzymes to use and to compare the activity of the VIM-7 wt, the VIM-7 D120A mutant and the VIM-7 H224Y mutant enzymes.

Enzyme kinetics

To study the enzyme activity and the reaction rates of the recombinantly produced proteins VIM-7 wt, VIM-7 D120A mutant and VIM-7 H224Y mutant, enzyme kinetic studies were performed. Six different antibiotics; ertapenem, meropenem, cefoxitin, cefepime, ceftazidime and cefuroxime, were used as substrates and dissolved in buffer E (Table 1). The substrate solutions for kinetic analyses were made as dilutions in the range of 2-1000 µM. The kinetic analysis was performed in two parallels to obtain reliable results. The TEV-cleaved and affinity purified proteins were diluted in buffer F (Table 1) to final concentrations of 10 µM or 50 µM. The measurements were performed using 96 well falcon UV microplates, because of the substrates' ability to interact with the plastic in 96 well non-binding microplates, which was used for activity assays with the substrate nitrocefin (Figure 28).

VIM-7 wt and VIM-7 H224Y mutant were able to hydrolyse all of the antibiotics tested (Figure 28). The concentration of VIM-7 D120A mutant was increased to a final concentration of 100 nM, which was ten times higher than the concentration of the VIM-7 wt and the VIM-7 H224Y, without the substrate ertapenem to be fully hydrolysed (Figure 29b, below). Thus, taken together with the activity measurement with nitrocefin (Figure 28), VIM-7 D120A mutant was considered inactive. Due to this conclusion, enzyme kinetic analysis of the VIM-7 D120A mutant with other substrates, were not conducted.
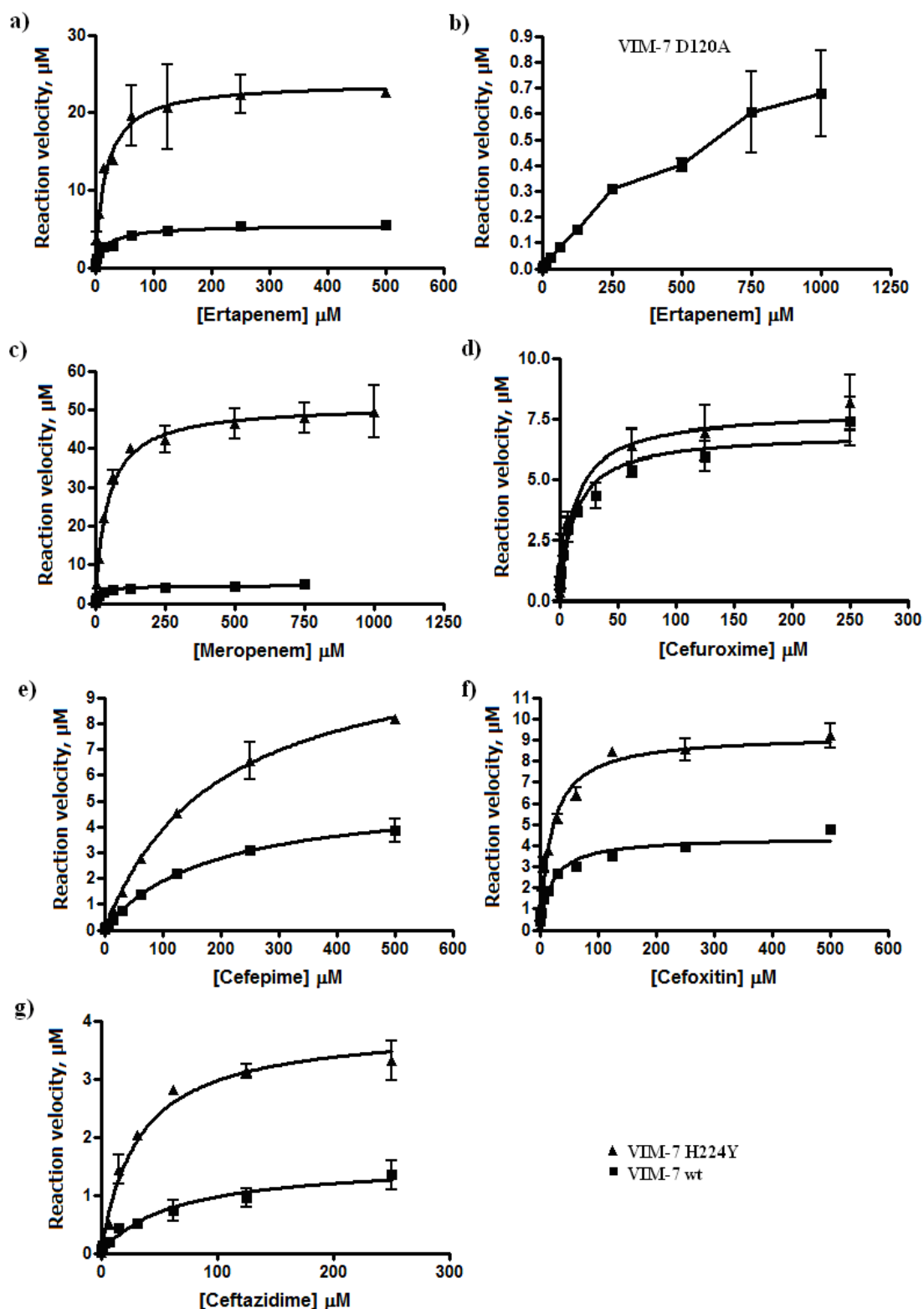
Figure 29: Enzyme kinetics VIM-7 wt (■), VIM-7 D120A (only in b) and VIM-7 H224Y (▲) with different substrates. a) Ertapenem using 10 nM VIM-7wt and 10 nM VIM-7 H224Y mutant, **b)** Ertapenem using 100 nM VIM-7 D120A mutant, **c)** Meropenem using 10 nM VIM-7 wt and 10 nM VIM-7 H224Y mutant, **d)** Cefuroxime using 10 nM VIM-7 wt and 10 nM VIM-7 H224Y mutant, **e)** Cefepime using 50 nM VIM-7 wt and 10 nM VIM-7 H224Y mutant, **f)** Cefoxitin using 50 nM VIM-7 wt and 10 nM VIM-7 H224Y mutant, **g)** Ceftazidime using 50 nM VIM-7 wt and 50 nM VIM-7 H224Y mutant.

First, assay trials with all enzymes were performed to get an indication of which enzyme concentration to use for complete hydrolysis of the substrates (Appendix).

The catalytic efficiency, k_{cat}/K_m (Table 4) of VIM-7 H224Y mutant was higher for four of six substrates when comparing with the VIM-7 wt. The substrates meropenem and cefuroxime had a higher catalytic efficiency with VIM-7 wt in comparison with VIM-7 H224Y mutant, with two times higher for meropenem and 1.5 times higher catalytic efficiency for cefuroxime. The fours substrates with higher catalytic efficiency with the VIM-7 H224Y mutant than the VIM-7 wt were ertapenem with four times higher, cefepime with ten times higher, cefoxitin with six times higher, and ceftazidime with five times higher catalytic efficiency.

The values for k_{cat}, the turnover number which indicates the reaction velocity of the hydrolysis, were higher for VIM-7 H224Y, compared to VIM-7 wt for all substrates.

K_m, gives an indication of how strong the substrates are bound to the active site. The lower the value of K_m, the more firm is the binding of substrate to enzyme. In our assay, K_m values are higher for VIM-7 wt with three of six substrates. The three substrates with higher K_m for VIM-7 wt are meropenem and cefuroxime, both with significant difference to the K_m of VIM-7 H224Y, while the substrate cefepime was not significantly higher when considering the high standard deviation of fourteen.

Table 4: Comparison of k_{cat}, K_m, with standard deviations, and catalytic efficiency k_{cat}/Km for VIM-7wt, VIM-7 H224Y and D120A mutants, with substrates ertapenem, meropenem, cefuroxime, cefepime, cefoxitin, and ceftazidime.

	VIM-7 wt			VIM-7 H224Y			VIM-7 D120A		
	k_{cat} (s⁻¹)	K_m (μM)	k_{cat}/K_m (1/M*s) *10³	k_{cat} (s⁻¹)	K_m (μM)	k_{cat}/K_m (1/M*s) *10³	k_{cat} (s⁻¹)	K_m (μM)	k_{cat}/K_m (1/M*s) *10³
Ertapenem	12.81 ± 0.013	18.9 ± 2.2	677	56.17 ± 0.06	18 ± 3	3150	0.030 ± 0.004	950 ± 380	0.03256
Meropenem	25.58 ± 0.026	20.0 ± 1.6	1280	27.96 ± 0.29	44.1 ± 4.2	634			
Cefuroxime	4.57 ± 0.05	12.9 ± 2.5	355	6.30 ± 0.07	25.1 ± 2.9	251			
Cefepime	0.45 ± 0.023	179 ± 14	2.50	4.86 ± 0.05	194 ± 14	25.1			
Cefoxitin	0.64 ± 0.030	20	31.3	3.94 ± 0.07	20.2 ± 2.1	195			
Ceftazidime	0.120 ± 0.007	61 ± 19	1.98	0.300 ± 0.016	31.9 ± 5	9.50			

Crystallization

The proteins VIM-7 wt, VIM-7 D120A and VIM-7 H224Y mutants were all expressed and purified, but because of the low protein concentration of VIM-7 D120A mutant, crystallization trials were performed for the VIM-7 H224Y mutant due to high amount of protein available.

In order to obtain a crystal structure of the VIM-7 H224Y mutant, crystallization trials, both by hand and by a robot, were set up. In both of these trials, the TEV-cleaved and affinity purified VIM-7 H224Y was used, thus, not gel filtered. One crystal was obtained with the robot, under the conditions of 25% PEG 3350, 0.1 M BisTris pH 5.5 and 0.2 M NaCl (Figure 30), was sent with researcher Hanna-Kirsti Schrøder Leiros (NorStruct, UiT) to the synchrotron at Max-LAB Lund, Sweden, for X-ray data collection.
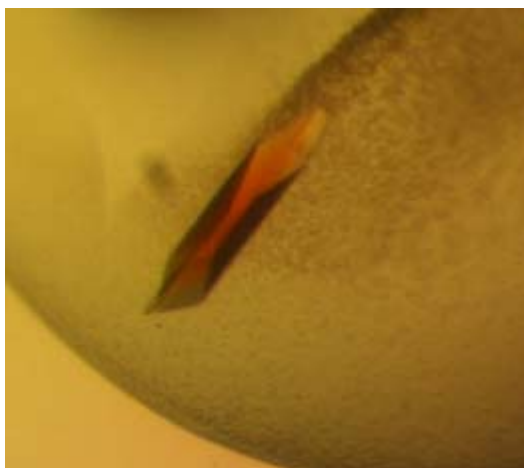
Figure 30: A crystal of VIM-7 H224Y. The enzyme was grown by using the KSCG screen, and used for X-ray data collection. The condition for the crystallization was 25% PEG 3350, 0.1M BisTris pH 5.5 and 0.2 M NaCl.

The crystal (Figure 30) was cryoprotected in 32% polyethylene glycol 5000 monomethyl ether (PEG 5K MME), 5% glycerol and 0.1 M succinate buffer pH 7.0, and then flash frozen in liquid nitrogen (performed by researcher Hanna-Kirsti Schrøder Leiros, NorStruct, UiT).
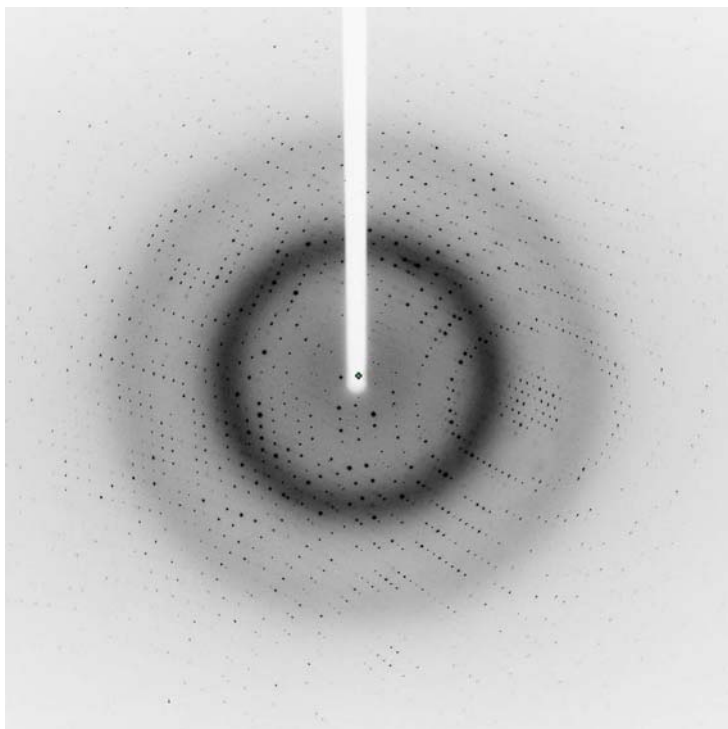
Figure 31: Diffraction image of VIM-7 H224Y mutant. The first image in the VIM-7 H224Y data set, collected with wavelength of 1.0000 Å, a crystal to detector distance of 135.47 mm and on a detector with height of 225 mm giving 1.45 Å resolution at the edge and 1.2 Å resolution in the corners of the detector.

The diffraction image of the VIM-7 H224Y mutant is shown in figure 31. The structure of VIM-7 H224Y mutant was solved by molecular replacement using VIM-7 wt as search model (PDB ID: 2Y87) [29]. The resolution, which is a measure of the resolvability in the electron density map of a molecule, was 1.40 Å in the final dataset. The space group P4$_3$ indicates that the crystal belongs to the tetragonal crystal class, which is the same as for VIM-7 wt. The unit cell parameters (Table 6) are very similar to the parameters from the VIM-7 wt [29] despite the different crystallization condition. The data collection at Max-LAB in Lund, Sweden, was done with a wavelength of 1.000 Å. I represent the measured intensity values of reflections, while σ_I represents the estimated standard deviation in the measurement of the intensity values. This means that $<I>/<\sigma_I>$ gives the average degree to which measured reflection intensities stand out over background. The unique reflections, $<I>/<\sigma_I>$ (Table 6), were approximately nine times greater than the background noise around the reflection. R_{sym} is a measurement of the agreement between the multiple recordings for a given unique reflection. It is a value of the degree to which each reflection deviates from the average of all of its multiply measured counterparts. A value of 6.6% is low, and indicates that the data are in good agreement with each other.

The model for VIM-7 H224Y mutant was refined to a low R value (11.78%, Table 6), which describes how well the model agrees with the experimental X-ray diffraction data [129]. The R_{free} value which is computed by a small set of intensities chosen randomly [134], had a value of 15.64%, which also is low. To describe the confidence of the model, a B-factor is introduced. High values of B-factor imply uncertainty in atom positions. The refinement showed a reasonable mean B-value (18.4 Å^2).

Table 6: Data collection from X-ray crystallization and crystallographic refinement statistics of VIM-7 H224Y. Values in parenthesis are for the highest resolution shell.

Data collection	
X-ray source	LUND I911-3
Space group	$P4_3$
Unit cell (Å)	a=b=70.23, c=47.03
Resolution (Å)	30-1.40 (1.48-1.40)
Wavelength (Å)	1.0000
No. unique reflections	43 649 (5 673)
Multiplicity	3.5 (2.0)
Completeness (%)	96.6 (86.8)
Mean ($<I> / <\sigma_I>$)	9.1 (3.1)
R_{sym} (%)[a]	6.6 (16.5)
Refinement	
Resolution (Å)	25-1.40
R-factor (all reflections) (%)	11.78
R-free (%)[b]	15.64
Average B-factor (Å^2)	
All atoms	18.4
Protein	16.4
Water molecules	31.8
Zn^{2+}	17.0

[a] $R_{sym} = \Sigma_j|I(h)_j - <I(h)>|/\Sigma_j I(h)_j$, where $I(h)_j$ is the scaled observed intensity of the jth observation of reflection h, and $<I(h)>$ is the mean value of corresponding symmetry-related reflection.

[b] $R_{free} = \Sigma h||F_{obs}| - |F_{calc}||/(\Sigma h|F_{obs}|)$, where $|F_{obs}|$ and $|F_{calc}|$ are the observed and calculated structure factor amplitudes for all reflections $(R\text{-}factor)$ and the reflections applied in the test R_{free} set.
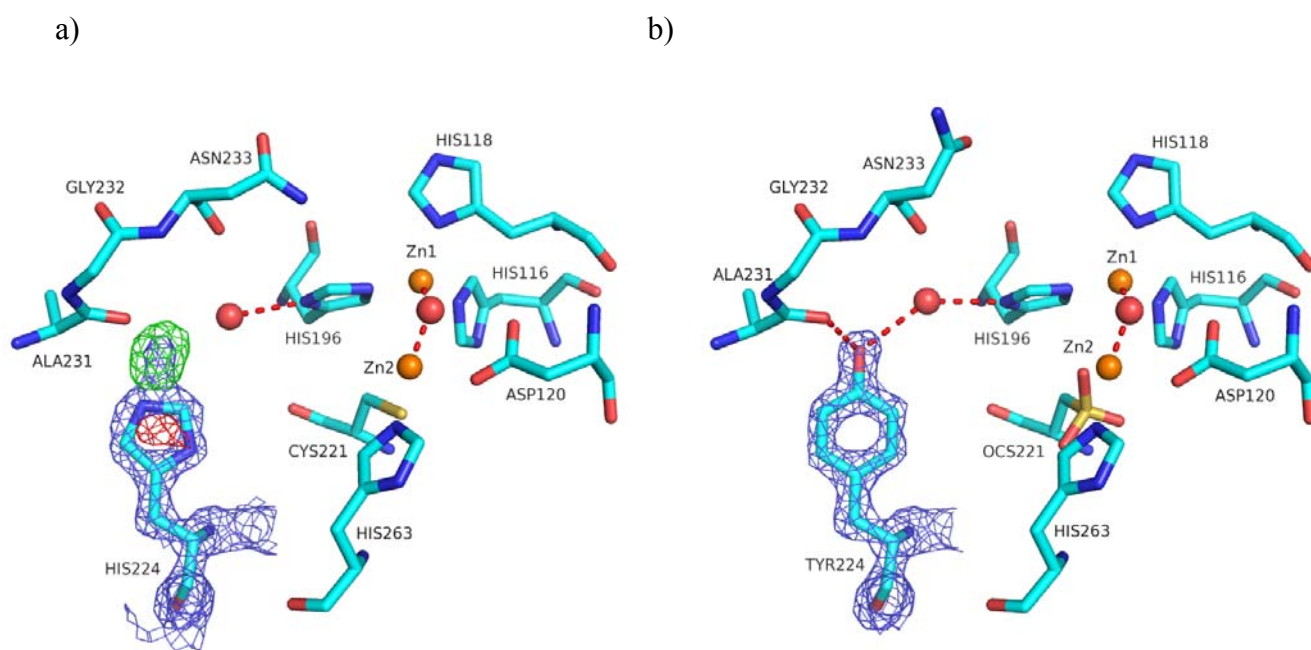
Figure 32: Electron density maps. a) The starting and b) final election density maps of residue 224 in the VIM-7 H224Y crystal structure. The $2F_o$-F_c map is displayed at 1.5 σ (blue) and the F_o-F_c maps at +3.5 σ (green) and -3.5σ (red). The atoms are colour-coded on the basis of atom type (cyan, carbon; blue, nitrogen; red, oxygen; yellow, sulfur; and orange, zinc).

The crystal structure of the VIM-7 H224Y mutant was solved with molecular replacement of VIM-7 wt (Figure 32). The Fourier difference map F_o-F_c is the difference map, where the green electron density represents the presence of electrons which are not provided by the structure of VIM-7 wt. The red electron density in the F_o-F_c represents the presence of excessive electrons, which is present when a histidine five-carbon-ring is substituting a tyrosine six-carbon-ring (Figure 32a). The blue electron density map is given by the $2F_o$-F_c, which is given by the F_o observed structure factors and F_c calculated structure factor (Figure 32b).

The cysteine 221 residue in VIM-7 wt (Figure 32a) was oxidized in the VIM-7 H224Y mutant (Figure 32b), which is a result of not sufficient amounts of β-mercaptoethanol in the protein solution prior to crystallization [29].

To conclude, the VIM-7 H224Y mutant was crystallized, and the structure of the mutant was successfully determined by molecular refinement.

Discussion

Cloning of VIM-7 wt and site-directed mutagenesis of VIM-7 D120A, VIM-7 D120N and VIM-7 H224Y

The *bla*$_{VIM-7}$ wild type gene, coding for the protein sequence A26-E264, was successfully cloned into the expression vector pDEST14 with an N-terminal his-tag and a TEV cleavage site, using the Gateway cloning system.

Mutations were introduced into *bla*$_{VIM-7}$, and the three different pDEST14 constructs encoding the VIM-7 mutations D120A, D120N and H224Y (Figure 18) were Sanger sequenced to analyse whether the desired point mutations were present (Figure 19). All mutants were successfully obtained.

Challenges with protein expression

The VIM-7 wt, VIM-7 D120A and VIM-7 H224Y mutants were all expressed in small scale in the *E. coli* strains Rosetta2(DE3)pLysS and BL21(DE3)star/pRARE/pLysS. The VIM-7 wt, VIM-7 D120A and VIM-7 H224Y mutants were produced in large scale expression in Rosetta2(DE3)pLysS successfully, and was purified and further used for enzyme kinetic studies and crystallization trials for the VIM-7 H224Y mutant.

The introduction of VIM-7 D120N mutant, on the other hand, was not observable in either small or large scale protein expression. The sequencing result of VIM-7 D120N mutant gave a low-intensity chromatogram (figure 19), which might indicate that the sequencing reaction was not optimal. However, even if the intensity was low, the spectre did show correct mutation nucleotide and the sequence was overall correct. In several attempts, in solubility experiments with different buffers, and in small and large scale expression experiments, the VIM-7 D120N mutant would not be induced. The reason for this is not known.

An alternative experiment to detect the recombinant VIM-7 D120N mutant would be to analyse the mutant by western blotting. In this method, proteins are initially separated by gel electrophoresis before the protein are transferred to a nitrocellulose membrane, where they are detected by using epitop specific antibodies [135]. This method would be much more sensitive than SimpleBlue Safe standard stained SDS-PAGE.

Screening for new clones of VIM-7 D120N mutant might, however, be a more promising way to obtain the recombinant protein.

Structure and enzymatic activity hypothesis for the VIM-7 D120N mutant

The VIM-7 D120N mutant was expected to be isostructural to the VIM-7 wt structure, because the atoms of the amino acid asparagine (N) fill the same space as the amino acid aspartic acid (D). The aspartic acid amino acid has a negative charge, whereas asparagine amino acid has a polar uncharged side chain, which, according to previous studies of D120N mutations [4], would have a great impact on the activity of the mutant.

The metal-binding of D120 in metallo-β-lactamases play an important role in catalysis. The position of D120, with a negatively charged oxygen located directly below the bridging group in the active site, shows how it coordinates Zn2 $^{2+}$ (Figure 6). Previous studies have shown that D120 plays an important role in the enzymatic activity. It has also been hypothesized that D120, in addition to being a metal-binding ligand, electrostatically interacts with the bridging hydroxide, properly positioning it for nucleophilic attack on the substrate (Figure 6) [4, 45, 136].

Previous studies of the D120N mutant in the L1 metallo-β-lactamase (L1) from *Stenotrophomonas maltophilia* have shown that the mutant conserves the dinuclear Zn center with a bridging water molecule present. The L1 D120N mutant is catalytically hindered, as the coordination of Zn2 is changed. The water molecule was also not coordinated by the L1 D120N mutant. The catalytic activity of the L1 D120N mutant was lower than the activity of the L1 wt, due to the loss of substrate-enzyme interaction and the loss of proton transfer to the substrate amide nitrogen [4, 45].

The effect of the D120N mutation in VIM-7, however, remains to be shown.

Purification of VIM-7 wt, VIM-7 D120A mutant and VIM-7 H224Y mutant

The proteins VIM-7 wt, VIM-7 D120A mutant and VIM-7 H224Y mutant were all successfully purified by the affinity purification method both before (Figures 21, 23 and 25) and after TEV-cleavage and dialysis (Figures 22, 24 and 26).

The SDS-PAGE analysis of the VIM-7 H224Y mutant was overloaded with protein. Hence, other proteins on the gel were more visible (Figure 26b). Size-exclusion purification, by gel filtration, was performed on the VIM-7 H224Y mutant (Figure 27). The observed shoulder in the gel filtration chromatogram (Figure 27) of the VIM-7 H224Y mutant indicates that the protein solution might contain multimeric complexes.

A pink colour of fractions 23 and 24 (Figure 25a) of the VIM-7 H224Y mutant after the first affinity purification appeared. This might be due to the presence of the two Zn ions in

the VIM-7 H224Y. Another assumption was a contamination, however, is less likely. The colour of the fractions had nothing to do with the high absorbance in the purification (Figure 25a), as the pink colour is measured at approximately 700 nm, and not 280 nm that was used in the purification. The SDS-PAGE analysis, however, showed extensive yields of the VIM-7 H224Y protein with contaminants. This was further supported by measuring the protein concentration of the pooled fractions, 7.7 mg/ml.

Epsilometer test

The results from the E-tests (Table 5) were not in accordance with the enzyme kinetic studies (Table 4). One reason for this might be that the expression vector, pDEST14, which is tightly regulated. The *E. coli* strain Rosetta2(DE3)pLysS has a pLysS plasmid with a T7 lysozyme site, which inactivated the T7 RNA polymerase, making it unable to bind to the T7 promoter of the pDEST14 vector, hence, not expressing the VIM-7 gene. The low degree of expression did not affect the antibiotics, which was tested. For E-tests performed in medicine, the pDEST14 vector is not used as expression vector. Had the genes been cloned into another vector with constitutive expression, or IPTG added to the genes, we would expect the result of the VIM-7, VIM-7 D120A and VIM-7 H224Y to be different.

Activity testing by using nitrocefin

The E-test did not show the difference in activity of the VIM-7 wt and the VIM-7 D120A mutant and the VIM-7 H224Y mutant, while the difference in activity was shown by testing with the substrate nitrocefin (Figure 28). The VIM-7 H224Y mutant had an activity which was similar, and slightly lower than VIM-7 wt, for the substrate nitrocefin. The nitrcefin assay showed that the VIM-7 D120A mutant was inactive compared to the VIM-7 wt and the VIM-7 H224Y mutant.

Comments on the enzyme kinetics experimental design of the enzyme kinetics assay

For the enzyme kinetic studies, duplicates of all reactions with fourteen different substrate concentrations, ranging from 0.2 µM to 1000 µM, were performed. The addition of enzymes was required to be done as simultaneously as possible, since the hydrolysis of the substrates starts immediately. For the adding of enzyme to substrate one was depended on a

multi-channel pipette. By having a 96-well plate and a pipette with eight functional pipette tips, the application of the enzyme was done in four operations manually with a few seconds between the applications. Hence, the values in the hydrolysis would be somewhat different, than values from an assay where the addition of enzymes was done simultaneously, for example by a robot that could handle the whole plate simultaneously. Fewer outliers would probably be defined.

The enzyme kinetics studies of VIM-7 wt and VIM-7 H224Y mutant were successfully performed with the antibiotics; ertapenem, meropenem, cefuroxime, cefepime, ceftazidime and cefoxitin. The VIM-7 D120A mutant was only tested with the substrate ertapenem. The VIM-7 D120A enzyme, even at a final concentration ten times higher than the VIM-7 wt and VIM-7 H224Y mutant, did still not hydrolyse the substrate. Taken together with the activity testing with nitrocefin (Figure 28), we concluded that the VIM-7 D120A mutant was inactive.

Enzyme kinetics and structure hypothesis for the VIM-7 D120A mutant

The VIM-7 D120A mutant was only tested with the carbapenem substrate, ertapenem. The reason for not screening the whole panel of substrates was its inactivity toward nitrocefin. By increasing the concentration of the VIM-7 D120A ten times, compared to the concentration of the VIM-7 wt and the VIM-7 H224, the substrate would still not be hydrolysed completely (Figure 29b). The K_m value of the VIM-7 D120A is relatively high, compared to all of the K_m values of the VIM-7 wt and the VIM-7 H224Y mutant, and the k_{cat}/K_m has a significantly low value. With such low rate efficiency, the enzyme-substrate complex converts a lesser proportion of the substrate to product. Thus, we concluded that the VIM-7 D120A mutant was inactive, and other substrates needed not to be tested for kinetic studies. The low activity of the VIM-7 D120A mutant was in accordance with previous studies of how alanine substitution of the D120 residue causes a decrease in catalytic efficiency in the metallo-β-lactamase IMP-1 [136]. As previously described, it is known that the D120 residue in metallo-β-lactamase is important for catalysis [4, 45].

As no crystallization trials for the VIM-7 D120A mutant were set up, due to a lack of protein, the structure is yet unknown. However, mutation of the D120 residue to alanine in metallo-β-lactamase IMP-1 did not show any modification in the overall protein fold [136]. By assuming that the overall fold of the VIM-7 D120A mutant is identical to the VIM-7 wild

type except for the substituted residue, one can predict that the activity of the mutant will be similar to previously described D120A mutations of metallo-β-lactamases.

In the predicted *in silico* structure of VIM-7 D120A mutant, the D120 residue is expected to be replaced by an alanine residue, while the other residues in the protein remain at the same position (Figure 33). The alanine at position 120, being hydrophobic and at a larger distance from Zn than aspartic acid, will most likely not bind and activate the metal-bridging water/hydroxide between the two Zn ions. The D120 residue does activate and bind to the Zn and the metal-bridging water/hydroxide via hydrogen bonding from its carboxylate side chain (Figure 6). The optimal position of the Zn ions for catalytic activity, which are coordinated by the D120 residue in the wild type, is most likely not facilitated by the D120A mutant. The loss of interaction with Zn is likely to result in a more flexible active site than in the VIM-7 wt, which further prevents productive substrate-binding. The D120A residue might also alter the process of proton transfer from water to nitrogen of the substrate. One of the Zn ions in the metallo-β-lactamase VIM-7 D120A might even be lost in a similar way to what was shown for IMP-1 [136].
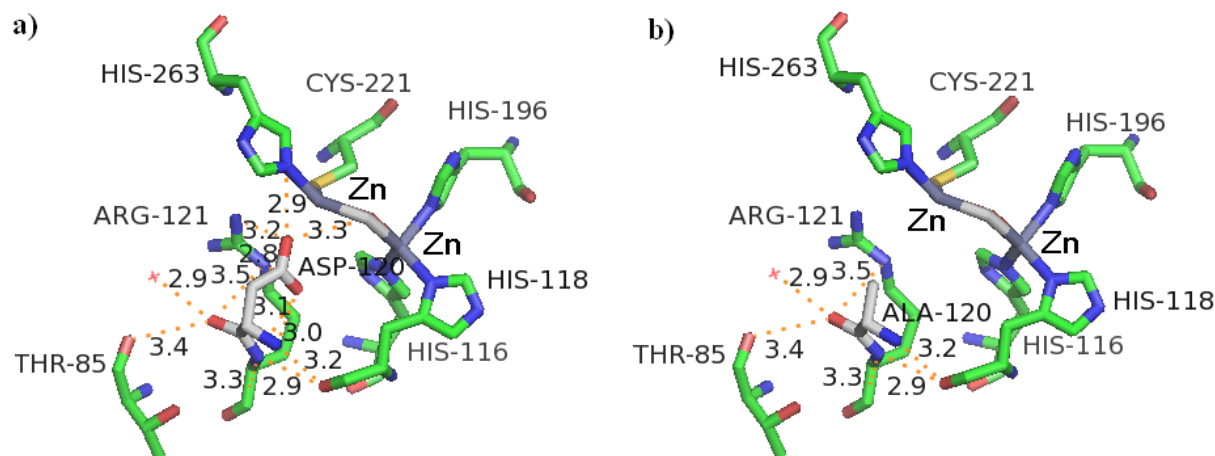
Figure 33: (a) The active site of VIM-7 wt PDB ID: 2Y87 [29], and (b) how the active site of the mutated VIM-7 D120A is predicted to be. The green indicate carbon atoms, red indicate oxygen, blue indicate nitrogen, yellow indicate sulphur, dark grey indicate Zn ions, light grey between the two Zn ions indicate the metal-bridging with water, and grey atoms indicate the target residue for mutation in a) and the mutation in b). The VIM-7 D120A was generated *in silico* in the PyMOL Molecular Graphics System.

Enzyme kinetics of the VIM-7 wt and the VIM-7 H224Y mutant

The enzyme kinetic assay results showed to have a higher catalytic efficiency for four of six substrates for the VIM-7 H224Y mutant compared to the VIM-7 wt (Table 4). The two β-lactam substrates, the carbapenem meropenem and the cephalosporin cefuroxime a higher catalytic efficiency was shown for the VIM-7 wt over the H224Y mutant.

The K_m values of the carbepenem substrate ertapenem (structure shown in Figure 34a) with the VIM-7 wt and the VIM-7 H224Y mutant is similar when considering the standard deviations (Table 4). The k_{cat} is four times higher for the VIM-7 H224Y mutant than for the VIM-7 wt. The catalytic efficiency is four times higher for the VIM-7 H224Y mutant, compared to the VIM-7 wt. The decisive factor for the higher catalytic efficiency for the VIM-7 H224Y mutant is the velocity of the reaction.

The K_m values of the VIM-7 wt and the VIM-7 H224Y mutant with the carbapenem substrate meropenem (structure shown in Figure 34b) shows a K_m value which is two times higher for the VIM-7 H224Y mutant, indicating that the substrate binds more firmly to the VIM-7 wt (Table 4). The turnover number k_{cat} of VIM-7 wt and the VIM-7 H224Y mutant are similar. The catalytic efficiency, k_{cat}/K_m, is two times greater for VIM-7 wt compared to the VIM-7 H224Y mutant, which implies that the increased binding of the meropenem substrate to the VIM-7 wt generates the higher catalytic efficiency compared to the VIM-7 H224Y mutant.
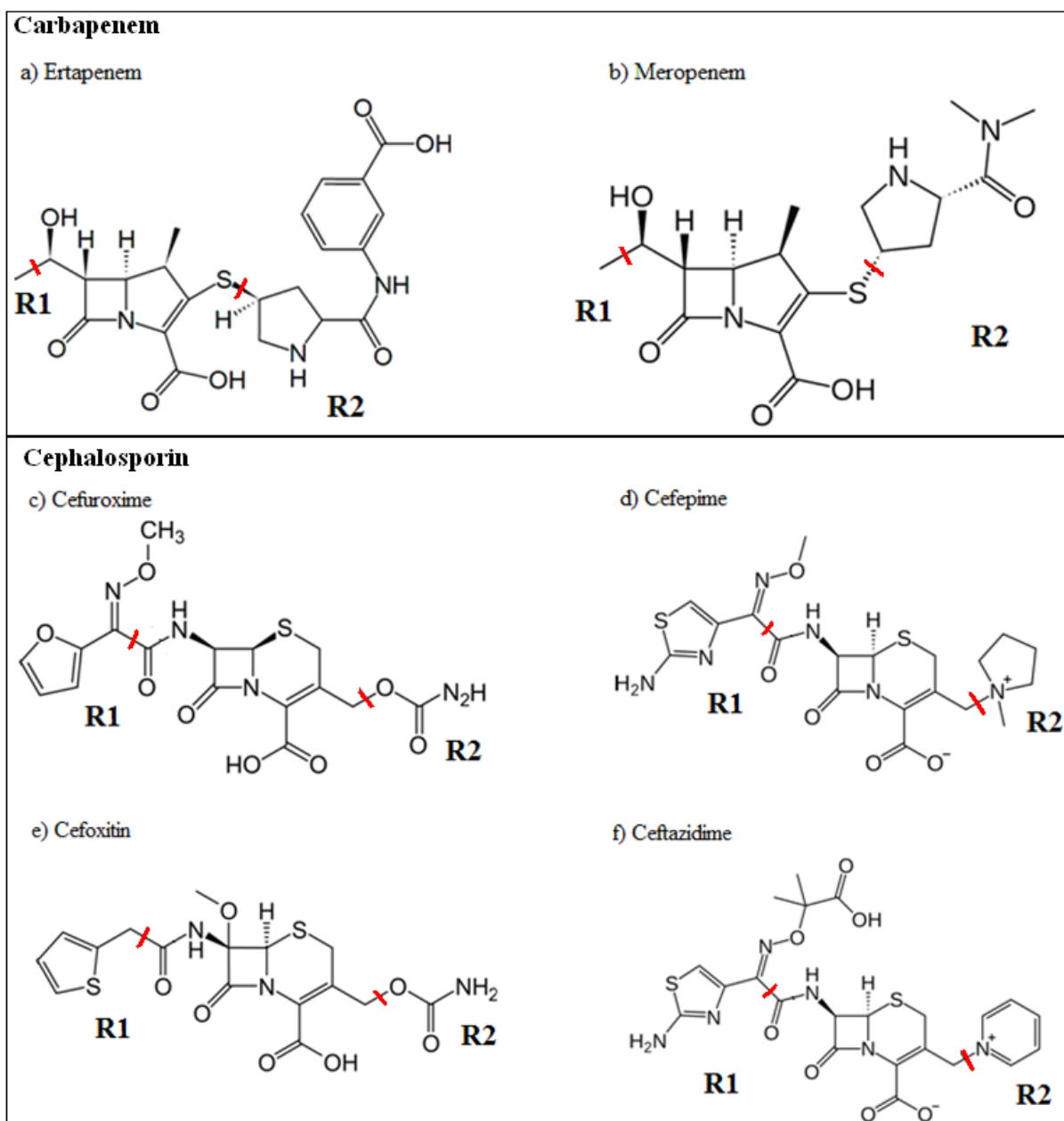
Figure 34: Structure formula of β-lactam substrates, the carbapenems a) ertapenem, b) meropenem and the cephalosporins c) cefuroxime, d) cefepime, e) cefoxitin and f) ceftazidime. The side groups R1 and R2 are indicated by red lines. The structure formulas were obtained from Wikipedia.

The enzyme kinetics with the cephalosporin substrate cefuroxime with a polar R2 group (structure shown in Figure 34c) showed a higher catalytic efficiency with VIM-7 wt compared to the VIM-7 H224Y mutant. The k_{cat} of VIM-7 wt was lower, by being approximately 70% of the k_{cat} of VIM-7 H224Y. The K_m of VIM-7 H224Y mutant is two times higher than the K_m of VIM-7 wt. Although the enzymatic reaction is faster for VIM-7 H224Y mutant, the binding affinity is the decisive factor, and this is stronger for the VIM-7 wt.

For the cephalosporin substrate cefoxitin with a polar R2 group (shown in Figure 34e), the binding affinity, K_m, of the VIM-7 wt and the VIM-7 H224Y mutant is similar. The turnover number, k_{cat}, is six times higher for the VIM-7 H224Y mutant than for the VIM-7 wt. The decisive factor for the catalytic efficiency, k_{cat}/K_m, for cefoxitin with the VIM-7 wt and the VIM-7 H224Y mutant is the k_{cat}, as the catalytic efficiency for the VIM-7 H224Y mutant is six times higher, than for cefoxitin with the VIM-7 wt.

Enzyme kinetics of the VIM-7 wt compared to the VIM-7 H224Y mutant with positively charged substrates

The cephalosporin substrate cefepime has a positively charged R2 group (Figure 34d). The catalytic efficiency was found to be ten times higher for the VIM-7 H224Y mutant, compared to the VIM-7 wt. The binding affinity, K_m, of the VIM-7 wt and the VIM-7 H224Y mutant is similar when considering the standard deviations. The turnover number, k_{cat}, is ten times higher for the VIM-7 H224Y mutant than for the VIM-7 wt. Hence, the decisive factor of the catalytic efficiency is the turnover number. The VIM-7 wt has a histidine residue which carries a positive charge when protonated, while the VIM-7 H224Y mutant, with a tyrosine in this position, has a neutral side chain. Two positive charges in the VIM-7 wt and cefepime may cause repulsion, and the binding of positively charged substrate to the positively charged active site may not be as firm as the binding of the substrate to a neutral active site. Hence, the cephalosporin substrate cefepime will bind more efficiently to the VIM-7 H224Y mutant.

The cephalosporin substrate ceftazidime was computationally docked into the VIM-7 H224Y structure. From the results in table 4, the VIM-7 H224Y mutant showed a five times higher catalytic efficiency k_{cat}/K_m than the VIM-7 wt. For ceftazidime the K_m of VIM-7 H224Y mutant is two times lower than the K_m for VIM-7 wt, which means that the substrate binds better to the VIM-7 H224Y mutant. The k_{cat} of VIM-7 H224Y mutant is three times higher than the wild type, which means that the reaction for the mutant is three times faster. The structure of the substrate ceftazidime (Figure 34f) has, like the substrate cefepime, a positively charged R2 group, the VIM-7 wt has a histidine residue which carries a positive charge when protonated, while the VIM-7 H224Y mutant has a neutral side chain. The active site of the VIM-7 H224Y mutant is less positively charged than the active site of the VIM-7 wt, and the positively charged substrate ceftazidime encounters less repulsion in the active site of the VIM-7 H224Y mutant. The ceftazidime might also form hydrogen bonding with the water molecule which is bound to the tyrosine 224 residue (TYR224 in Figure 35). This

strong bonding between the water and the tyrosine residue is not present in the wild type. Hence, the substrate ceftazidime will bind more efficiently to the H224Y mutant.

To sum up, the catalytic efficiencies of the cephalosporin substrates carrying a positively charged R2 group seem to be higher for the VIM-7 H224Y mutant than the catalytic efficiency for the VIM-7 wt.
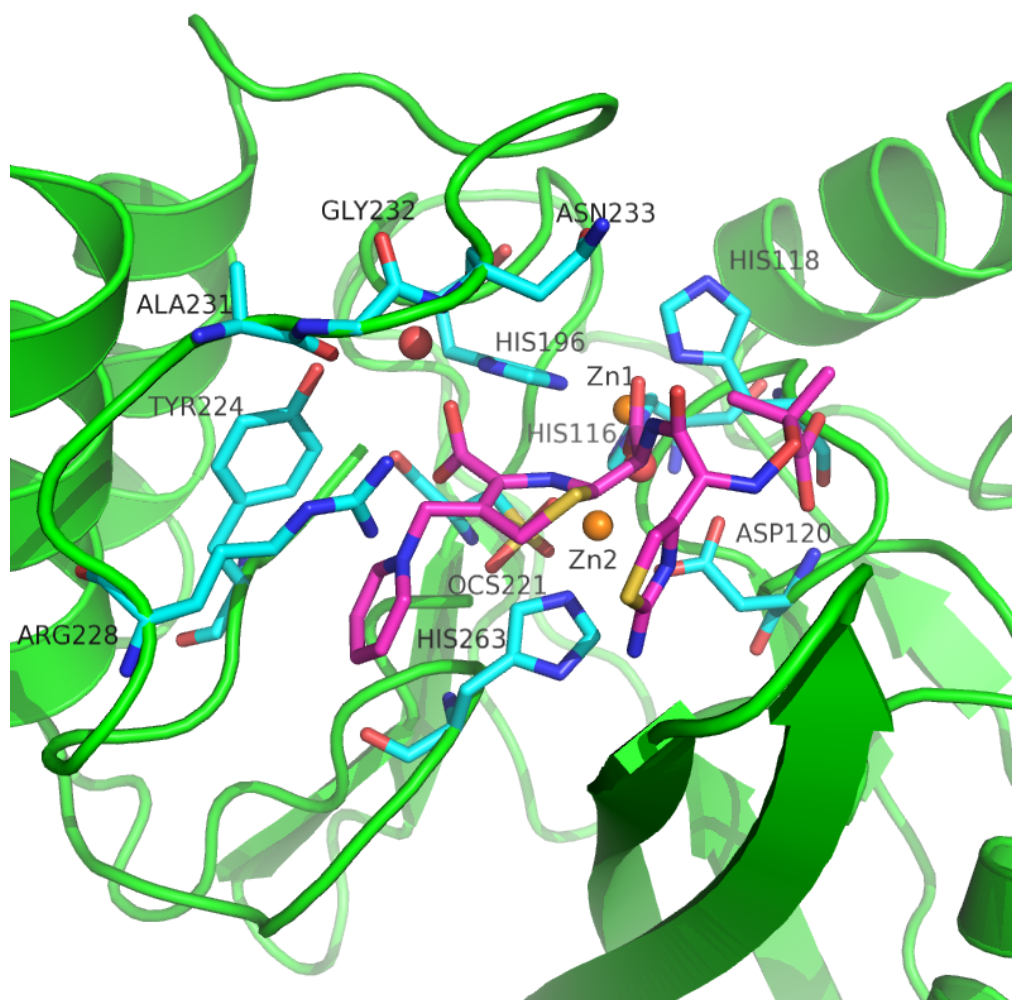

Figure 35: The cephalosporin substrate ceftazidime computationally docked in the VIM-7 H224Y mutant. The docking was performed using the structure of the VIM-7 which has been docked with ceftazidime, superimposed on the solved crystal structure of the VIM-7 H224Y mutant. green indicate the secondary structure of the VIM-7 H224Y mutant, the cyan indicate the carbon atoms in the active site residues, the blue indicate the nitrogen atoms, the red indicate the oxygen atoms, yellow indicate the sulphur atoms. The red spheres indicate water molecules, while orange spheres indicate Zn ions. The magenta indicates the carbons in the cephalosporin substrate ceftazidime. The positively charged R2 group (Figure 35f) is in the left of the ceftazidime substrate. The docking was performed in the PyMOL Molecular Graphics System.

The VIM-7 H224Y structure

The overall structure of the VIM-7 H224Y mutant had a αββα fold, as the solved crystal structure of VIM-7 [29].

The obtained VIM-7 H224Y crystal structure, although not located close enough to directly form bonding with the Zn ions, shows to influence the catalytic efficiency. One observation made was that the Arginine residue at position 228 in the VIM-7 H224Y mutant had changed the conformation when comparing to the previously solved VIM-7 structure. The tyrosine at position 224 makes two hydrogen bonds; one hydrogen binds to an A231, and another hydrogen binds to a water molecule, which again, hydrogen binds to His196, which is one of the Zn coordinating residues (Figure 32). The two hydrogen bonds formed in the VIM-7 H224Y mutant make the active site of the protein more rigid compared to the active site in the wild type. This may result in reduced flexibility for the other residues in the active site, and the β-lactam substrates may form tighter bonding in the active site, compared to the wild type.

Conclusion

The VIM-7 wild type gene, coding for the protein sequence A26-E264, with an N-terminal hexahis-tag and a TEV cleavage site was cloned. The VIM-7 mutations D120A, D120N and H224Y were designed, produced and sequenced. The VIM-7 wt, the VIM-7 D120A mutant and the VIM-7 H224Y mutant were produced, affinity purified and activity tested with the nitrocefin assay. In addition, the VIM-7 H224Y mutant was purified with gel filtration. Enzyme kinetic studies were performed on the VIM-7 wt and the VIM-7 H224Y mutant. The VIM-7 D120A mutant was tested against the substrate ertapenem, and showed to be inactive. The crystal structure of the VIM-7 H224Y mutant was solved, and the overall structure fold was maintained compared to the native VIM-7. The

The mutation of D120 residue to an alanine amino acid results in an inactive enzyme, which strengthen the hypothesis of the importance of the D120 residue in the active site. The mutation of H224 residue to a tyrosine amino acid results in a significantly higher catalytic efficiency when comparing to the VIM-7 wt. For substrates like the carbapenem substrate ertapenem, the cephalosporin substrates cefepime, the ceftazidime and the cefoxitin the mutant showed four, ten, five and six times higher catalytic activity respectively.

In this study, it was shown that the mutation of one single amino acid had a huge impact on the catalytic properties of the enzyme, as shown with the VIM-7 D120A mutant and the VIM-7 H224Y mutant.

Future work

There were not set crystallization trials for the VIM-7 D120A mutant, and this would be the next natural step in studying the structure of the VIM-7 D120A mutant in detail. For the VIM-7 D120N mutant, new clones would be screened in order to obtain the recombinant protein. The VIM-7 D120N mutant would further contribute in the studies of the importance of the D120 residue in the active site of the VIM-7. Further, the VIM-7 D120A mutant, the VIM-7 D120N mutant and the VIM-7 H224Y mutant should be docked with different antibiotic substrates in order to study their interaction. The inactive VIM-7 D120A mutant is more likely to obtain an enzyme-substrate crystal structure, compared to active mutants, as the substrate in the inactive D120A mutant probably will be remained intact and not enzymatically cleaved.

The next step is to screen for inhibitors and perform cocrystallization of the inhibitor-enzyme complex, to study what effect the inhibitor would have on the active site of the enzyme.

References

1. Levy, S.B. and B. Marshall, *Antibacterial resistance worldwide: causes, challenges and responses.* Nat Med, 2004. 10(12 Suppl): p. S122-9.
2. Molstad, S., C.S. Lundborg, A.K. Karlsson and O. Cars, *Antibiotic prescription rates vary markedly between 13 European countries.* Scandinavian Journal of Infectious Diseases, 2002. 34(5): p. 366-371.
3. Walsh, T.R., M.A. Toleman, L. Poirel and P. Nordmann, *Metallo-beta-lactamases: the quiet before the storm?* Clinical Microbiology Reviews, 2005. 18(2): p. 306-+.
4. Garrity, J.D., A.L. Carenbauer, L.R. Herron and M.W. Crowder, *Metal binding Asp-120 in metallo-beta-lactamase L1 from Stenotrophomonas maltophilia plays a crucial role in catalysis.* J Biol Chem, 2004. 279(2): p. 920-7.
5. *Usage of antimicrobial agents and occurrence of antimicrobial resistance in Norway*. 2006 10.05.2012]; Available from: http://www.vetinst.no/nor/Publikasjoner/Norm-Norm-Vet-rapporten.
6. Page, M.I. and A.P. Laws, *The mechanism of catalysis and the inhibition of beta-lactamases.* Chemical Communications, 1998(16): p. 1609-1617.
7. Matagne, A., A. Dubus, M. Galleni and J.M. Frere, *The beta-lactamase cycle: a tale of selective pressure and bacterial ingenuity.* Nat Prod Rep, 1999. 16(1): p. 1-19.
8. Ambler, R.P., *The structure of beta-lactamases.* Philos Trans R Soc Lond B Biol Sci, 1980. 289(1036): p. 321-31.
9. Bush, K. and G.A. Jacoby, *Updated functional classification of beta-lactamases.* Antimicrob Agents Chemother, 2010. 54(3): p. 969-76.
10. Hall, B.G. and M. Barlow, *Evolution of the serine beta-lactamases: past, present and future.* Drug Resist Updat, 2004. 7(2): p. 111-23.
11. Walsh, T.R., M.A. Toleman, L. Poirel and P. Nordmann, *Metallo-beta-lactamases: the quiet before the storm?* Clin Microbiol Rev, 2005. 18(2): p. 306-25.
12. Galleni, M., J. Lamotte-Brasseur, G.M. Rossolini, J. Spencer, O. Dideberg and J.M. Frere, *Standard numbering scheme for class B beta-lactamases.* Antimicrob Agents Chemother, 2001. 45(3): p. 660-3.
13. Rasmussen, B.A. and K. Bush, *Carbapenem-hydrolyzing beta-lactamases.* Antimicrob Agents Chemother, 1997. 41(2): p. 223-32.
14. Felici, A., G. Amicosante, A. Oratore, R. Strom, P. Ledent, B. Joris, L. Fanuel and J.M. Frere, *An overview of the kinetic parameters of class B beta-lactamases.* Biochemical Journal, 1993. 291 (Pt 1): p. 151-5.
15. Sabath, L.D. and E.P. Abraham, *Zinc as a Cofactor for Cephalosporinase from Bacillus Cereus 569.* Biochemical Journal, 1966. 98(1): p. C11-&.
16. Hussain, M., A. Carlino, M.J. Madonna and J.O. Lampen, *Cloning and Sequencing of the Metallothioprotein Beta-Lactamase-Ii Gene of Bacillus-Cereus 569/H in Escherichia-Coli.* Journal of Bacteriology, 1985. 164(1): p. 223-229.
17. Jacobson, R.K., N. Minenza, M. Nicol and C. Bamford, *VIM-2 metallo-beta-lactamase-producing Pseudomonas aeruginosa causing an outbreak in South Africa.* J Antimicrob Chemother, 2012.
18. Senda, K., Y. Arakawa, S. Ichiyama, K. Nakashima, H. Ito, S. Ohsuka, K. Shimokata, N. Kato and M. Ohta, *PCR detection of metallo-beta-lactamase gene (blaIMP) in gram-negative rods resistant to broad-spectrum beta-lactams.* J Clin Microbiol, 1996. 34(12): p. 2909-13.

19.   Mulvey, M.R., J.M. Grant, K. Plewes, D. Roscoe and D.A. Boyd, *New Delhi metallo-beta-lactamase in Klebsiella pneumoniae and Escherichia coli, Canada.* Emerg Infect Dis, 2011. 17(1): p. 103-6.

20.   Marumo, K., A. Takeda, Y. Nakamura and K. Nakaya, *Purification and characterization of metallo-beta-lactamase from Serratia marcescens.* Microbiol Immunol, 1995. 39(1): p. 27-33.

21.   Felici, A., M. Perilli, N. Franceschini, G.M. Rossolini, M. Galleni, J.M. Frere, A. Oratore and G. Amicosante, *Sensitivity of Aeromonas hydrophila carbapenemase to delta3-cephems: comparative study with other metallo-beta-lactamases.* Antimicrob Agents Chemother, 1997. 41(4): p. 866-8.

22.   Walsh, T.R., W.A. Neville, M.H. Haran, D. Tolson, D.J. Payne, J.H. Bateson, A.P. MacGowan and P.M. Bennett, *Nucleotide and amino acid sequences of the metallo-beta-lactamase, ImiS, from Aeromonas veronii bv. sobria.* Antimicrob Agents Chemother, 1998. 42(2): p. 436-9.

23.   Ullah, J.H., T.R. Walsh, I.A. Taylor, D.C. Emery, C.S. Verma, S.J. Gamblin and J. Spencer, *The crystal structure of the L1 metallo-beta-lactamase from Stenotrophomonas maltophilia at 1.7 angstrom resolution.* J Mol Biol, 1998. 284(1): p. 125-136.

24.   Yang, Y., B.A. Rasmussen and K. Bush, *Biochemical characterization of the metallo-beta-lactamase CcrA from Bacteroides fragilis TAL3636.* Antimicrob Agents Chemother, 1992. 36(5): p. 1155-7.

25.   Edwards, R., C.V. Hawkyard and P.S. Hashmi, *Biological assay for the detection of metallo-beta-lactamases in Bacteroides fragilis.* Br J Biomed Sci, 1998. 55(3): p. 169-71.

26.   Bebrone, C., *Metallo-beta-lactamases (classification, activity, genetic organization, structure, zinc coordination) and their superfamily.* Biochem Pharmacol, 2007. 74(12): p. 1686-1701.

27.   Gomes, C.M., C. Frazao, A.V. Xavier, J. Legall and M. Teixeira, *Functional control of the binuclear metal site in the metallo-beta-lactamase-like fold by subtle amino acid replacements.* Protein Sci, 2002. 11(3): p. 707-12.

28.   Thornalley, P.J., *The glyoxalase system: new developments towards functional characterization of a metabolic pathway fundamental to biological life.* Biochemical Journal, 1990. 269(1): p. 1-11.

29.   Borra, P.S., H.K. Leiros, R. Ahmad, J. Spencer, I. Leiros, T.R. Walsh, A. Sundsfjord and O. Samuelsen, *Structural and computational investigations of VIM-7: insights into the substrate specificity of vim metallo-beta-lactamases.* J Mol Biol, 2011. 411(1): p. 174-89.

30.   Iversen, B.G., T. Jacobsen, H.M. Eriksen, G. Bukholm, K.K. Melby, K. Nygard and P. Aavitsland, *An outbreak of Pseudomonas aeruginosa infection caused by contaminated mouth swabs.* Clin Infect Dis, 2007. 44(6): p. 794-801.

31.   Itah, A.Y. and J.P. Essien, *Growth profile and hydrocarbonoclastic potential of microorganisms isolated from tarballs in the Bight of Bonny, Nigeria.* World Journal of Microbiology & Biotechnology, 2005. 21(6-7): p. 1317-1322.

32.   Homma, H., A. Yamanaka, S. Tanimoto, M. Tamura, Y. Chijimatsu, S. Kira and T. Izumi, *Diffuse Panbronchiolitis - a Disease of the Transitional Zone of the Lung.* Chest, 1983. 83(1): p. 63-69.

33.   Lauretti, L., M.L. Riccio, A. Mazzariol, G. Cornaglia, G. Amicosante, R. Fontana and G.M. Rossolini, *Cloning and characterization of blaVIM, a new integron-borne metallo-beta-lactamase gene from a Pseudomonas aeruginosa clinical isolate.* Antimicrob Agents Chemother, 1999. 43(7): p. 1584-90.

34.   Vatopoulos, A., *High rates of metallo-beta-lactamase-producing Klebsiella pneumoniae in Greece--a review of the current evidence.* Euro Surveill, 2008. 13(4).

35.   Bogaerts, P., T.D. Huang, H. Rodriguez-Villalobos, C. Bauraing, A. Deplano, M.J. Struelens and Y. Glupczynski, *Nosocomial infections caused by multidrug-resistant Pseudomonas putida isolates producing VIM-2 and VIM-4 metallo-beta-lactamases.* J Antimicrob Chemother, 2008. 61(3): p. 749-51.

36.   Tsakris, A., S. Pournaras, N. Woodford, M.F. Palepou, G.S. Babini, J. Douboyas and D.M. Livermore, *Outbreak of infections caused by Pseudomonas aeruginosa producing VIM-1 carbapenemase in Greece.* J Clin Microbiol, 2000. 38(3): p. 1290-2.

37.   Poirel, L., T. Naas, D. Nicolas, L. Collet, S. Bellais, J.D. Cavallo and P. Nordmann, *Characterization of VIM-2, a carbapenem-hydrolyzing metallo-beta-lactamase and its plasmid- and integron-borne gene from a Pseudomonas aeruginosa clinical isolate in France.* Antimicrob Agents Chemother, 2000. 44(4): p. 891-7.

38.   Villegas, M.V., K. Lolans, M. del Rosario Olivera, C.J. Suarez, A. Correa, A.M. Queenan and J.P. Quinn, *First detection of metallo-beta-lactamase VIM-2 in Pseudomonas aeruginosa isolates from Colombia.* Antimicrob Agents Chemother, 2006. 50(1): p. 226-9.

39.   *Update: Detection of a Verona Integron-Encoded Metallo-Beta-Lactamase in Klebsiella pneumoniae-United States, 2010 (Reprinted from MMWR, vol 59, pg 1212, 2010).* Jama-Journal of the American Medical Association, 2010. 304(19): p. 2122-2122.

40.   Toleman, M.A., D. Biedenbach, D.M. Bennett, R.N. Jones and T.R. Walsh, *Italian metallo-beta-lactamases: a national problem? Report from the SENTRY Antimicrobial Surveillance Programme.* J Antimicrob Chemother, 2005. 55(1): p. 61-70.

41.   Oteo, J., J.L. Hernandez-Almaraz, J. Gil-Anton, A. Vindel, S. Fernandez, V. Bautista and J. Campos, *Outbreak of vim-1-carbapenemase-producing Enterobacter cloacae in a pediatric intensive care unit.* Pediatr Infect Dis J, 2010. 29(12): p. 1144-6.

42.   Toleman, M.A., K. Rolston, R.N. Jones and T.R. Walsh, *blaVIM-7, an evolutionarily distinct metallo-beta-lactamase gene in a Pseudomonas aeruginosa isolate from the United States.* Antimicrob Agents Chemother, 2004. 48(1): p. 329-32.

43.   Samuelsen, O., M. Castanheira, T.R. Walsh and J. Spencer, *Kinetic characterization of VIM-7, a divergent member of the VIM metallo-beta-lactamase family.* Antimicrob Agents Chemother, 2008. 52(8): p. 2905-8.

44.   Garau, G., I. Garcia-Saez, C. Bebrone, C. Anne, P. Mercuri, M. Galleni, J.M. Frere and O. Dideberg, *Update of the standard numbering scheme for class B beta-lactamases.* Antimicrob Agents Chemother, 2004. 48(7): p. 2347-9.

45.   Crisp, J., R. Conners, J.D. Garrity, A.L. Carenbauer, M.W. Crowder and J. Spencer, *Structural basis for the role of Asp-120 in metallo-beta-lactamases.* Biochemistry, 2007. 46(37): p. 10664-74.

46.   Glick, B.R., J.J. Pasternak and C.L. Patten, *Molecular biotechnology : principles and applications of recombinant DNA.* 4th ed2010, Washington, DC: ASM Press. xvii, 1000 p.

47.   Fleming, A., *On the Antibacterial Action of Cultures of a Penicillium, with Special Reference to Their Use in the Isolation of B. Influenzae.* British Journal of Experimental Pathology, 1929. 10(3): p. 226-236.

48.   Waksman, S.A., *Antagonistic Relations of Microorganisms.* Bacteriol Rev, 1941. 5(3): p. 231-91.

49.   Waksman, S.A., *What Is an Antibiotic or an Antibiotic Substance.* Mycologia, 1947. 39(5): p. 565-569.

50.   Pankey, G.A. and L.D. Sabath, *Clinical relevance of bacteriostatic versus bactericidal mechanisms of action in the treatment of gram-positive bacterial infections.* Clinical Infectious Diseases, 2004. 38(6): p. 864-870.

51.   Goossens, H., M. Ferech, R.V. Stichele, M. Elseviers and E.P. Grp, *Outpatient antibiotic use in Europe and association with resistance: a cross-national database study.* Lancet, 2005. 365(9459): p. 579-587.

52.   Kanoh, S. and B.K. Rubin, *Mechanisms of Action and Clinical Application of Macrolides as Immunomodulatory Medications.* Clinical Microbiology Reviews, 2010. 23(3): p. 590-+.

53.   Gaynor, M. and A.S. Mankin, *Macrolide antibiotics: Binding site, mechanism of action, resistance.* Current Topics in Medicinal Chemistry, 2003. 3(9): p. 949-960.

54.   Vazquez, D., M. Barbacid and L. Carrasco, *Inhibitors of mammalian protein synthesis.* Hamatol Bluttransfus, 1974. 14: p. 327-40.

55.   Wierzbowski, A.K., D.J. Hoban, T. Hisanaga, M. DeCorby and G.G. Zhanel, *The use of Macrolides in treatment of upper respiratory tract infections.* Current Allergy and Asthma Reports, 2006. 6(2): p. 171-181.

56.   Kudoh, S., A. Azuma, M. Yamamoto, T. Izumi and M. Ando, *Improvement of survival in patients with diffuse panbronchiolitis treated with low-dose erythromycin.* American Journal of Respiratory and Critical Care Medicine, 1998. 157(6): p. 1829-1832.

57.   Cooper, M.R., C.R. Durand, M.T. Beaulac and M. Steinberg, *Single-agent, broad-spectrum fluoroquinolones for the outpatient treatment of low-risk febrile neutropenia.* Ann Pharmacother, 2011. 45(9): p. 1094-102.

58.   Oliphant, C.M. and G.M. Green, *Quinolones: a comprehensive review.* American Family Physician, 2002. 65(3): p. 455-64.

59.   Wispelwey, B., *Clinical implications of pharmacokinetics and pharmacodynamics of fluoroquinolones.* Clin Infect Dis, 2005. 41 Suppl 2: p. S127-35.

60.   Yoshida, H., M. Nakamura, M. Bogaki, H. Ito, T. Kojima, H. Hattori and S. Nakamura, *Mechanism of Action of Quinolones against Escherichia-Coli DNA Gyrase.* Antimicrob Agents Chemother, 1993. 37(4): p. 839-845.

61.   Hooper, D.C., *Emerging mechanisms of fluoroquinolone resistance.* Emerg Infect Dis, 2001. 7(2): p. 337-41.

62.   Holten, K.B. and E.M. Onusko, *Appropriate prescribing of oral beta-lactam antibiotics.* American Family Physician, 2000. 62(3): p. 611-620.

63.   Wang, Z., W. Fast, A.M. Valentine and S.J. Benkovic, *Metallo-beta-lactamase: structure and mechanism.* Curr Opin Chem Biol, 1999. 3(5): p. 614-22.

64.   Tenover, F.C., *Mechanisms of antimicrobial resistance in bacteria.* American Journal of Infection Control, 2006. 34(5): p. S3-S10.

65.   McManus, M.C., *Mechanisms of bacterial resistance to antimicrobial agents.* American Journal of Health-System Pharmacy, 1997. 54(12): p. 1420-1433.

66.   Elander, R.P., *Industrial production of beta-lactam antibiotics.* Applied Microbiology and Biotechnology, 2003. 61(5-6): p. 385-392.

67.   Antunez, C., N. Blanca-Lopez, M.J. Torres, C. Mayorga, E. Perez-Inestrosa, M.I. Montanez, T. Fernandez and M. Blanca, *Immediate allergic reactions to cephalosporins: evaluation of cross-reactivity with a panel of penicillins and cephalosporins.* J Allergy Clin Immunol, 2006. 117(2): p. 404-10.

68.   Dalhoff, A., N. Janjic and R. Echols, *Redefining penems.* Biochem Pharmacol, 2006. 71(7): p. 1085-95.

69.   Ligon, B.L., *Penicillin: its discovery and early development.* Semin Pediatr Infect Dis, 2004. 15(1): p. 52-7.

70.   *The Official Web Site of the Noble Prize*. [Web Page: www.nobelprize.org/].

71.   Malik, Z.A. and N. Litman, *Ampicillin and amoxicillin.* Pediatr Rev, 2006. 27(11): p. 434-6.

72.   Gonzaga, A.J., M. Antonio-Velmonte and T.E. Tupasi, *Cyclacillin: a clinical and in vitro profile.* J Infect Dis, 1974. 129(5): p. 545-51.

73.   Sykes, R.B., D.P. Bonner, K. Bush and N.H. Georgopapadakou, *Azthreonam (SQ 26,776), a synthetic monobactam specifically active against aerobic gram-negative bacteria.* Antimicrob Agents Chemother, 1982. 21(1): p. 85-92.

74.   Thompson, R.L., *Cephalosporin, carbapenem, and monobactam antibiotics.* Mayo Clin Proc, 1987. 62(9): p. 821-34.

75.   McPhee, S.J., M.A. Papadakis and M.W. Rabow, *Current medical diagnosis & treatment, 2012*. 51st ed2012, New York: McGraw-Hill. 1867 p.

76.   Livermore, D.M. and N. Woodford, *Carbapenemases: a problem in waiting?* Curr Opin Microbiol, 2000. 3(5): p. 489-95.

77.   Birnbaum, J., F.M. Kahan, H. Kropp and J.S. MacDonald, *Carbapenems, a new class of beta-lactam antibiotics. Discovery and development of imipenem/cilastatin.* American Journal of Medicine, 1985. 78(6A): p. 3-21.

78.   Pryka, R.D. and G.M. Haig, *Meropenem: a new carbapenem antimicrobial.* Ann Pharmacother, 1994. 28(9): p. 1045-54.

79.   Zhanel, G.G., C. Johanson, J.M. Embil, A. Noreddin, A. Gin, L. Vercaigne and D.J. Hoban, *Ertapenem: review of a new carbapenem.* Expert Rev Anti Infect Ther, 2005. 3(1): p. 23-39.

80.   Lang, M., P. Schneider, W. Tosch, R. Scartazzini and O. Zak, *The Penems, a New Class of Beta-Lactam Antibiotics .7. Synthesis and Antimicrobial Activity of 2-Hetero-Cyclylmercaptoalkyl Derivatives.* Journal of Antibiotics, 1986. 39(4): p. 525-534.

81.   Burton, H.S. and E.P. Abraham, *Isolation of Antibiotics from a Species of Cephalosporium - Cephalosporins P1,P2,P3,P4 and P5.* Biochemical Journal, 1951. 50(2): p. 168-174.

82.   Stapley, E.O., J. Birnbaum, A.K. Miller, H. Wallick, D. Hendlin and H.B. Woodruff, *Cefoxitin and cephamycins: microbiological studies.* Rev Infect Dis, 1979. 1(1): p. 73-89.

83.   Stapley, E.O., M. Jackson, S. Hernandez, S.B. Zimmerman, S.A. Currie, S. Mochales, J.M. Mata, H.B. Woodruff and D. Hendlin, *Cephamycins, a new family of beta-lactam antibiotics. I. Production by actinomycetes, including Streptomyces lactamdurans sp. n.* Antimicrob Agents Chemother, 1972. 2(3): p. 122-31.

84.   Birnbaum, J., E.O. Stapley, A.K. Miller, H. Wallick, D. Hendlin and H.B. Woodruff, *Cefoxitin, a semi-synthetic cephamycin: a microbiological overview.* J Antimicrob Chemother, 1978. 4(B): p. 15-32.

85.   Grzelak, E.M., I. Malinowska and I.M. Choma, *Determination of Cefacetrile and Cefuroxime Residues in Milk by Thin-Layer Chromatography.* Journal of Liquid Chromatography & Related Technologies, 2009. 32(14): p. 2043-2049.

86.   Tartaglione, T.A. and R.E. Polk, *Review of the new second-generation cephalosporins: cefonicid, ceforanide, and cefuroxime.* Drug Intell Clin Pharm, 1985. 19(3): p. 188-98.

87.   Antunes, N.T., H. Frase, M. Toth, S. Mobashery and S.B. Vakulenko, *Resistance to the third-generation cephalosporin ceftazidime by a deacylation-deficient mutant of the TEM beta-lactamase by the uncommon covalent-trapping mechanism.* Biochemistry, 2011. 50(29): p. 6387-95.

88.   Angelescu, M. and A. Apostol, *[Cefepime (maxipime), large spectrum 4th generation cephalosporin, resistant to beta-lactamases].* Chirurgia (Bucur), 2001. 96(6): p. 547-52.

89. Widmer, A.F., *Ceftobiprole: A new option for treatment of skin and soft-tissue infections due to methicillin-resistant Staphylococcus aureus.* Clinical Infectious Diseases, 2008. 46(5): p. 656-658.

90. Uri, J.V., *Detection of Beta-Lactamase Activity with Nitrocefin of Multiple Strains of Various Microbial Genera.* Acta Microbiologica Hungarica, 1985. 32(2): p. 133-145.

91. Livermore, D.M., *Interplay of Impermeability and Chromosomal Beta-Lactamase Activity in Imipenem-Resistant Pseudomonas-Aeruginosa.* Antimicrob Agents Chemother, 1992. 36(9): p. 2046-2048.

92. Murray, B.E. and B. Mederski-Samaroj, *Transferable beta-lactamase. A new mechanism for in vitro penicillin resistance in Streptococcus faecalis.* J Clin Invest, 1983. 72(3): p. 1168-71.

93. Peter-Getzlaff, S., S. Polsfuss, M. Poledica, M. Hombach, J. Giger, E.C. Bottger, R. Zbinden and G.V. Bloemberg, *Detection of AmpC beta-lactamase in Escherichia coli: comparison of three phenotypic confirmation assays and genetic analysis.* J Clin Microbiol, 2011. 49(8): p. 2924-32.

94. Simm, A.M., E.J. Loveridge, J. Crosby, M.B. Avison, T.R. Walsh and P.M. Bennett, *Bulgecin A: a novel inhibitor of binuclear metallo-beta-lactamases.* Biochemical Journal, 2005. 387(Pt 3): p. 585-90.

95. Walsh, T.R., S. Gamblin, D.C. Emery, A.P. MacGowan and P.M. Bennett, *Enzyme kinetics and biochemical analysis of ImiS, the metallo-beta-lactamase from Aeromonas sobria 163a.* J Antimicrob Chemother, 1996. 37(3): p. 423-31.

96. Bebrone, C., C. Moali, F. Mahy, S. Rival, J.D. Docquier, G.M. Rossolini, J. Fastrez, R.F. Pratt, J.M. Frere, and M. Galleni, *CENTA as a chromogenic substrate for studying beta-lactamases.* Antimicrob Agents Chemother, 2001. 45(6): p. 1868-71.

97. Danzer, L.A., *Liquid-Chromatographic Determination of Cephalosporins and Chloramphenicol in Serum.* Clinical Chemistry, 1983. 29(5): p. 856-858.

98. O'Callaghan, C.H., A. Morris, S.M. Kirby and A.H. Shingler, *Novel method for detection of beta-lactamases by using a chromogenic cephalosporin substrate.* Antimicrob Agents Chemother, 1972. 1(4): p. 283-8.

99. WHO. *Global Strategy for Containment of Antimicrobial Resistance.* 2001.

100. Levy, S.B., *The antibiotic paradox : how the misuse of antibiotics destroys their curative power*. 2nd ed2002, Cambridge, MA: Perseus Pub. xx, 353 p.

101. Bloom, B.R. and C.J.L. Murray, *Tuberculosis - Commentary on a Reemergent Killer.* Science, 1992. 257(5073): p. 1055-1064.

102. Bradford, P.A., *Extended-spectrum beta-lactamases in the 21st century: characterization, epidemiology, and detection of this important resistance threat.* Clinical Microbiology Reviews, 2001. 14(4): p. 933-51, table of contents.

103. Nordmann, P. and L. Poirel, *Emerging carbapenemases in Gram-negative aerobes.* Clinical Microbiology and Infection, 2002. 8(6): p. 321-331.

104. Nandi, S., J.J. Maurer, C. Hofacre and A.O. Summers, *Gram-positive bacteria are a major reservoir of Class 1 antibiotic resistance integrons in poultry litter.* Proc Natl Acad Sci U S A, 2004. 101(18): p. 7118-22.

105. Dowson, C.G., T.J. Coffey and B.G. Spratt, *Origin and molecular epidemiology of penicillin-binding-protein-mediated resistance to beta-lactam antibiotics.* Trends in Microbiology, 1994. 2(10): p. 361-6.

106. Spratt, B.G., *Resistance to antibiotics mediated by target alterations.* Science, 1994. 264(5157): p. 388-93.

107. Soares, S., K.G. Kristinsson, J.M. Musser and A. Tomasz, *Evidence for the introduction of a multiresistant clone of serotype 6B Streptococcus pneumoniae from Spain to Iceland in the late 1980s.* J Infect Dis, 1993. 168(1): p. 158-63.

108. Olson, B., R.A. Weinstein, C. Nathan, W. Chamberlin and S.A. Kabins, *Epidemiology of Endemic Pseudomonas-Aeruginosa - Why Infection Control Efforts Have Failed.* Journal of Infectious Diseases, 1984. 150(6): p. 808-816.

109. Colgan, R. and J.H. Powers, *Appropriate antimicrobial prescribing: Approaches that limit antibiotic resistance.* American Family Physician, 2001. 64(6): p. 999-1004.

110. Lawson, M. and A.L. Lawson, *Investigating the antibiotic resistance problem.* American Biology Teacher, 1998. 60(6): p. 412-417.

111. Atkins, P.W. and J. De Paula, *Atkins' Physical chemistry.* 8th ed2006, Oxford ; New York: Oxford University Press. xxx, 1064 p.

112. Price, N.C. and L. Stevens, *Fundamentals of enzymology : the cell and molecular biology of catalytic proteins.* 3rd ed1999, Oxford ; New York: Oxford University Press. xviii, 478 p., 7 col. plates.

113. Lehninger, A.L., D.L. Nelson and M.M. Cox, *Lehninger principles of biochemistry.* 4th ed2005, New York: W.H. Freeman.

114. Illanes, A., *Enzyme biocatalysis principles and applications*, 2008, Springer: [New York]. p. x, 391 p.

115. Nielsen, H., J. Engelbrecht, S. Brunak and G. von Heijne, *Identification of prokaryotic and eukaryotic signal peptides and prediction of their cleavage sites.* Protein Eng, 1997. 10(1): p. 1-6.

116. *The Signal P 4.0 Server.* [cited 12 21.03]; Available from: http://www.cbs.dtu.dk/services/SignalP/.

117. Esposito, D., L.A. Garvey and C.S. Chakiath, *Gateway cloning for protein expression.* Methods Mol Biol, 2009. 498: p. 31-54.

118. *The Basics of Gateway® Reactions.* 2012; Available from: https://www.invitrogen.com/site/us/en/home/Products-and-Services/Applications/Cloning/Gateway-Cloning/GatewayC-Misc/Protocols.html.

119. *ZR Plasmid Miniprep™-Classic.* Available from: http://www.zymoresearch.com/media/downloads/39/D4015i.pdf.

120. *DNA sequencing core facility.* Available from: http://www.unn.no/dna-sequencing/category11734.html.

121. *BioEdit Sequence Aligment Editor* Available from: http://www.mbio.ncsu.edu/bioedit/bioedit.html.

122. *Instruction manual - Z-Competent E. coli Transformation Kit & Buffer Set*, Z. Research, Editor.

123. *Superior Performance of Laemmi PAGE with Extended Self Life.* [cited 12 21.03]; Available from: http://www.bio-rad.com/webroot/web/pdf/lsr/literature/Bulletin_5871D.pdf.

124. Kapust, R.B., J. Tozser, T.D. Copeland and D.S. Waugh, *The P1' specificity of tobacco etch virus protease.* Biochem Biophys Res Commun, 2002. 294(5): p. 949-55.

125. Waugh, D.S. *TEV Protease FAQ* 2010; Available from: http://mcl1.ncifcrf.gov/waugh_tech/faq/tev.pdf.

126. *ProtParam.* Available from: http://web.expasy.org/protparam/.

127. Huang, M.B., C.N. Baker, S. Banerjee and F.C. Tenover, *Accuracy of the E test for determining antimicrobial susceptibilities of staphylococci, enterococci, Campylobacter jejuni, and gram-negative bacteria resistant to antimicrobial agents.* J Clin Microbiol, 1992. 30(12): p. 3243-8.

128. Siemann, S., D.P. Evanoff, L. Marrone, A.J. Clarke, T. Viswanatha and G.I. Dmitrienko, *N-arylsulfonyl hydrazones as inhibitors of IMP-1 metallo-beta-lactamase.* Antimicrob Agents Chemother, 2002. 46(8): p. 2450-7.

129. Rhodes, G., *Crystallography made crystal clear : a guide for users of macromolecular models*. 3rd ed. Complementary science series2006, Amsterdam ; Boston: Elsevier/Academic Press. xxv, 306 p.

130. Stevens, R.C., *High-throughput protein crystallization.* Curr Opin Struct Biol, 2000. 10(5): p. 558-63.

131. Hert, D.G., C.P. Fredlake and A.E. Barron, *Advantages and limitations of next-generation sequencing technologies: a comparison of electrophoresis and non-electrophoresis methods.* Electrophoresis, 2008. 29(23): p. 4618-26.

132. GenePool. *Sanger Sequencing Troubleshooting Guide*. 2009 [cited 12 17.04.]; http://genepool.bio.ed.ac.uk/sanger/Sanger_troubleshooting_guide_v1.pdf].

133. *HiLoad Superdex 30 prep grade, HiLoad Superdex 75 prep grade, HiLoad Superdex 200 prep grade*, G. Healthcare, Editor 2011: http://www.gelifesciences.co.jp/catalog/pdf/18110052.pdf.

134. Lattman, E. and P. Loll, *Protein crystallography : a concise guide*2008, Baltimore: Johns Hopkins University Press. viii, 136 p.

135. Towbin, H., T. Staehelin and J. Gordon, *Electrophoretic Transfer of Proteins from Polyacrylamide Gels to Nitrocellulose Sheets - Procedure and Some Applications.* Proceedings of the National Academy of Sciences of the United States of America, 1979. 76(9): p. 4350-4354.

136. Yamaguchi, Y., T. Kuroki, H. Yasuzawa, T. Higashi, W. Jin, A. Kawanami, Y. Yamagata, Y. Arakawa, M. Goto, and H. Kurosaki, *Probing the role of Asp-120(81) of metallo-beta-lactamase (IMP-1) by site-directed mutagenesis, kinetic studies, and X-ray crystallography.* J Biol Chem, 2005. 280(21): p. 20824-32.
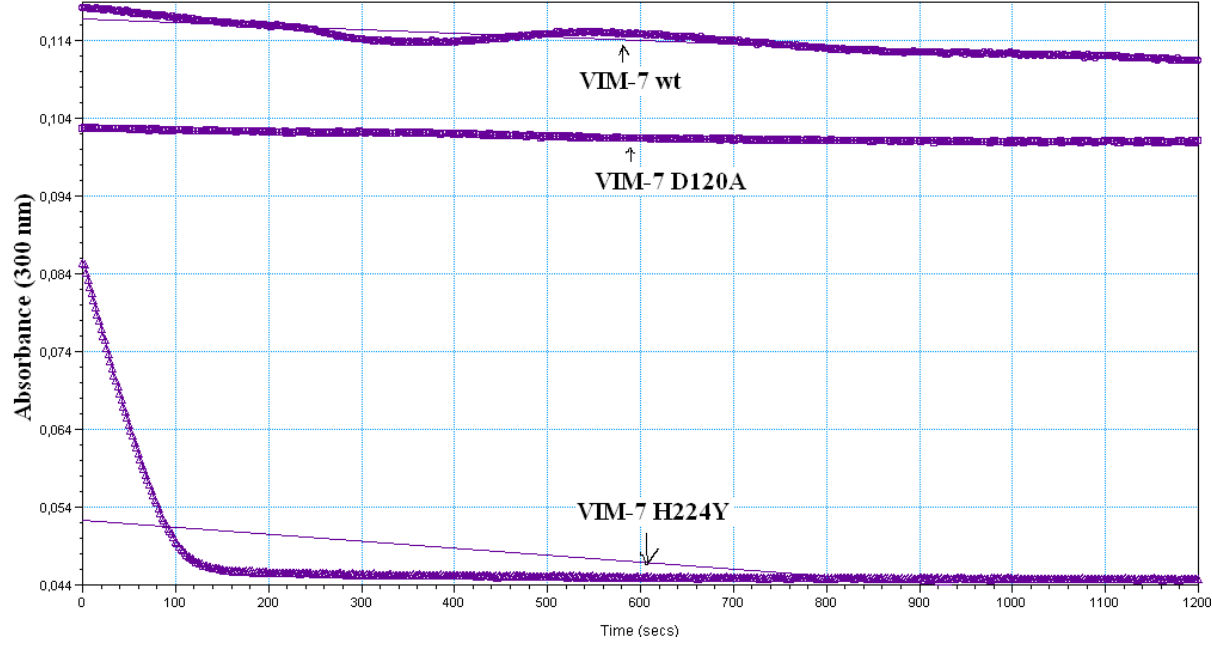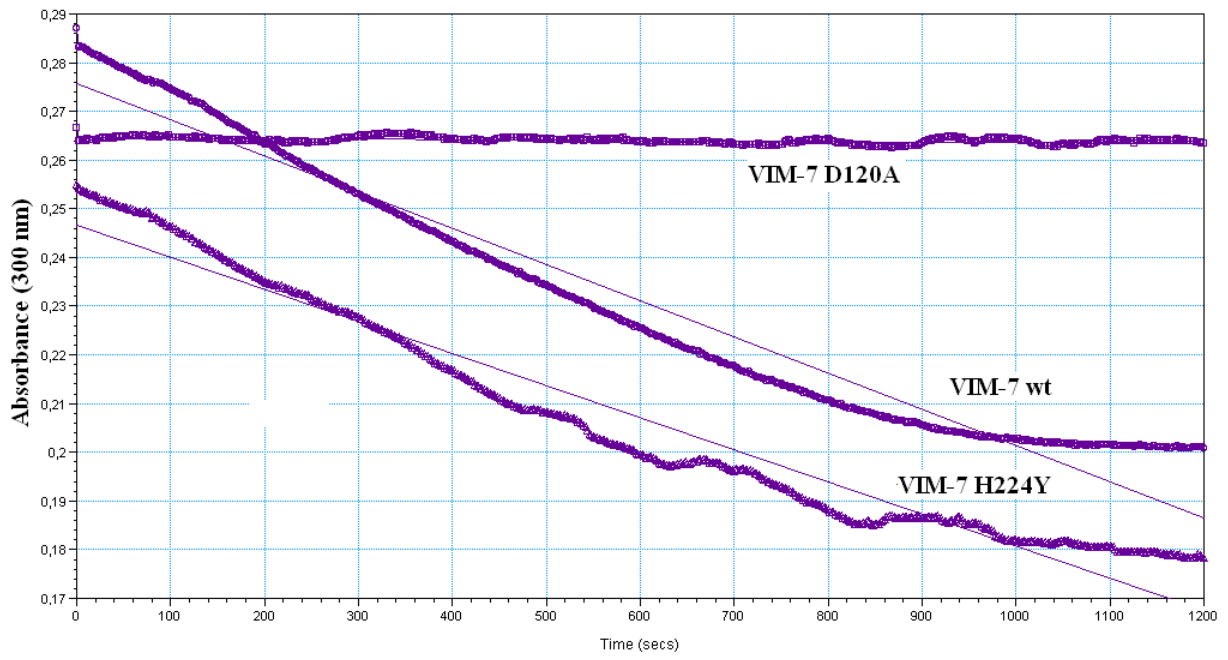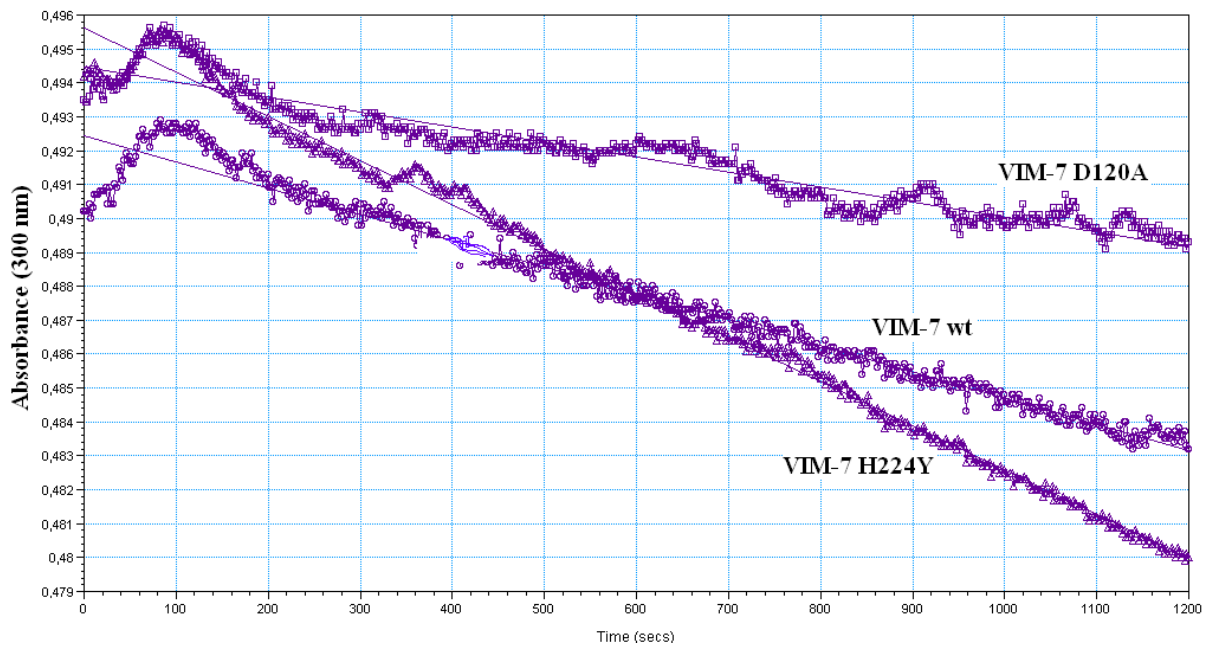
Appendix

Kinetics data

a)
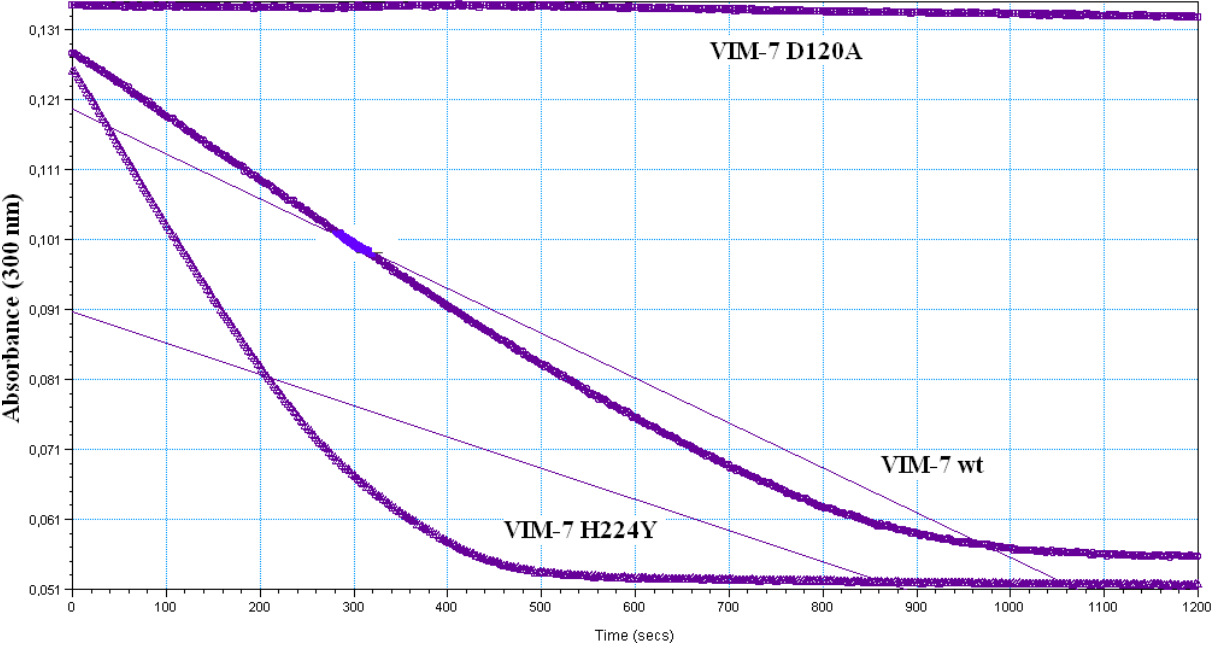
b)

c)

d)

e)

f)

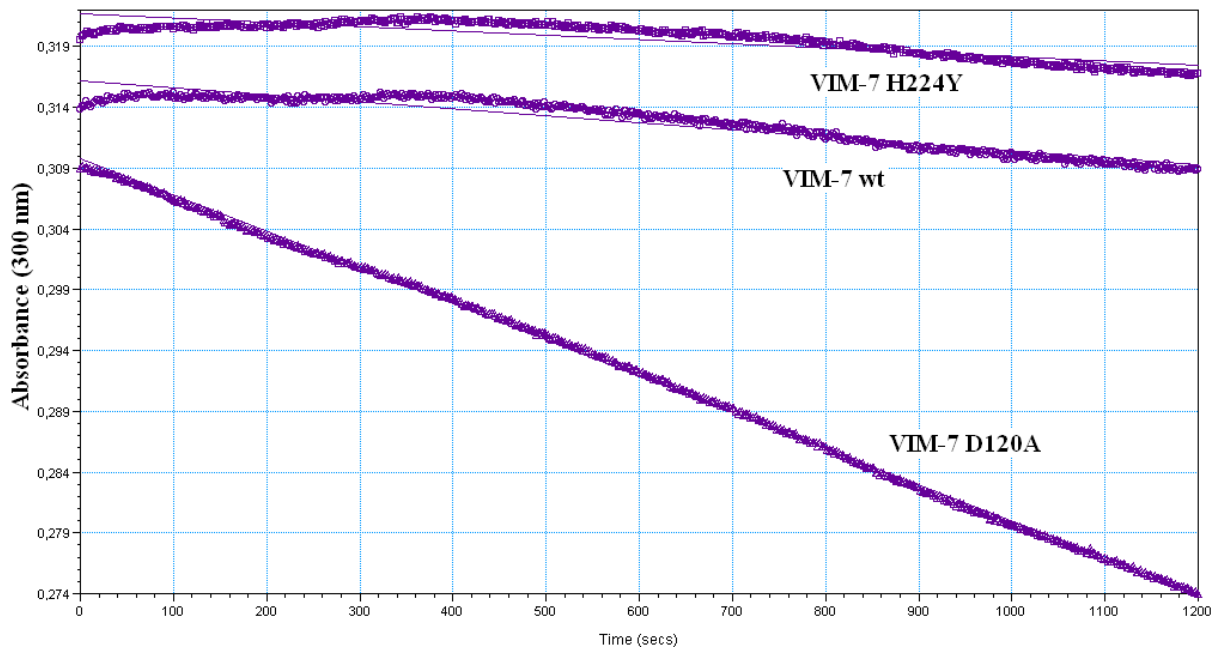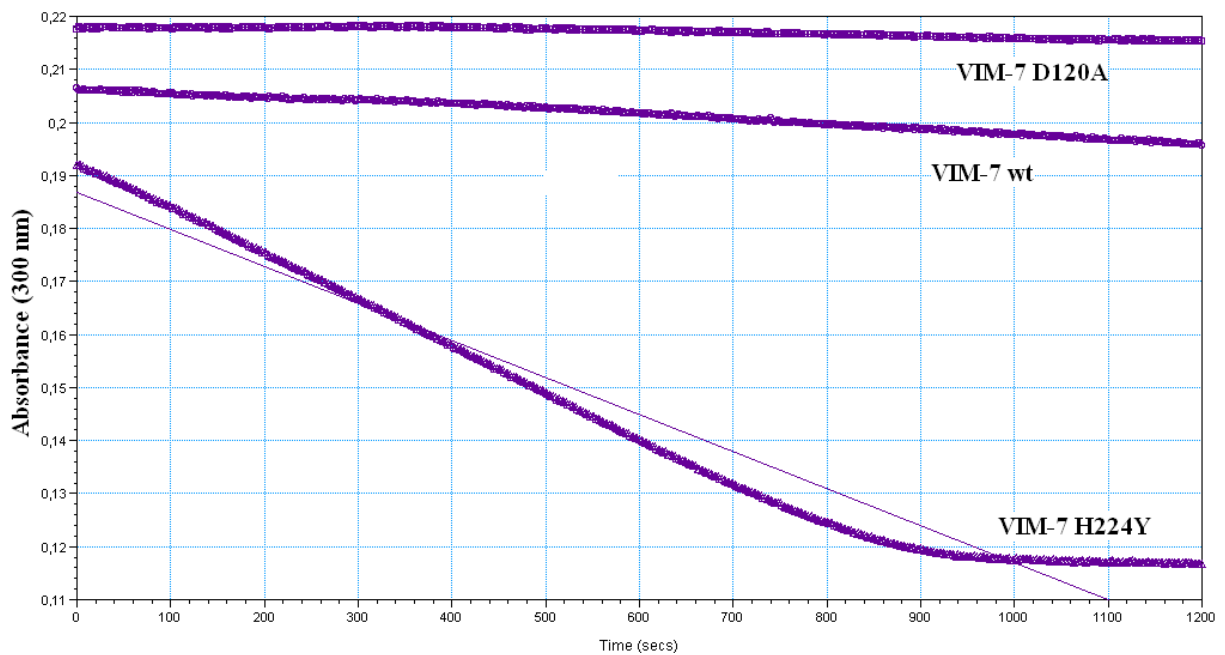**Figure 50: Enzyme kinetics for comparing the activity of VIM-7wt, VIM-7 D120A and VIM-7 H224Y.** The protein concentration of all the proteins was 0.1 µM. The measurement was done by starting with 990 µl of buffer A together with 10 µl substrate. 2 µl of the protein with a final concentration of 0.1 µM was added to the solution, and the concentration was measured for 20 min.

a) Ertapenem, b) Meropenem, c) Cefuroxime, d) Ceftazidime, e) Cefepime and f) Cefoxitin.